THÈSE

En vue de l'obtention du
DOCTORAT DE L'UNIVERSITÉ DE TOULOUSE

Délivré par :
Université Toulouse III Paul Sabatier (UT3 Paul Sabatier)

Présentée et soutenue par
Mathieu Fogel
le : 6 juillet 2015

Titre :
Mise en œuvre de composites structuraux conducteurs par pulvérisation de dispersions NTC / résine époxy sur nappes fibres de carbone

---

École doctorale et discipline ou spécialité :
ED SDM : Science et Génie des Matériaux

Unité de recherche :
CIRIMAT / Physique des Polymères

Directeurs de thèse :
Dr. Éric Dantras (CIRIMAT / Physique des Polymères)
Pr. Philippe Olivier (Institut Clément Ader)

Jury :

Pr. Jean Grenet	Université de Rouen	Président du jury
Pr. Christophe Derail	Université de Pau et des pays de l'Adour	Rapporteur
Pr. Marco Gigliotti	Université de Poitiers	Rapporteur
Pr. Christophe Laurent	Université de Toulouse	Examinateur
Dr. Patricia Parlevliet	Airbus Group Innovations	Invitée
Dr. Éric Dantras	Université de Toulouse	Directeur de thèse
Pr. Philippe Olivier	Université de Toulouse	Directeur de thèse

Manufacturing of conductive structural composites through spraying of CNTs / epoxy dispersions on dry carbon fiber plies

by

Mathieu Fogel

A thesis submitted in partial fulfillment of the requirements for the degree of Doctor of Philosophy

Université Toulouse III - Paul Sabatier

École Doctorale Sciences De la Matière - ED482

July 6th 2015

Keywords: Carbon fiber-reinforced Polymer, Carbon Nanotubes, Nanocomposites, Electrical Properties

Mots-clés: Polymère à renfort fibre de carbone, Nanotubes de carbone, Nanocomposites, Propriétés électriques

This thesis has been prepared as a collaboration between:

Airbus Group Innovations
Composite Technologies
81663 Munich, Germany

☎+49 (0)89 607 20103
🖷+49 (0)89 604 27796
www.airbus-group.com

Université Paul Sabatier
Institut Carnot CIRIMAT
Physique des Polymères
31062 Toulouse CEDEX 9, France

☎+33 (0)5 61 55 64 56
🖷+33 (0)5 61 55 62 21
www.cirimat.cnrs.fr

Acknowledgments

Firstly, I would like to express my sincere gratitude to the professor Jean Grenet for accepting to participate and chair my thesis committee. My sincere thanks also goes to the professors Christophe Derail and Marco Gigliotti for accepting to examine my manuscript. I would also like to thank the professor Christophe Laurent for accepting to participate to my thesis committee.

Foremost, I would like to express my deepest gratitude to my advisors Dr. Éric Dantras and Pr. Philippe Olivier for the continuous support during my PhD, for their patience, motivation, and immense knowledge. Their guidance and availability helped me in throughout the research and writing of this thesis. I want to thank them from the bottom of my heart for accepting to take up this challenge with me.

A very special thank goes out to my supervisor at Airbus Group Innovations, Dr. Patricia Parlevliet, for guiding my research for the past several years as well as for her motivation and encouragement. Her insightful comments and observations helped me perfect my research from many perspectives.

I would like to thank all my colleagues at Airbus Group Innovations in Munich, for the technical assistance and interesting discussions, which helped me a lot along the way. I also want to thank the members of the Laboratoire de Physique des Polymères in Toulouse for welcoming me into the team while I was working there.

I thank also my fellow labmates for the stimulating discussions, support and for all the fun we had in the last four years.

Last but not least, I would like to thank my parents, my brother as well as my girlfriend, Anna, for supporting me throughout this thesis.

Abstract

Carbon-Fiber-Reinforced Polymer (CFRP) have gained popularity over the years, replacing traditional metallic-based structures due to the fact that they offer a much better mechanical properties / weight ratio, allowing manufacturers to reduce the weight per passenger ratio of their airplanes. Unlike their metallic counterparts, CFRPs are significantly less conductive, due to the interleaving polymeric matrix which prohibits the electrical charges to flow through the material especially in the through-thickness direction.

In response to these issues, the concept of multifunctional CFRP has been developed. Nowadays, composite materials are mostly meant to be "single-skill" materials as they only are load-bearing materials. In the future, composites will also have multifunctional properties, as they are meant to integrate properties such as electrical conductivity. The main goal of this work is to create multiscale Carbon Fiber-Reinforced Polymers by inserting carbon nanotubes in the matrix of the composite material to improve and homogenize the through-thickness conductivity of the composite. Multiscale composites are created when nanoparticules are added to a standard composite (referred to as macro-composite) conferring a nano-dimension to the material.

A first part of this work looks into the dispersion process used to obtain the epoxy matrix doped with carbon nanotubes. It also presents an analysis of the cure kinetics, rheological and electrical behavior of the CNT doped epoxy polymers. A second part introduces a spraying technique and manufacturing process followed to produce the CNT-doped multiscale CFRP. This section also presents a quality assessment of the produced composite material. A last part investigates the electrical conductivity, as well as a few mechanical properties of the newly manufactured material, to be able to conclude on the viability and potential of this technique.

Contents

Glossary

AITM Airbus Test Method

CFRP Carbon-Fiber-Reinforced Polymer

CNT Carbon Nanotube

CVD Chemical Vapour Deposition

DC Direct Current

DDS Dynamic Dielectric Spectroscopy

DMA Dynamic Mechanical Analysis

DTA Differential Thermal Analysis

DWCNT Double-Walled Carbon Nanotube

FVF Fiber Volume Fraction

FWHM Full Width at Half Maximum

GI Interlaminar Fracture Toughness in mode I

ILSS Interlaminar Shear Strength

MWCNT Multi-Walled Carbon Nanotube

RTM Resin Transfer Molding

SEM Scanning Electron Microscopy

SWCNT Single-Walled Carbon Nanotube

TEM Transmission Electron Microscopy

UDR Universal Dielectric Response

VAP Vacuum Assisted Process

VARI Vacuum Assisted Resin Infusion

VARTM Vacuum Assisted Resin Transfer Molding

Introduction

Composites for aeronautical and space applications

One hundred years ago, on January 1^{st} 1914, the world's first scheduled commercial passenger flight took place when Antony H. Jannus flew across the Tampa Bay (Florida, United States) [1]. Since then, commercial aviation has been growing steadily. Alone in the last 30 years, the International Air Transport Association (IATA) reported an average annual growth rate of around 5 % [2]. The democratization of flying is mainly due to the dramatically falling prices. Indeed the real cost per flown mile has been divided by two since 1979, with prices rising less than the overall inflation [3]. Today, for airline companies, fuel represents around 30 % of the operating costs. Furthermore, kerosene consumption correlates directly to greenhouse gases emissions and thus represent not only an economical but also an environmental issue. That is why all aircraft manufacturers have been trying to reduce the weight per passenger of their airplanes, as it is one of three main areas which may be improved to reduce the overall fuel consumption of the aircraft together with engines and aerodynamics.

Carbon-Fiber-Reinforced Polymers (CFRPs) have gained popularity over the years, replacing traditional metallic-based structures due to the fact that they offer much better performances. Indeed the mechanical properties / weight ratio of composite materials is far better than for any other material, allowing manufacturers to reduce the weight per passenger ratio of their airplanes. As a result, fuel consumption is reduced, flight range, payload and environmental balance are increased.

Large commercial jets are vulnerable to lightning strike, being typically struck once or twice a year [4]. Unlike their metal counterparts, composite structures do not readily conduct the extreme electrical currents and electromagnetic forces generated by lightning strikes. CFRPs are significantly less conductive than metals, due to the interleaving

polymeric matrix which prohibits the electrical charges to flow through the material especially in the through-thickness direction. For that reason, Lightning Strike Protection (LSP) has been a significant point of interest since the first composites were used on aircraft more than 30 years ago.

If a lightning bolt strikes an unprotected composite structure, up to 200000 A of electricity seeks the path of least resistance. Direct effects typically include degradation of the resin in the immediate strike area, with possible burn-through of the laminate. Indirect effects occur when magnetic fields and electrical potential differences in the structure induce transient voltages, which can damage and even destroy on-board electronics that have not been shielded against Electromagnetic Fields (EMFs) or lightning protected.

Another example concerns the cut laminate edges of aircraft fuel tanks formed of CFRP which have nowadays to be sealed to prevent the exposure of carbon fibers to combustible fuel. This sealing also prevents forming capacitor-like gaps (occurring when insulating layers of matrix are sandwiched between layers of conductive carbon fibers), where a phenomenon referred to as "edge-glow" could happen. The edge seal acts as a dielectric layer that both electrically insulates the cut laminate edges from the fuel and prevent sparking at the edges as an indirect effect of lightning strikes.

Multifunctional, Multiscale CFRP: Goal, Motivation, Concept

In response to these issues, the concept of multifunctional CFRP has been developed. Nowadays, composite materials are mostly meant to be "single-skill" materials as they only are load-bearing materials. In the future, composites will not only have structural but also multifunctional properties, as they are meant to integrate assignments such as acoustic damping, self-sensing combined with self-healing and electrical conductivity.

The main goal of this work is to create multiscale Carbon Fiber-Reinforced Polymers by inserting carbon nanotubes in the matrix of the composite material to improve and homogenize the through-thickness conductivity of the composite. This homogenization of the through-thickness conductivity is crucial to avoid the above-mentioned phenomenon of "edge-glow". Multiscale composites are created when nanoparticules are added to a

standard composite (referred to as macro-composite) conferring a nano-dimension to the material.

Carbon Nanotubes (CNTs) and carbon nanotubes based nanocomposites have been the subject of intense research since the discovery of CNTs in 1991 by Iijima [5]. Their high aspect ratio as well as electrical properties makes them especially attractive when trying to improve matrix dominated properties of CFRPs used in the aeronautical and space industries. Inserting CNTs in the polymer matrix of CFRPs may lead to the increase in through thickness electrical conductivity expected in order to partially fulfill electrical conductivity requirements traditionally met by metallic structures.

However, although the introduction of CNTs into conventional fiber-reinforced polymer composites is assumed to significantly improve the electrical performances of the composite, several processing challenges have to be overcome, which will be detailed in chapter 1. That is why, one of the goals of this work is to develop a processing technique suitable for manufacturing CNT doped CFRP. This method will consist of spraying a CNT / epoxy dispersion on the dry carbon plies as a pre-impregnation method.

Framework and Roadmap of the work

Figure 1 presents a schematic representation of the roadmap followed in this work. As a foreword, the first chapter will review the state of the art on the defined subject. As this covers a wide spectrum of research, this literature review will focus on CNT/epoxy matrices and their application into carbon fiber reinforced polymers modified with carbon nanotubes.

Chapter two will present the materials (Epoxy matrix, MWCNTs and carbon fibers), analysis methods and experimental procedures used in this work.

The third chapter will describe the dilution and calendering processes used to obtain the epoxy matrix doped with carbon nanotubes. This chapter also represents a crucial step before moving on to the mentioned spraying process. It deals with the investigation of the cure kinetics, rheological and electrical behavior of the epoxy matrix doped with carbon nanotubes. Besides the scientific interest of such a study, it helped settle several essential parameters used in the spraying process.

Having performed this important analysis, chapter four will introduce in detail the spraying technique and manufacturing process followed to produce the CNT-doped multiscale composite. A second part of this chapter will present the characterization of the produced materials and will feature a quality assessment, as well as the analysis of the electrical and mechanical properties of the newly manufactured material, to be able to conclude on the viability and potential of this technique.

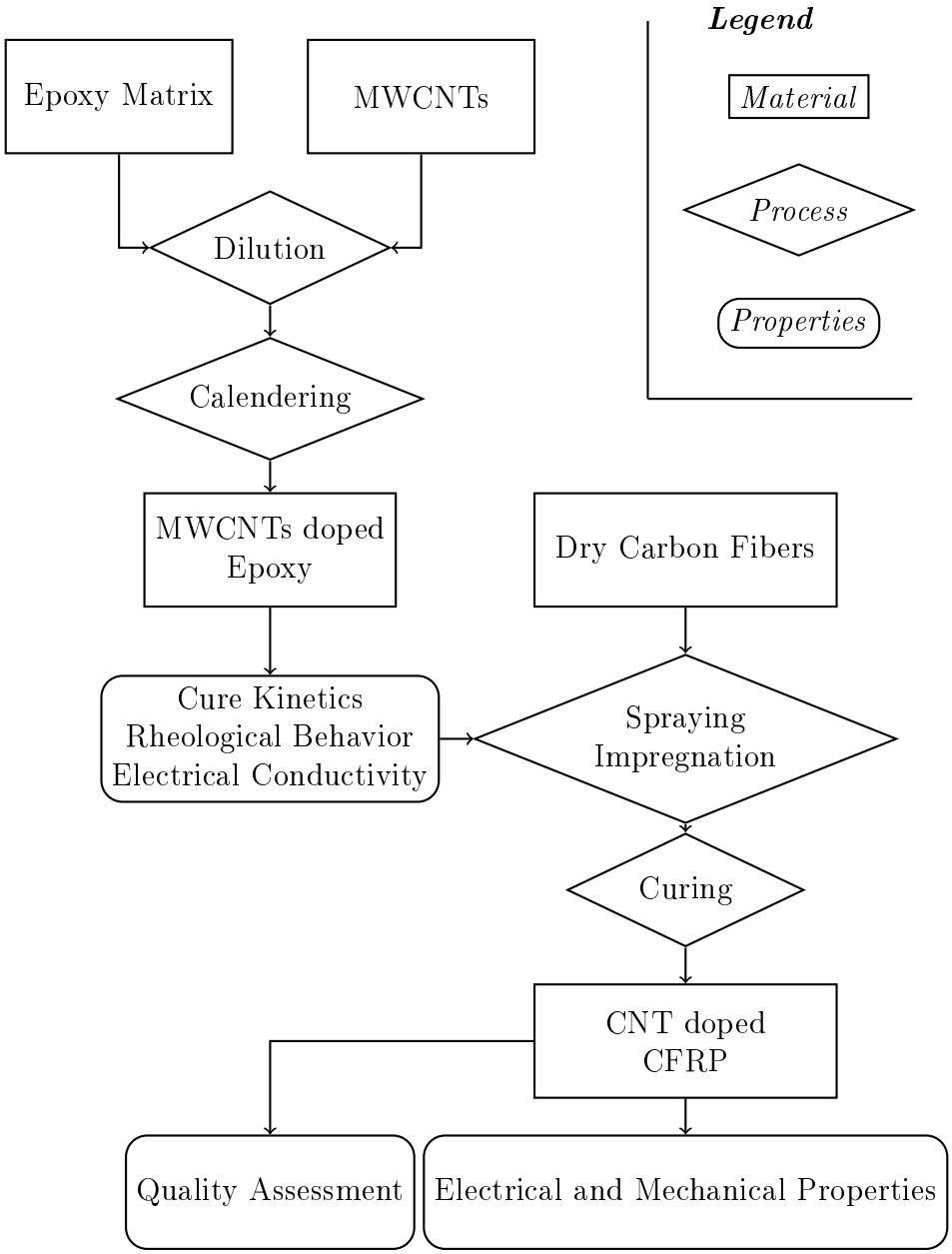

Figure 1 – Experimental procedure used in this work

Chapter 1

Literature Review

Contents

1.1 Introduction

In this first chapter, the state of the art preexisting this work will be presented and reviewed. An exhaustive literature review of composite materials and carbon nanotubes will not be reported in this chapter as they both belong to the state of the art for respectively more than 50 and 20 years. Nevertheless, interested readers can refer to the following books: *Composite Materials : Science and Applications* [6] as well as *Understanding Carbon Nanotubes* [7] and the chapter *Properties of Carbon Nanotubes* in the *Handbook of Nanomaterials Properties* [8], for more information on respectively composite materials and carbon nanotubes.

A first section of this chapter will be dedicated to study the processing methods and properties enhancement of the epoxy matrices doped with carbon nanotubes. In a second section, the state of the art concerning the performance enhancement of CFRP with the use of CNTs will be reviewed. The challenges and expectations this technology is facing will be reviewed as well.

1.2 Carbon Nanotube/Epoxy Nanocomposites

Tremendous efforts have been made in order to insert CNTs into epoxy polymers to address the challenges mentioned previously. Various approaches to improve the dispersion, orientation and chemical and physical bonding of CNTs will be reviewed in this section. The resulting properties of the obtained nanocomposites will be discussed. Further research approaches in CNT/epoxy nanocomposites will be presented as well.

1.2.1 Epoxy Matrices

Many aspects of the performance of composite are shaped or determined by the matrix. It determines the mechanical properties such as the strength transverse to the fiber direction, it provides stability to the fiber in the case of a compression loading and overall transmits the force application to the fibers and between the individual fibers. Furthermore, the matrix governs the electrical and thermal behavior of the CFRP material in the through-thickness direction (for directions perpendicular to the reinforcement fibers).

Organic matrices include elastomer materials, thermoplastic and thermoset resins. Thermosets before hardening, in the same way as thermoplastics, are independent macromolecules. But in their final state, after curing, they build a three-dimensional structure obtained by chemical cross-linking. The links created between the chains of the thermosets limit their mobility and possibilities of relative displacement [9]. Generally for composite materials manufacturing, low molecular weight polymers are used: unsaturated polyester or epoxy resins. They exhibit a low viscosity and are therefore easy to process and are usually initiated by thermal curing for production of the finished parts.

Epoxy prepolymers are typically formed by the reaction of epichlorohydrin and bisphenol A (see figure 1.1). The step polymerization is actually carried out in the presence of sodium salt. Side reactions (hydrolysis of epichlorohydrin, reaction of epichlorohydrin with hydroxyl groups of polymer or impurities) as well as the stoichiometric ratio need to be controlled to produce a prepolymer with two epoxide end groups [10].

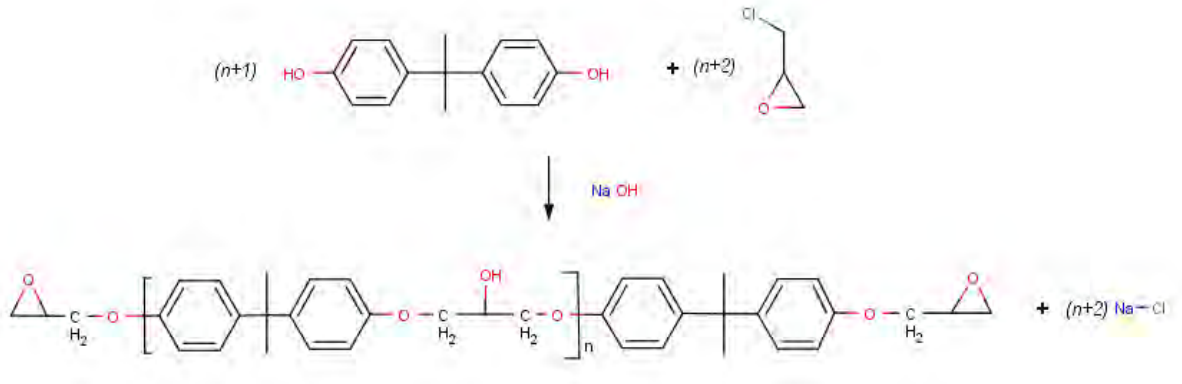

Figure 1.1 – Synthesis of the epoxy prepolymer

A variety of co-reactants can be used to cure epoxy resins, either through the epoxide or hydroxyl groups. Polyamines are the most common curing agents with a reaction involving ring-opening addition of amines. The formation of the three dimensional network between the epoxy resin and the amine curing agent can be described by the three following reactions (figure 1.2). First the primary amine provided by the hardener opens the oxirane cycle of the epoxy prepolymer to create a secondary amine (figure 1.2a). Then the secondary amine reacts in the same way with the prepolymer to form a tertiary amine (figure 1.2b). The reactivity of the primary amine with the epoxy group is higher than the reactivity of the secondary amine $k_1 > k_2$. The value of the ratio k_2/k_1 is usually

found between 0.5 and 0.8 [11]. At last the hydroxyl groups (R-O) formed can react with the prepolymer to form an ether bond (R-O-R') as seen on figure 1.2c. Multiple authors suggest that this third reaction can be neglected [10].

Epoxy resins formulations possess high chemical and corrosion resistance, toughness and flexibility, good mechanical behavior and outstanding adhesion to many different substrates. A wide range of products varying in properties and curing temperatures are obtained for dedicated applications by proper selection of monomers, additives and curing agents [12]. The applications for epoxy fall into two categories: coatings and structural. Structural composites are used in the oil & gas, chemical, construction and transportation (automotive, rail, watercraft and aerospace). More information and characteristics of the structural epoxy matrix used in this study can be found in section 2.2.1.

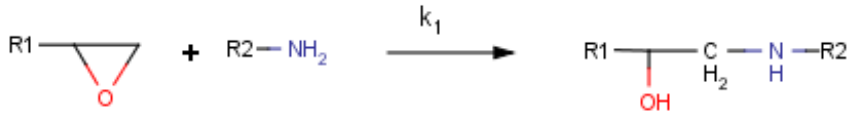

(a) Reaction I: Addition epoxy - primary amine

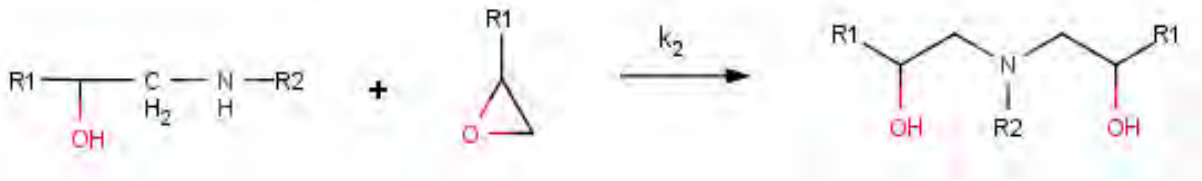

(b) Reaction II: Addition Epoxy - secondary amine

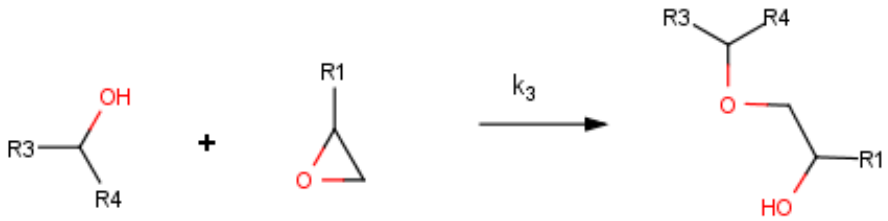

(c) Reaction III: Etherification

Figure 1.2 – Cross-linking mechanism of an epoxy system

Cross-linked epoxy matrices exhibit outstanding properties in most domains, placing them as the standard option for a variety of applications such as adhesives, coatings or composites for structural applications. Incorporation of CNTs into epoxy is expected to further enhance the already high performance of epoxy and epoxy composites by bringing additional functional functionalities such as electrical conductivity.

1.2.2 Preparation of Epoxy/CNT Nanocomposites

A high degree of dispersion of CNTs inside the epoxy matrix is often a prerequisite to obtain optimal properties of the nanocomposites. Many processing techniques coexist together with functionalization treatments to promote CNT adhesion and dispersion.

Processing Techniques

Various processing methods are used to manufacture CNT/epoxy nanocomposites. Ultrasonication is probably one of the most widely used dispersion methods. It is generally accepted that ultrasonic waves promote CNT bundles break-up and scatter individual CNTs, resulting in nanoparticules dispersion [13]. However, high density and long duration treatments can induce localized damage and shorten the CNTs, decreasing their mechanical, thermal and electrical properties [14]. Ultrasonication is often used together with functionalization treatments of the nanotubes described in the following section.

Mechanical dispersion of CNTs in an epoxy polymer is more challenging because of the relatively low shear forces exerted on the high viscosity epoxy. During regular mechanical or magnetic stirring, the shear forces are usually not sufficient to disperse the nanotubes. Increasing the temperature (or adding solvent) to decrease the viscosity of the polymer has been reported and helps promote the dispersion process [15]. This high shear mixing process led to a high degree of dispersion but upscaling this process remains a challenge.

A third approach consists in the use of adjacent cylinders rotating a different rotation velocities to transmit high shear forces to the material flowing in-between the cylinders. This technique is known as calendering or three-roll milling (figure 1.3). The detailed experimental calendering procedure can be found in chapter 3. The general configuration of a three-roll mill can be found in figure 1.3a. The narrow gap between the rolls (δ_1 and δ_2) combined with the difference in roll velocity ($\omega_{apron} = 3\,\omega_{center} = 9\,\omega_{feed}$) results in high shear at the gap between the rolls (see figure 1.3b). Both gaps and rotational speed are adjustable, allowing the generation of various shear intensities. During processing, the CNT / epoxy mixture is poured between the feed and center roll and passes through the two gaps between the rotating cylinders, shearing uniformly the entire volume of the material. The shearing / collecting process is repeated until the desired CNT dispersion

is achieved.

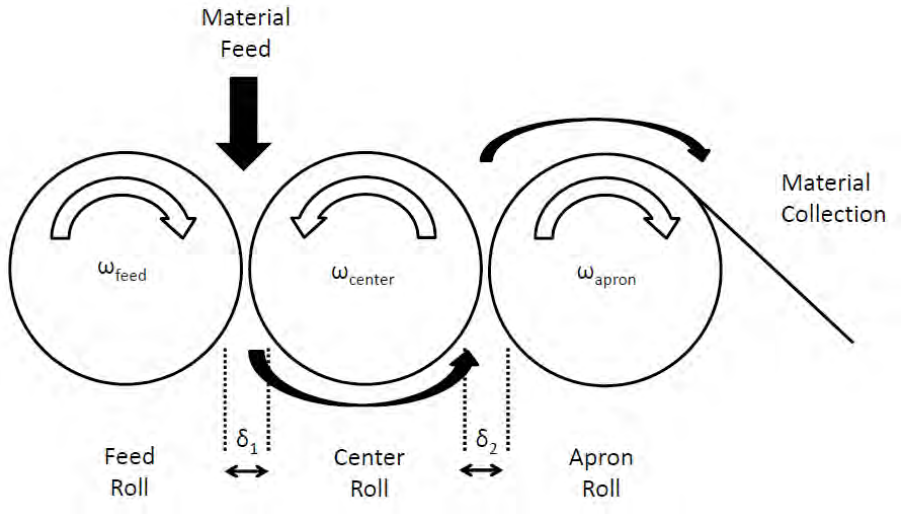

(a) Schematic representation of a three-roll mill

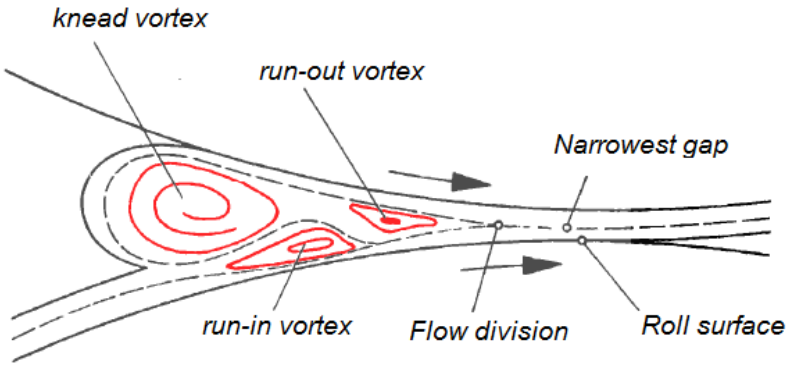

(b) Flow conditions at roll interface [16]

Figure 1.3 – Working principle of a three-roll mill

Gojny et al. [17, 18] obtained a very good dispersion of carbon nanotubes using this technique (qualitatively determined by Transmission Electron Microscopy (TEM)). They manufactured nanocomposites containing 0.1 wt.% of carbon nanotubes by calendering with a gap size between the ceramic rolls of 5 µm and a roll speed set to 20 (1st roll), 60 (2nd roll), and 180 rpm (3rd roll). The nanocomposite produced showed a satisfying dispersion state (only some small agglomerates with a diameter below 1.5 µm were observed). This processing route enables shear forces to be homogeneously introduced over the whole volume of dispersed material.

In the same way, Thostenson et al. [19] milled CNTs into the epoxy matrix with the same laboratory scale three-roll mill (Exakt 80E). Their initial gap width was set to

50 μm because of the large size of the initial MWCNT agglomerates. The mixture was then processed at progressively smaller gap settings of 50, 30, 20, 10 and 5 μm. The speed of the apron roll was set to 250 rpm. The nanocomposite structure evolution after processing at different gap settings (from 50 to 5 μm) was studied (TEM). It appeared that after processing at progressively smaller gaps down to 5 μm there is a much larger quantity of nanotubes dispersed in the matrix and substantially less agglomerates (with smaller size).

Furthermore, Olowojoba et al. [20] prepared MWCNT / epoxy dispersions using two different apron roll speeds (180 and 270 rpm), and subjected these to either one or five calendering runs. Agglomerate statistics, as well as rheological and dielectric spectroscopy indicated that milling at 180 rpm might promote CNT exfoliation but that the higher speed of 270 rpm might promote the shortening of CNT leading to lower aspect ratios.

At last, the work of Maillot [21] showed that CNT could be well dispersed in the epoxy matrix using calendering. A calendering sequence of decreasing gaps (120 to 5 μm) and increasing rotational speed (100 to 500 rpm) was used (see also the table 3.1 in chapter 3). Small agglomerates could still be found but the overall quality of the dispersion was good (determined by Scanning Electron Microscopy (SEM) and statistical observation via optical microscopy). Concerning the calendering process, the dispersion of CNTs in epoxy will be based in this work on these observations (see further in section 3.2).

While the above-mentioned techniques clearly improve the dispersion of CNTs, they do not address the adhesion of the interface between CNT and epoxy. That is why, a surface treatment of the CNTs may in some cases be required.

Functionalizations

Functionalization of carbon nanotubes can solve both issue of adhesion and dispersion, with the help of either covalent or non-covalent functionalization.

Non-Covalent Functionalization

Non-covalent functionalization takes advantage of amphiphilic interactions with CNT surfaces in a non-covalent way, mainly based on van der Waals forces. In order to optimize the dispersion, molecules preventing re-agglomeration are usually attached by creating electrostatic repulsion [22] and/or steric stabilization between CNTs [23]. The attached

molecules may modify the surface properties of the CNTs improving their compatibility with solvents and epoxy monomers. The major advantage of this technique is that it improves the dispersion without damaging the integrity of the nanotube [13]. Even though non-covalent functionalization may improve the CNT/epoxy interface and in that way promote adhesion, the lack of interfacial chemical bonding does not enable an effective load transfer, limiting the mechanical performance improvement [24].

One of the most used non-covalent method is the use of amphiphilic molecules as surfactants. The hydrophobic side of the surfactant interacts preferentially with the nanotube, while the hydrophilic part induces electrostatic repulsion between the CNTs, helping the dispersion process. A high number of surfactants is suitable to be added to the epoxy system for nanocomposite manufacturing. For instance, Barrau et al. [22, 25, 26] achieved a high CNT dispersion degree (as proved by the low electrical percolation threshold they obtained) by adding palmitic acid and dispersing with the help of ultrasonication.

A second group of special surfactants is composed of amphiphilic block copolymers. It has been showed that in a selected solvent, the lyophilic blocs (strong affinity with the liquid in which it is dispersed) are readily dissolved and have a decreased radius of gyration (used to describe the dimensions of the polymer chain), while the lyophobic blocs (lack of attraction with the dispersion medium) are absorbed onto the CNT surface. During the ultrasonication step, the CNT agglomerates are broken up and the lyophilic blocs form steric stabilization layers (see figure 1.4). This allows the CNTs to remain in a dispersed state. Courbaron Gilbert et al. [27] studied the effect of amphiphilic block copolymers (in this case a diblock PAA-PMMA) on the carbon nanotubes dispersion in an epoxy matrix. They proved the effectiveness of this method to improve CNT dispersion.

A last group of non-covalent functionalization agents are nitrogen-containing compounds. Because diamines are typical curing agents for epoxy systems, this chemical compound appears to be appropriate for CNT dispersion in epoxy. Brown et al. [28] dispersed Single-Walled Carbon Nanotubes (SWCNTs) in a diamine with the use of ultrasound. It was the same amine which was used to cure the epoxide prepolymer. Due to the preferred interaction between the diamine and the SWCNT surface and the steric stabilization by the long alkyl chain of the diamine, the CNT dispersion was improved significantly and a very low electrical percolation threshold of 0.05 wt.% was obtained.

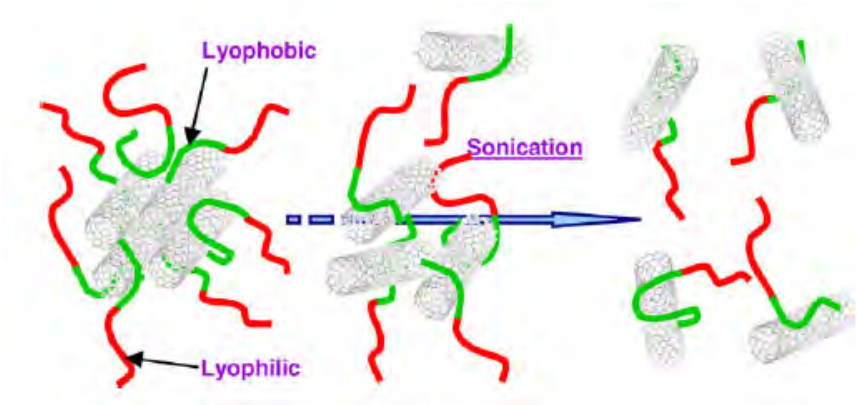

Figure 1.4 – Suspension of CNTs in solution with block copolymers [23]

Covalent Functionalization

Unlike non-covalent functionalization, covalent functionalization not only helps CNT dispersion in the matrix, but also promotes chemical bonding between the functionalized CNTs and the epoxy polymer. This makes covalent functionalization particularly interesting for resin toughening and load-bearing applications. In order to foster the interactions between CNTs and epoxy, functionalized CNTs are usually designed to serve as cross-linkers, integrating them de facto in the polymer network [29]. According to numerical simulations [30], the shear strength of the CNT / matrix interface can be enhanced by over an order of magnitude with the formation of cross-links involving less than 1% of the nanotube carbon atoms. On the other hand, a decrease in electrical conductivity may appear, as each covalent functionalization site scatters electrons [31]. This observation recommends against the use of functionalized nanotubes in the case of our work, intending to increase the electrical conductivity of the material.

Most CNT functionalization processes begins with the oxidation of the CNT surface (either acid, ozone, plasma oxidation or fluorination). These oxidized CNTs typically contain carboxylic acid (-COOH), carbonyl [-C(O)-] and hydroxy (-OH) groups on their outer wall surface and tube ends. Oxidized nanotubes present better solubility and can form better, electrostatically dispersed, CNT dispersion. Oxidized CNTs can directly be used for nanocomposite production and already present better mechanical and thermal properties, because of their improved dispersion state [32].

The functional groups on the oxidized CNT surface (especially carboxilic groups) provide a large versatility for subsequent functionalization thanks to their versatile chem-

istry. Quite a few derivatization routes have been developed so far. The carboxilic acid groups can either: directly interact with the epoxy polymer via a ring opening reaction [33]; interact with amines especially di- or polyamines [34]; treated with ozone [35] or plasma [36]; or fluorinated [37] and sometimes further functionalized by reacting with amine groups [38].

Effect of CNTs on the Curing of Epoxies

In this section the influence of nanotubes on the polymerization of epoxy resins will be reviewed. Additional experimental observations on this subject can be found in section 3.3. The effect of CNTs on polymerization can be divided into two mechanisms. On one side the functional groups on the surface of the nanotubes can participate in the polymerization mechanism. On the other side, CNTs themselves may not be involved in the curing but change the physical properties of the epoxy matrix, which subsequently influences the polymerization kinetics.

Non-functionalized CNTs have been reported to speed up the epoxy polymerization, as showed by a higher initial reaction rate [39], by the fact that CNTs can initiate cure at a lower temperature [40], and a shift of the exothermal reaction peak to lower temperatures [41] during isothermal characterization of the polymerization kinetics. The explanation for this acceleration effect of these pristine nanotubes is caused by their extremely high thermal conductivity. This analysis is shared by Coubaron Gilbert [42], who investigated the effects of MWCNTs on the cross-linking reaction of a DGEBA/DDS epoxy resin. They demonstrated that CNTs initiate epoxy curing at lower temperatures, accelerate the reaction and produce a higher degree of curing. At the same time the activation energy of the cure reaction was unchanged compared to results already reported in the literature. This behavior was attributed to the high thermal conductivity of the MWCNTs, which favors polymerization inside the bulk epoxy resin. On the other hand, it has been found that the addition of nanotubes can lower the degree of cure compared to the reference epoxy material, which may be due to the steric hindrance caused by the CNTs decreasing the mobility of the epoxy monomers and hardener. As a result, the glass transition temperature was lowered for the CNT-modified sample [40].

Concerning the use of covalently functionalized CNTs, three cases have to be distin-

guished. For carboxylic acid and hydroxy groups and if amine curing agents are used, they can both react together and modify the stoichiometry. Abdalla et al. [43] reported a lower curing rate in that case, while other works (Bae et al. [44]) demonstrated that oxidized CNTs increased the initial rate by decreasing the activation energy. Such an opposite behavior is probably due to the fact that CNT oxidation promotes dispersion, which helps heat transfer in the material, accelerating the curing reaction. When amine groups are grafted onto CNTs, they can serve as curing agent and thus promote curing (although this might be counterbalanced by the steric hindrance of CNTs) [45]. At last, fluorinated CNTs have been reported to alter the curing kinetics as well, by reacting with the amino groups of the amine curing agent. This translates into a stoichiometric imbalance, and in that case, in a lower glass transition temperature and cross-linking density [46] resulting in decreased mechanical properties of the polymer.

As showed, both unfunctionalized and functionalized CNTs can have a significant impact on the curing behavior of the epoxy polymer and further on the thermal, mechanical and electrical properties of the epoxy material as discussed further in section 1.2.3.

Orientation of CNTs in Nanocomposites

After dispersing the carbon nanotubes inside the polymeric matrix, it might be interesting for some applications to give the CNTs a preferential orientation. A few approaches have been investigated to align CNTs.

Aligning CNTs using a magnetic field is possible thanks to the anisotropic magnetic susceptibility (i.e. the degree of magnetization of a material in response to an applied magnetic field). Application of a sufficiently strong magnetic field should be able to orient the nanotubes. Choi et al. [47] have observed the enhancement of the thermal (300% with 3 wt.%) and electrical (one order of magnitude compared to the control CNT/epoxy nanocomposite without applying the magnetic field) conductivities with magnetic field. However a decrease in mechanical properties [48] was caused, supposedly by a decoupled orientation between the polymer chains due to inhibited chain movements caused by the presence of aligned nanotubes.

In the presence of an electric field, carbon nanotubes experience polarization. This generates a torque force applied on the CNT, which gives the alignment motion to the

tube. Martin et al. [49] observed that the application of an electric field on CNT dispersed in epoxy can be used to induce the formation of aligned carbon nanotube network. With increasing field strength, high quality networks and higher volume electrical conductivity (up to 2.10^{-4} S.m^{-1} for a 0.01 wt.% nanocomposite under AC field of 200 V.cm^{-1}, with a control sample exhibit a conductivity of 10^{-10} S.m^{-1}) can be achieved.

Mechanical deformation is typically an orientation method used for thermoplastic nanocomposites (for instance using spinning, stretching or extrusion molding). Wang et al. [50] aligned SWCNT in epoxy films by repeated stretching of the semicured matrix. They reported a good alignment of the nanotubes and an increase in electrical conductivity, Young's modulus and tensile strength. The main drawback of this technique is the use of large amount of solvent (here ethanol) in both dispersion and stretching steps.

1.2.3 Properties of CNT/Epoxy Nanocomposites

Even though the initial aim of incorporating CNTs into epoxy matrices was originally to enhance the mechanical properties of the polymeric material, additional possibilities have been identified and pursued. The influence of CNTs on the mechanical, electrical and thermal properties of epoxy / CNT nanocomposites, as presented in the literature, will be reviewed in the next section.

Influence of CNTs on the Mechanical Properties

Due to the brittle nature of epoxy matrices various methods have been used to improve their toughness. One of the most common way to do so is to insert dispersed modifiers in the material (for instance: rubbers, thermoplastic and inorganic particles). When such modifiers are included below a certain concentration (to avoid phase separation), the following toughening mechanisms can be proposed, as presented in figure 1.5 [51]: *a)* crack bridging; *b)* crack path deflection; *c)* crack pinning / branching; *d)* particle yielding; *e)* particle yielding-induced shear branching; *f)* microcracking; *g)* particle-matrix debonding.

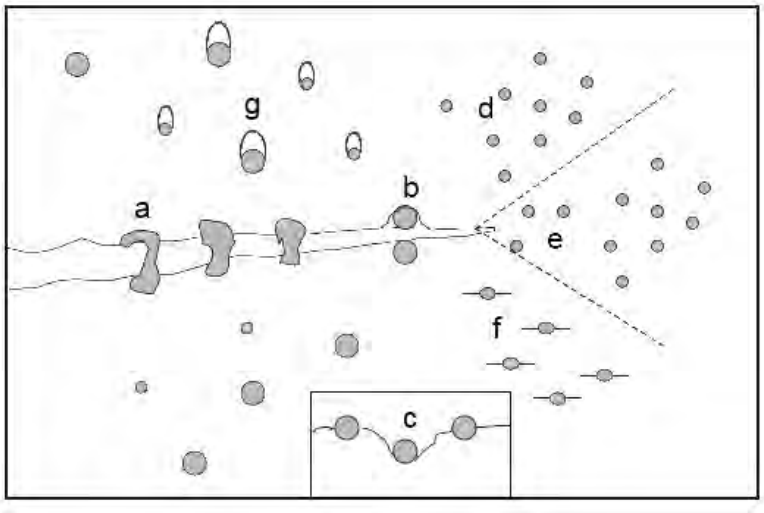

Figure 1.5 – Toughening mechanisms for epoxy resins [51]

The main mechanisms that contribute to the increase in fracture toughness in the case of rigid fillers such as CNTs are *a)* crack bridging; *b)* crack path deflection, *f)* micro-cracking and *g)* particle-matrix debonding. Gojny et al [52] adapted this rigid particle approach in the particular case of carbon nanotubes and proposed fracture mechanisms as presented in figure 1.6. Representation *a)* depicts the initial state of the CNT; *b)* presents a pull-out caused by CNT/matrix debonding in case of weak interfacial interaction; *c)* shows the rupture of the CNT due to a strong interfacial adhesion in combination with extensive and local deformations; *d)* exhibits a telescopic pull-out where the outer layer fractures due to strong interfacial bonding and pull-out of the inner tube; *e)* presents the bridging and partial debonding of the interface caused by the local bonding to the matrix which enables crack bridging and interfacial failure in the non-bonded regions. Furthermore they presented that the CNTs may represent a potential possibility for toughness improvement, possibly because of the bridging effect during loading. However, formation of voids because of either incomplete degassing of CNT agglomerates easily minimized the observed improvement. At last, these theoretical mechanisms still need to be backed up by sufficient experimental data.

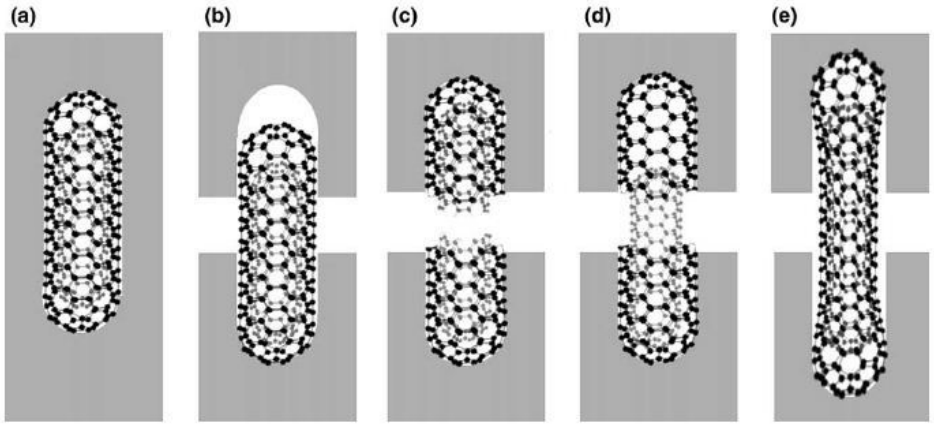

Figure 1.6 – CNT fracture mechanisms [52]

By infusing epoxy into vertically grown CNT forests (see also section 1.3.2), Garcia et al. [53] increased the Young's modulus by 220 % compared to the neat epoxy. The CNT loading in that case reached 2 wt.%.

Overall, the literature results tends to depict that CNTs are effective tools to improve the mechanical properties of epoxy / CNT nanocomposites. However, the mechanical performance improvement reached so far is still far behind the general expectations, no consensus having been reached to explain this discrepancy. There remains significant interest in the further improvement of stiffness and strength of epoxy modified CFRP for structural applications which will be reviewed in section 1.3.3.

Influence of CNTs on the Electrical Properties

A lot of studies have been performed to analyze the electrical properties of CNT-doped epoxy matrices. Table 1.1 reviews the most relevant works found in the literature. This table includes: the CNT type and synthesis technique; their dispersion method; the percolation threshold (p_c) and the maximal conductivity achieved σ_{max} and the corresponding weight percentage. This table focuses on epoxy polymers only.

The key to achieve good electrical properties (low percolation threshold) is to form a conductive CNT network and minimize the aggregation of CNTs.

The percolation theory is a statistical theory, which describes a transition from a state to another. The electrical conductivity of composite material is one of the phenomena where this theory can be applied, by describing the transition from an insulating to

Type	Dispersion Process	p_c (wt.%)	σ_{max} (S.m^{-1}) and CNT wt.%	Source
SWCNT (Arc discharge)	Sonication	0.074	$1.25.10^{-3}$ (0.20)	[54]
SWCNT (CVD) DWCNT (CVD)	Sonication	0.3	10^{-2} (2.5)	[22]
MWCNT (CVD)	Mechanical stirring	0.0025	2 (0.01)	[55]
MWCNT (CVD)	Mechanical stirring	0.5 - 1	5.10^{-2} (4)	[56]
MWCNT (CVD)	Sonication + Mechanical stirring	5	10^{-4} (12)	[57]
DWCNT (CVD)	Sonication + Mechanical stirring	0.04	1 (0.7)	[58]
DWCNT (CVD)	Calendering	0.05	10^{-2} (0.5)	[59]
DWCNT-NH_2 (CVD)	Calendering	0.1 - 0.3	2.10^{-4} (0.5)	
MWCNT (CVD)	Calendering	0.05	8.10^{-3} (0.5)	
MWCNT-NH_2 (CVD)	Calendering	0.3 - 0.35	4.10^{-4} (1)	

Table 1.1 – Literature review of the electrical properties of CNT doped epoxies

a conductive state above a critical filler concentration called percolation threshold (see figure 1.7).

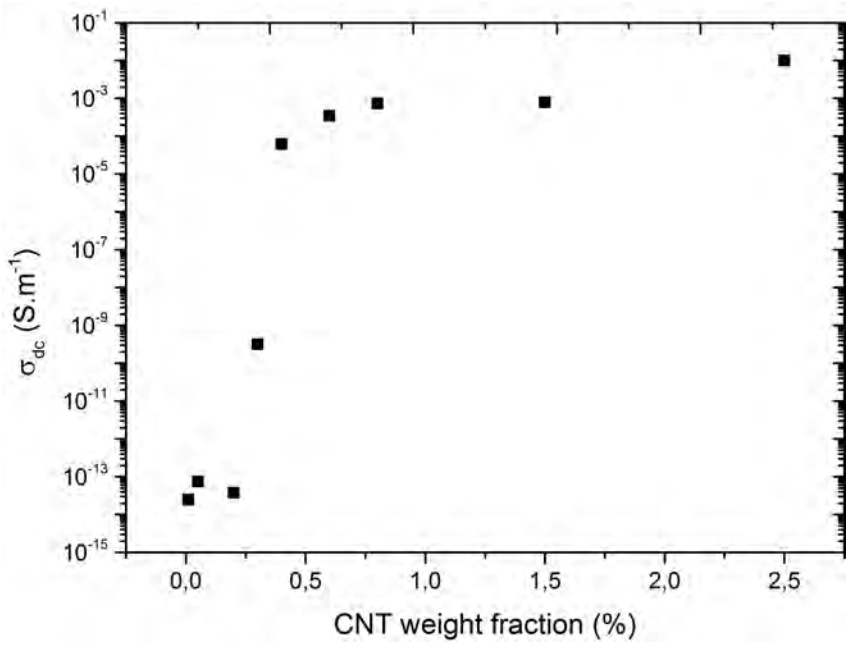

Figure 1.7 – Percolation phenomenon in a CNT / epoxy dispersion [22]

It can be noted that the functionalization usually improves the CNT dispersion and lowers the percolation threshold. However, molecules grafted on the CNT surface lower the volume conductivity as noted by Gojny and al. [59] with amine groups -NH_2 (see table). The thin functionalization groups layers on the CNTs act as a barrier to the electrical charges, and therefore functionalized CNTs will not be investigated in this work. Moreover, the same work showed that when using unfunctionalized MWCNTs and dispersing them with a calendering process a percolation threshold of 0.05 wt.% and a maximal conductivity of 8.10^{-3} S.m^{-1} can be achieved.

At last, it can be observed that the electrical behavior resulting from the dispersion of CNTs can also be used to evaluate the dispersion level of the CNT network. Hsu et al. [60] developed a technique to characterize the degree of dispersion of carbon nanotubes in polymer matrices using the AC impedance spectra. The state of dispersion of the nanotubes inside the epoxy matrix can be accessed via the measure of the DC conductivity of the nanocomposite [61]. The lower the percolation threshold is, the better the CNTs are dispersed. A low percolation threshold signifies the presence of a homogeneous dispersion state, with few to no CNT bundles present.

Influence of CNTs on the Thermal Properties

In the same way as for electrical properties, the enhancement of thermal properties with the help of carbon nanotubes rests upon the formation of a percolating network of nanofillers. That is why a sufficient dispersion of the CNTs is crucial in order to increase thermal conductivity. While CNT functionalization promotes dispersion and thus heat transfer, the functionalization agents create an insulation interface on the CNT surface impeding thermal conductivity [62].

Biercuk et al. [63] reported that loading epoxy matrices with 1 wt.% SWCNTs showed a 125 % increase in thermal conductivity at room temperature. Their results suggest that thermal, electrical (a percolation threshold between 0.1 and 0.2 wt.% was reported) and mechanical properties (here an increase in the Vickers hardness) can be improved without the need for chemical functionalization.

Furthermore, Yu et al. [64] achieved a high thermal conductivity enhancement of 200 % by adding 4 wt. % of oxidized SWCNTs. The need for a higher quantity of nanofiller seems to indicate the detrimental effect of functionalization. Moreover, they demonstrated that the purity of the nanotubes dramatically affects the thermal conductivity of the nanocomposites. CNTs with a high impurity degree are low efficiency fillers which make little contribution to heat transfer.

1.3 Carbon Nanotubes modified CFRP

In this section, the development and processing of nanoreinforced composites (also called multiscale, hierarchical, hybrid or nanoengineered composites [65]) will be briefly reviewed. Particular attention will be paid to review the various techniques used to manufacture nanoreinforced CFRP. Two main manufacturing routes consist of either attaching a nanoreinforcement to the surface of conventional reinforcing fibers or adding CNTs directly to the polymer matrix (see also figure 1.8). The electrical and mechanical properties of these composites will be reviewed in order to provide perspectives for this work.

Although CNT-modified polymer nanocomposites have received most of the attention in the last two decades (as reviewed in the previous section), the work on CNT-modified CFRP has emerged in the last few years. Challenges and drawbacks resulting from matrix and interface dominated properties (particularly fracture toughness and electrical conductivity) have been driving the research. Nano-scale reinforcement, especially carbon nanotubes, may have the potential to provide further improvement to the state of the art CFRPs. Various methods have been tried to enhance conventional CFRP materials, but the solution which fulfills the requirements without notable drawbacks has yet to emerge. Introducing nanoreinforcement in to the matrix could be the most promising solution as it could lead to improvements in matrix dominated properties without affecting the overall architecture or performances of the carbon-fiber reinforced polymer.

1.3.1 CFRP Processing

Nowadays, two main families of composite processing techniques coexist for industrial applications: pre-impregnated materials and liquid composite molding.

Prepreg

The particularity of this technique is the use of intermediate or semi-finished products commonly named prepregs consisting in a layer of carbon fibers already pre-impregnated with the desired amount of matrix. The prepreg material has then to be given their final shape and cured mostly with the use of an autoclave (the pressure applied reduces the

void content inside the final laminate). The main advantage of the prepreg technology is the possibility to obtain end-products with a high and precisely controlled fiber volume content. On the other hand, the costs associated with this technology are quite important. First, such pre-impregnated materials are expensive. Moreover, production and investment overheads are costly as specific equipment is needed to stock (industrial freezers) and process (autoclaves) the semi-finished products. At last, although automated fiber placement technologies are more and more used, hand-layup is still the preferred way of manufacturing composite parts using prepregs, generating high labor costs. That is why, as a response to these cost issues, liquid molding processes are gaining interest.

Liquid Composite Molding

Liquid composite molding technologies (such as Resin Transfer Molding (RTM), Vacuum Assisted Resin Transfer Molding (VARTM) and infusion) share some common features. All of them use a dry fiber preform (without matrix) which is placed into an "open" (with a soft vacuum bag as upper part of the mold) or closed mold (with both upper and lower parts of the mold made of a rigid material, metal for instance) where the resin is injected so that the preform is fully wet with the polymer. Afterwards the resin is cured and the part can be extracted from the mold. The advantages of these processes are especially: the good quality and good tolerance obtained (especially in closed molds), the lower labor and investment costs, and the degree of flexibility in terms of part design. Table 1.2 presents a comparison between various liquid resin infusion technologies and their relevant attributes and features.

Multiscale Composite Processing: Challenges

The introduction of CNTs into conventional fiber-reinforced polymer composites is assumed to significantly improve composite performances. However, in order to manufacture such multiscale composites, three processing challenges have to be overcome.

The first issue to be addressed is the dispersion of the nanotubes in the final composite material. As reviewed in the previous section, a variety of methods enables CNTs to be properly dispersed in the matrix. Issues such as CNT re-agglomeration in the final cross-linked epoxy material have been for instance reported by Li et al. [61].

Process	Features
Resin Transfer Molding (RTM)	• Resin injected into matched mold under pressure • Excellent tolerance compliance • Can obtain high fiber volume fractions (55–65%)
Vacuum Assisted Resin Transfer Molding (VARTM)	• Vacuum pulls liquid resin into preform (no applied pressure) • Requires low-viscosity resins • Sometimes referred as Vacuum Assisted Liquid Resin Infusion
Resin Film Infusion (RFI)	• Resin placed on the bottom of tool and autoclave heat/pressure cycle is applied to force resin into preform • Based on prepreg B-staged resin formulations

Table 1.2 – Review of various liquid resin infusion processes based on [66]

The second difficulty to be overcome is the increase in viscosity appearing when mixing CNTs into the epoxy matrix. This increase in viscosity is a challenge for both prepreg and resin infiltration routes. For instance, Godara et al. [67] incorporated CNTs into prepregs using a drum-winding technique. In order to counterbalance the viscosity increase compatibilizers and other additives had to be used. Concerning resin infiltration, Kim et al. [68] dispersed CNTs in epoxy via sonication and then manufactured CFRP using RTM processing. They observed an extensive increase in infiltration time (3 hours instead of 20 min for the unmodified CFRP). To solve this issue, some groups have tried to modify the RTM process but still with limited to no success.

A last challenge concerns the filtration of the CNTs by the carbon fiber plies during the infiltration process. A few research groups reported noticeable filtration effects leading to a non-homogeneous density of CNTs inside the composite material [67].

1.3.2 Processing of nanotube modified CFRP

The various processing techniques in order to produce multiscale composites can be classified in two categories: dispersing CNTs solely throughout the polymeric matrix,

or grafting CNTs directly on the reinforcing carbon fibers (see figure 1.8). The various manufacturing techniques will be presented, yet the discussion will be focused on the technology selected: the matrix modification approach.

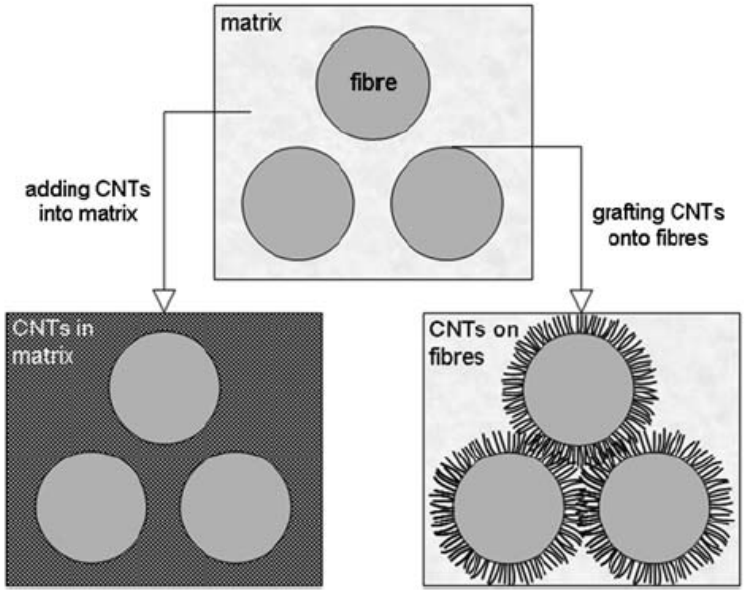

Figure 1.8 – Schematic representation of the two multiscale composite manufacturing routes [65]

CNT-modified carbon fibers

The first potential approach is based on the growth or attachement of CNTs to regular carbon fibers [65]. Grafting CNTs onto conventional fibers could provide higher loadings and CNTs exhibiting a radial orientation, which is expected to be the best configuration for enhancing matrix dominated properties. On the other hand, attaching CNTs on large quantities of carbon fibers requires process development in order to offer up-scalability. Four different grafting techniques have been reported so far:

- direct growth of CNTs on the fiber (via Chemical Vapour Deposition (CVD))
- electrophoretic deposition
- chemical reactions between functionalized CNTs and fibers
- coating of fibers with a CNT-containing sizing

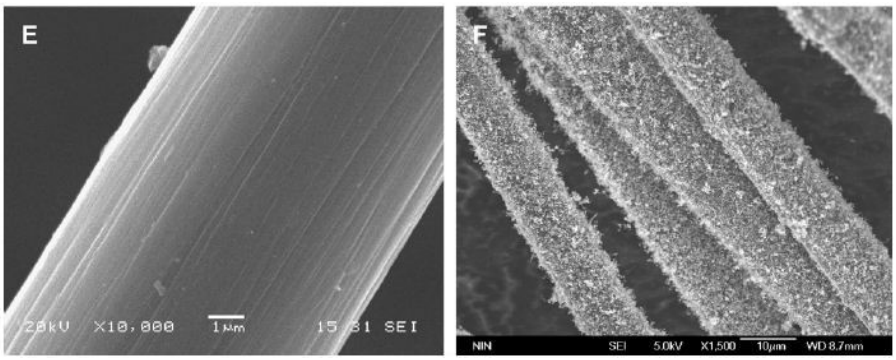

Figure 1.9 – SEM images of pitch carbon fibers before (left) and after (right) CVD growth of CNT [69]

Although CVD deposition being the earliest and most investigated grafting method, other techniques to deposit CNTs have been investigated in order to avoid the potential damage of the carbon fiber during CNT growth (the high temperature required for CVD processing tends to degrade the fiber) and to identify the difficulty of controlling the uniformity and purity of the deposit. Bekyarova et al. [70] showed that a uniform deposition can be obtained by using EPD (Electrophoretic deposition), in which CNTs were deposited onto the carbon fiber electrodes under an applied electric field. Alternatively, a sizing material containing carbon nanotubes has been deposited on glass fibers [71]. The feasibility of this technique for carbon fibers remains to be investigated. More recently chemical methods to covalently graft functionalized CNTs (e.g. with amine groups) onto functionalized carbon fibers (e.g. with acid chlorides) have been investigated [72]. However compared to the direct growth method (CVD), methods using either EPD, sizing or chemical grafting provide little to no control over the CNT orientation. It has been observed that, in theses cases, the CNTs were parallel to the C-fiber plies, limiting their potential applications.

CNT-reinforced matrix

A second approach for producing multiscale composites consists in inserting carbon nanotubes directly into the matrix of the fiber-reinforced polymer. Again this approach includes three different methods.

A first method involves impregnating the continuous fibers with the CNT loaded polymer using a pre-impregnation process. Godara et al. [67] presented an approach

involving a drum winder where carbon fibers were pulled through the modified epoxy containing 0.5 wt.% of CNTs. They reported many critical issues that needed to be optimized such as stability of the dispersion, viscosity control and optimization of surface modification. Nevertheless, they reported a substantial increase in crack propagation energy (+75 %, see next section).

The second method, maybe more straightforward, consists in dispersing the nanotubes into a polymeric matrix used further in a resin transfer molding or vacuum-assisted resin transfer infusion process. Both of these methods, when used with CNT modified resin, face substantial drawbacks. As mentioned in the previous section, increase in resin viscosity, filtration effect and dispersion issues are known to make this technique difficult to implement. Nevertheless, El Sawi et al. [73] manufactured carbon fiber / epoxy / DWCNTs composite laminates using a liquid resin infusion process in order to impregnate individual UD plies of carbon fibers by the epoxy filled with Double-Walled Carbon Nanotubes (DWCNTs). Series of eight individual plies were impregnated using this technique. In spite of the low resin permeability of carbon fibers in regards to the CNTs, evidence of CNT migration through the thickness was found. The electrical characterization of the materials was performed and results can be found further in this chapter.

The limitations imposed by this technique have thus led several groups to look for alternatives. These alternatives aim at inserting the nanoreinforcement in the interlaminar region only. Complex approaches involves, for instance, growing aligned CNTs (often named VACNTs for vertically-aligned carbon nanotubes or *CNT forests*) onto a substrate followed by placing them between prepreg plies. Garcia et al. [53] used aligned CNTs as interlaminar reinforcement for prepregs. Carbon nanotubes were grown onto a silicon substrate in an aligned fashion (at high temperature) and then transfer-printed into a prepreg (at room temperature) maintaining alignment in the transverse direction (see figure 1.10). Although some questions can arise about the influence of such a high temperature treatment on the physical integrity of the carbon fiber, an increase in fracture toughness in both mode I and II was observed. In the same way, Wicks and al. [74, 75] manufactured multiscale composites by growing CNTs onto weaves which could then be placed around the midply of an infused laminate.

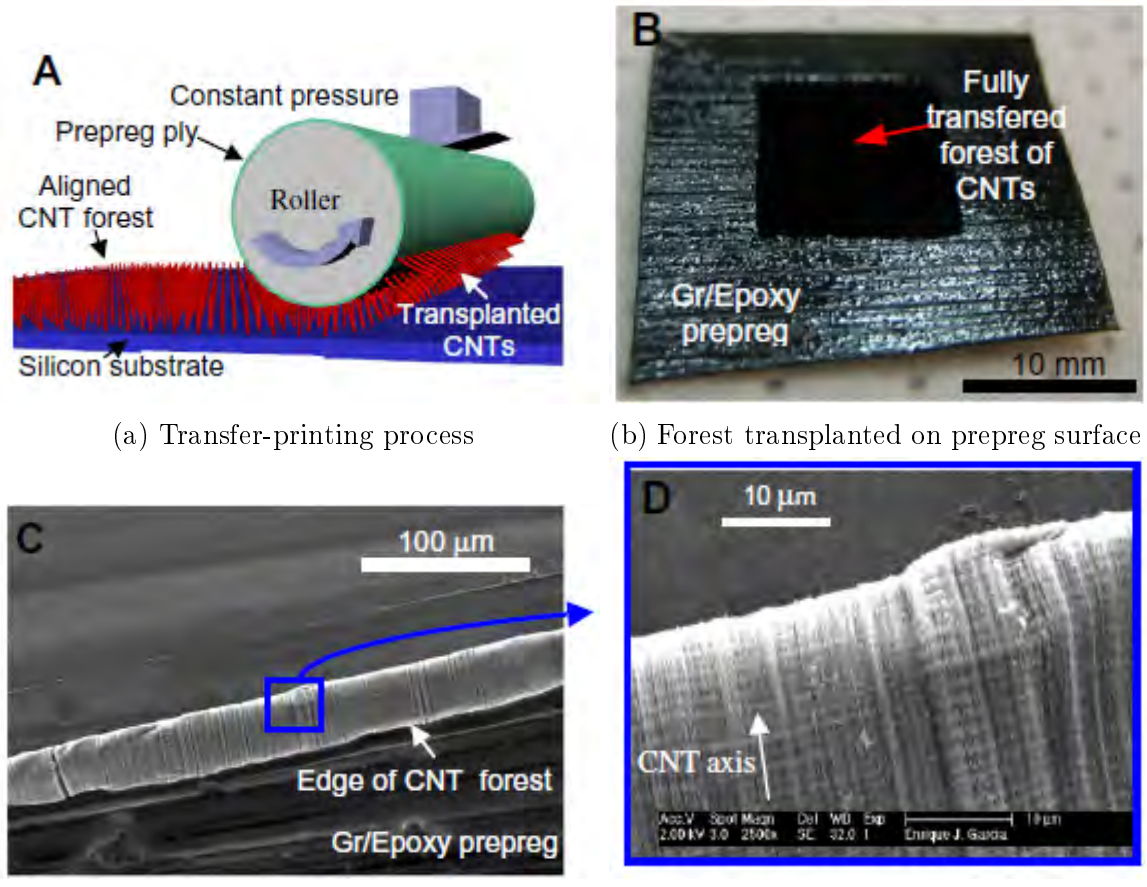

(a) Transfer-printing process

(b) Forest transplanted on prepreg surface

(c) SEM image of CNT forest

(d) CNT alignment after transplantation

Figure 1.10 – Transfer-printing of VACNTs to prepreg [53]

Although this technique is particularly interesting for crack-stopping applications, it might be inappropriate when trying to increase the transverse electrical conductivity of a composite. Despite the fact that both techniques aim at bridging the gap between carbon fiber plies with CNTs, the transverse orientation of the nanotubes might in that case (see figure 1.11) be a handicap for conductivity applications where a random orientation of the nanotubes is preferential.

Furthermore, other approaches explored have consisted in either mixing epoxy with CNTs and use it to glue carbon plies together [76], or applied the CNTs onto prepregs with a roller [77], or at last disperse CNTs in a solvent and spray the mixture onto fiber plies.

Davis et al. [78] developed a spraying technique to deposit fluorine functionalized carbon nanotubes, which were dispersed in an ethanol solution using a high-shear mixer, before being sonicated for 30 minutes. After the spraying process, the solvent is evapo-

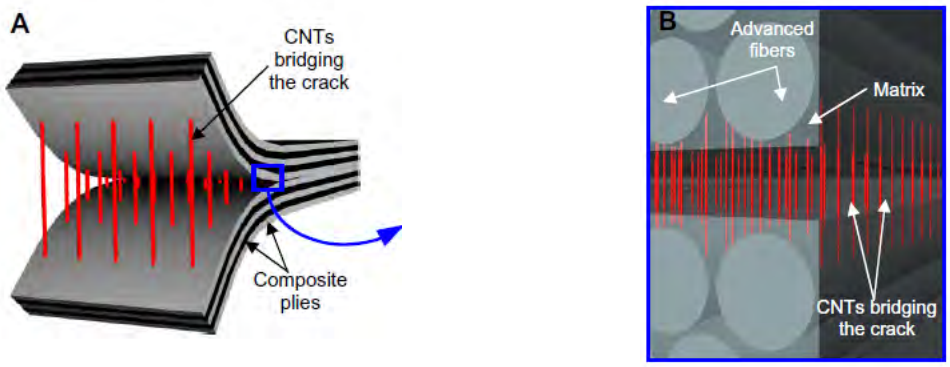

(a) VACNTs between two plies of a laminated composite

(b) VACNTS bridging the interface between two plies

Figure 1.11 – Illustration of the ideal hybrid interlaminar architecture [53]

rated and deposits of CNTs at the desired weight percentage (up to 0.5 wt.%) remain on the fabric surface. They assumed that during the subsequent VARTM laminate fabrication CNTs remained in and on the fabric surface but that some are dispersed in the matrix to produce what they believed to be a toughened fiber-matrix interface. Nevertheless, the potential wash-out effect of the infiltration process was not investigated.

In the same way, Shan et al. [79] developed a spraying technique used to deposit carboxylic acid functionalized MWCNTs on the surface of carbon fiber fabrics via a three steps process. First, a solution of ethanol-dispersed CNTs was sprayed and dried on the fibers, followed in a second step by the spraying of an epoxy binder with a higher viscosity used to anchor the CNTs on the fabric. Finally, the laminate was infused using vacuum-assisted resin infusion. They reported a good CNT dispersion and that this anchoring technique was effective. The composite modified with the CNTs and binder material exhibited increased interlaminar properties (GIc increased by 24 %, GIIc by 11 % and ILSS by 12 %), while the CNT doped laminate without binder showed a decrease in these properties. While this processing methods and results are interesting, the influence of the epoxy binder alone may explain this increase in properties.

This spraying method is particularly interesting as it may overcome the issues of filtration and viscosity, and, combined with the use of the calendering technique can lead to the development of process which do not require the use of a solvent and enables a nanoreinforcement targeted to the interlaminar region, for a bridging effect between carbon fiber plies to seek for an increase in through thickness conductivity.

1.3.3 Mechanical reinforcement of CFRPs with CNTs

Attempts to improve mechanical properties of CFRP by adding carbon nanotubes have been widely documented in the literature. Fracture toughness and Interlaminar Shear Strength (ILSS) are of particular interest as they are matrix-dominated properties which have the potential to be enhanced using nanotechnology. Along with considering whether nano-reinforcement indeed enhances interfacial properties, it is also critical understand the mechanisms involved in these behaviors.

Fracture Toughness

A number of studies [53, 74, 77, 80] have reported the toughening of CFRP thanks to the introduction of CNTs at the interlaminar region. The toughness enhancement reported must be considered carefully knowing that the presence of a thick resin layer alone enhances the mode I fracture toughness [81]. The results of these works can be found in table 1.3.

For long-fiber composites cracks mostly advance either along the fiber / matrix interface or by cleaving the matrix layer. Mechanisms that improve the fracture toughness of nanocomposites (see figure 1.5) such as pull-out, crack path deflection, bridging also apply to crack propagation inside a multiscale composite. In most studies, extensive crack deflection in the crack plane was observed, correlating with increases in fracture toughness because of the energy required to generate additional crack surface area. The deflection can be so important that the crack is deviated from the interlaminar plane leading to fiber bridging and interlaminar cracking (see figure 1.12).

Interlaminar Shear Strength

An additional matrix-dominated property to be considered is the interlaminar shear strength where improvements ranging from 8 to 30 % have been claimed for a CNT volume fraction of respectively 0.25 and 0.1 wt.% [70, 83]. In these cases, failure often involves pull-out or rupture of the nanotube, which, as mentioned previously, is supposed to consume additional energy and thus increase the ILSS [18].

Interesting is the work of Thakre et al. [83] where a SWCNT-containing ethanol

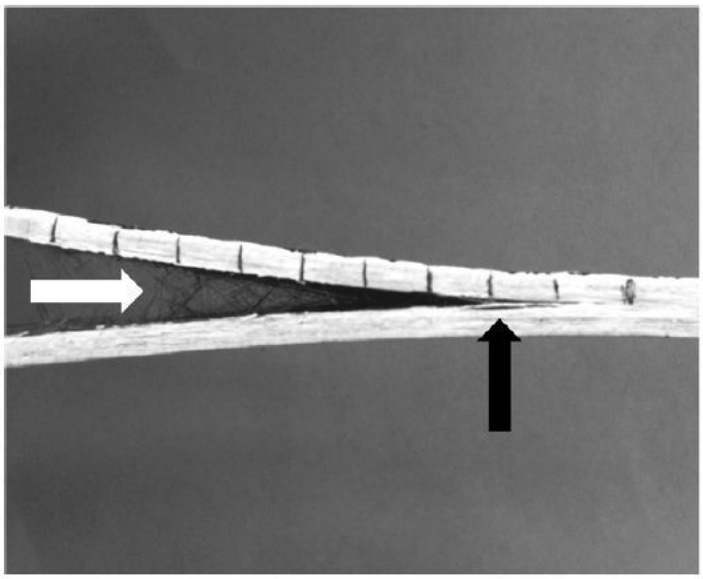

Figure 1.12 – Fiber bridging (white arrow) and interlaminar cracking (black arrow) in mode I specimen [82]

solution was sprayed on carbon fibers. The ILSS was found to be slightly improved by using functionalized nanotubes, while little to no improvement was noticed when using pristine nanotubes. Again, it may be necessary to interpret some of these results (summarized in table 1.3) with caution, as increasing the thickness of the resin layer between carbon fiber plies alone also increases the ILSS [84].

	Modification Process	Fiber	Matrix	CNTs	Baseline	CNT Modified	Source
GIc ($J.m^{-2}$)	Forest on prepreg	IM7	epoxy	Forest	370	530	[53]
	Hand-rolling on prepreg	T700S	epoxy	Carbon nanofibers	500	700	[77]
					221	432	
GIIc ($J.m^{-2}$)	Forest on prepreg	IM7	epoxy	Forest	350	1100	[53]
	Hand-rolling on prepreg	T700S	epoxy	Carbon nanofibers	N/A	2000	[77]
ILSS (MPa)	Electrodeposition on CF	IM7	Epon 862	MWCNTs (0.25 wt.%)	39	50	[70]
	Solvent Spray	T300	Epon 862	pristine SWCNTs	58	59	[83]
				functionalized SWCNTs	58	60.5	

Table 1.3 – Review of mechanical properties of multiscale composite

1.3.4 Electrical Conductivity of CNT modified CFRP

Electrical conductivity improvements of multiscale composites are commonly reported for glass-fiber reinforced polymer [18]. Due to the low conductivity of the baseline materials (in opposition to CFRP), CNTs provide in that case a substantial improvement.

On the other hand, very few results concerning the electrical conductivity of CNT doped carbon-fiber reinforced composite have been reported in the literature. A few reasons may account for this under-investigated domain. First, most of the research focuses on the enhancement of interlaminar properties as seen in the previous section. Second, the insulating nature of glass or alumina fibers (in comparison to carbon) makes for a higher improvement potential. At last, the issues related to processing mentioned in the previous sections hinder the development of such materials.

Nevertheless, three important works deserve to be mentioned. First, the work of Bekyarova et al. [70] reported the use of electrophoresis to depose MWCNTs on woven carbon fabric. These were subsequently infiltrated with epoxy resin using VARTM. The through-thickness conductivity was measured by four-probes testing and compared to a reference sample manufactured in the same conditions. Baseline samples exhibited a through-thickness conductivity (also known as Z-conductivity) of 6.8 $S.m^{-1}$ while the CNT-treated samples reached 8.9 $S.m^{-1}$. Although the authors reported this as a 30 % improvement, the electrical conductivity of a reference CF/epoxy sample is reported to

fluctuate between 2 and 6.8 S.m^{-1}. This variance of results calls this improvement into question. The authors anticipate that this might be due to the variation in thickness of the specimens.

Another interesting results are provided in the work of Lin et. al. [85]. In this work, the thermoelectric behavior of carbon nanotube-charged CFRP materials was investigated. CNTs were attached on the surface of carbon fibers up to a weight percentage of 1 wt.%. Their results showed that the presence of carbon nanotubes increased the value of longitudinal electric conductivity (X axis, fiber direction) of about 10 %.

El Sawi et al. [73] presented a suitable technique to insert DWCNTs in an unidirectional CFRP. To do so, they developed a liquid resin infusion process in order to impregnate individual UD plies of carbon fibers by an epoxy matrix where DWCNTs had been previously dispersed. The electrical conductivity measurement were performed using dynamic dielectric spectroscopy (see section 2.3.4) in the frequency range of 10^{-2} to 10^{7} Hz at isothermal temperatures ranging from -150 to +130°C. Figure 1.13 presents the transverse electrical conductivity for these frequency and temperature parameters. At room temperature, the reference CFRP reached a through-thickness conductivity of 6.6 $\times$ 10^{-5} S.m^{-1}, while for the 0.4 wt.% doped CFRP it reached 5.3 $\times$ 10^{-4} S.m^{-1}. Carbon nanotubes increase the electrical conductivity through the thickness by one order of magnitude, while in the two other directions (X and Y) the conductivity was not affected. Moreover, an evolution in the conduction regime can also be noted.

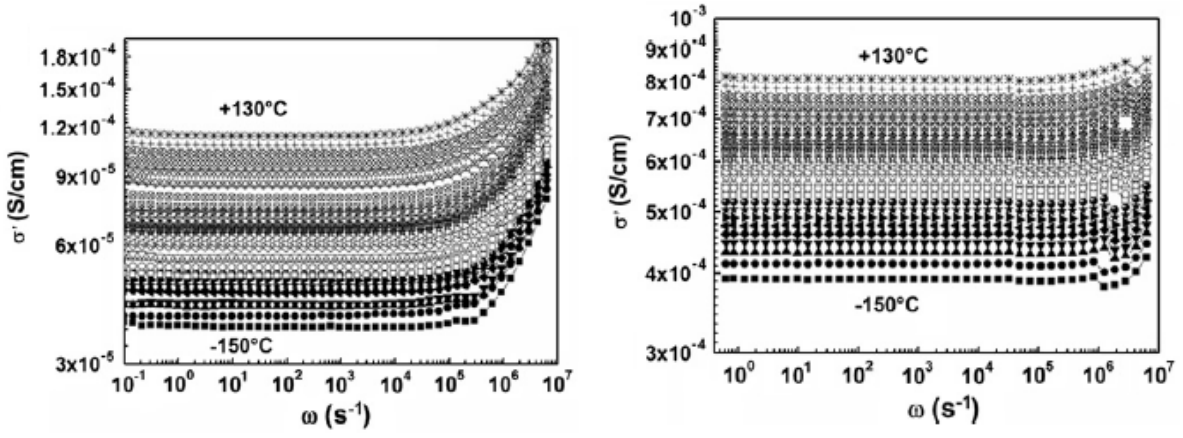

(a) Undoped CFRP (b) CFRP doped with 0.4 wt.% CNTs

Figure 1.13 – Frequency dependence of the through-thickness conductivity for temperatures from -150° to 130°C [73]

1.4 Outlook

In a first section of the literature survey, up-to-date research in epoxy / CNT nanocomposite has been reviewed. It has been discussed how materials and processing techniques influence the obtained properties. Their improvement and applications will strongly depend on how well they are prepared. It is now evident that properties such as electrical conductivity of nanocomposites depend on many factors such as type of CNTs, dispersion process and alignment.

For the experimental part of this research, it has been decided to work with MWCNTs (for their commercial availability and industrial production), which will be unmodified (as functionalization seems to lower electrical conductivity). The calendering technique is chosen to disperse CNTs, as it provides a good dispersion state leading to good electrical properties. Furthermore, it is upscalable (allows to manufacture larger quantities of CNT modified material) and does not require the use of solvent. At last, no alignment of CNTs will be pursued, because of the negative effects on electrical properties.

In a second part, it has been presented how a number of methods based on both conventional composite processing technologies and innovative techniques are being used to process good quality multiscale composites. Although they only contained modest CNT contents, enhancement of interlaminar properties have been reported by some authors. Concerning electrical properties very few groups have been able to demonstrate property improvements, leaving an interesting gap to fill. As revealed by the previous works, great care must be taken concerning the evaluation of the quality of the samples produced, the measurement methodology and the baseline materials, the CNT innovative materials are compared to.

Progress in this area may require to look at new manufacturing processes to produce CNT doped CFRP. The spraying method which will be further developed in chapter 4 appears to be an appropriate candidate. The study of multiscale composites is still in its beginning, but shows great promise for creating both structural and functional composites with improved performance. That is why, we propose to integrate the function "electrical conductivity" into a carbon-fiber reinforced material.

Chapter 2

Materials and Analysis Methods

Contents

2.1 Introduction

This second chapter presents the materials and analysis techniques used in this work. It is composed of two subsections. The first part will be dedicated to a brief presentation of the used materials: epoxy matrix, carbon fiber reinforcement and carbon nanotubes. In a second part, the methods used in order to characterize the materials will be introduced.

2.2 Materials

2.2.1 Epoxy Matrix

The epoxy matrix used in this study is the commercially available MVR 444 provided by Cytec Industries Inc. (formerly Advanced Composite Group, United Kingdom). This epoxy matrix is a single-component resin where the epoxy prepolymer and amine hardener are already mixed together and degassed. It is typically used to manufacture aerospace composite components using VARTM (having a low viscosity at processing temperatures) and is usually cured at 180°C.

The exact composition of the MVR444 resin is unfortunately not publicly available. Nevertheless, based on the information provided by Cytec in the safety data sheet, it can be assumed that this thermosetting resin is based on four chemical components:

a Tetraglycidyl 4,4'-diaminodiphenylmethane (CAS-No: 28768-32-3), representing between 50 and 100% of the resin preparation

b 4,4'-Methylenebis(2,6-diethylaniline) (CAS-No: 13680-35-8), representing between 10 and 25% of the resin preparation

c 4,4'-Methylenebis(2-Isopropyl-6-Methylaniline (CAS-No: 16298-38-7), representing between 5 and 10% of the resin preparation

d Diethyltoluenediamine (CAS-No: 68479-98-1), representing between 5 and 10% of the resin preparation.

The overall reaction system is a classical epoxy / amine system. The glycidylamine epoxy groups are high functionality epoxies which, coupled with a high reactivity, high

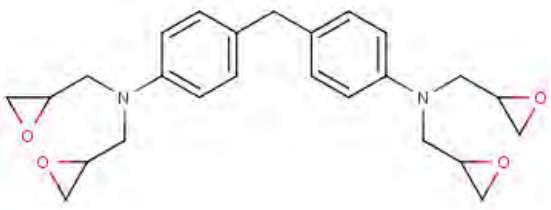

(a) Tetraglycidyl 4,4'-diaminodiphenylmethane

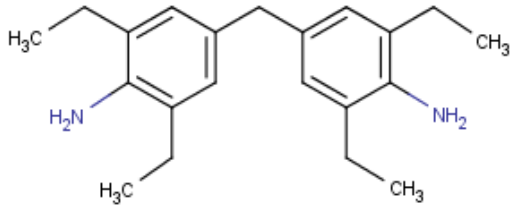

(b) 4,4'-Methylenebis(2,6-diethylaniline)

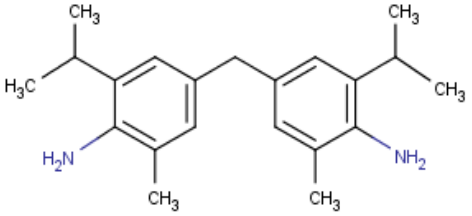

(c) 4,4'-Methylenebis(2-Isopropyl-6-Methylaniline)

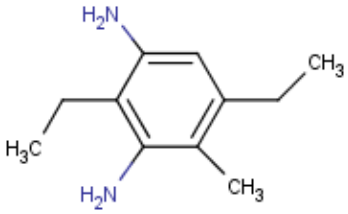

(d) Diethyltoluenediamine

Figure 2.1 – Chemicals molecules composing the MVR444 resin

temperature resistance and good mechanical properties of the resulting cured network, fulfills the requirements for aerospace composite applications. These epoxy groups react with the amine functions of the components shows in figures 2.1b, 2.1c and 2.1d. The presence of tetra-functional groups enables this system to have a high reactivity and an elevated degree of conversion after curing.

Figure 2.2 shows the typical cure cycle used to process the CFRP with this resin material. It is composed of four steps. First, the resin is heated up to 90°C, which induces a decrease in viscosity so that the component (dry preform) can be infused. After being injected the resin is heated to 120°C (heat rate of 2 K/min) and held at this temperature for one hour, to enable the resin to completely wet the fibers. Then, the resin is heated again (2 K/min) this time to 180°C, to be cured during two hours. After this step, the whole setup is cooled down with a rate of 2 K/min.

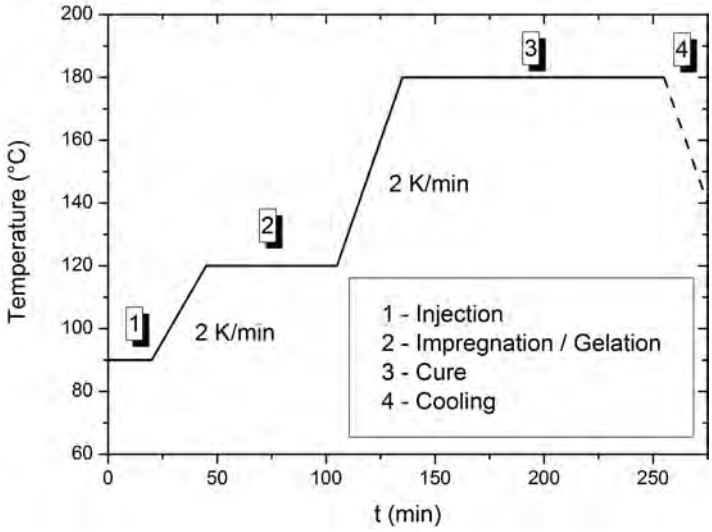

Figure 2.2 – Cure cycle of the MVR444 resin (based on [86])

Table 2.1 presents some of the key properties of the MVR444 resin (uncured and cured following the cycle presented on figure 2.2).

Property	Value	Unit	Source
T_{g0}	-18 ± 1	°C	Measured in this work
$T_{g\,cured}$	214 ± 2	°C	Measured in this work
Viscosity at 80°C	0.1	Pa.s	Measured in this work
Cured Resin Density	1.16 ± 0.01	g.cm^{-3}	Measured in this work
Compression Modulus	2.2	GPa	[86]
Compression Yield Strength	146.0	MPa	[86]
Compression Strain to Yield	13.5	%	[86]
Tensile Modulus	3.1	GPa	[86]
Tensile Strength	77.6	MPa	[86]
Poisson's ratio	0.35		[86]
Fracture Toughness (G_C)	300	J.m^2	[86]

Table 2.1 – Key properties of the MVR444 resin

Up to this date, most of the research concerning liquid resin molding infusion resin for aerospace structural composites, have been mainly focused on the RTM6 resin from Hexcel (see for instance [87, 88]). In chapter 3, we propose to investigate in detail the

cure kinetics, rheological properties and electrical behavior of the MVR444 epoxy polymer both pristine and doped with CNTs.

2.2.2 Carbon Fiber Reinforcement

Figure 2.3 presents the unidirectional carbon fabric used in this work. It is manufactured by SAERTEX, Germany, based on carbon fibers manufactured by Toho Tenax, Japan.

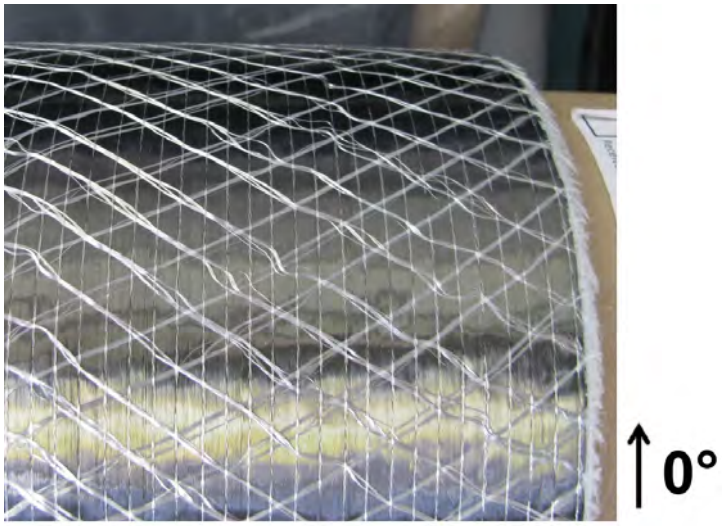

Figure 2.3 – Unidirectional carbon fiber non-crimp fabric

Table 2.2 presents the construction of the unidirectional carbon fabric. The carbon fiber reinforcement is composed of the TENAX J IMS60 E13 24K in the 0° direction, reinforcing threads made of glass-reinforced polypropylene (PP-Glass) in the 90° and ± 60° directions and stitching threads made of polyester (here is PES misleadingly used as abbreviation for polyester by SAERTEX) along the carbon fibers tows. In this table, tex refers to a unit of measure for the linear mass density of fibers, yarns and threads which can defined as the mass in grams per 1000 meters.

Construction	Areal Weight ($g.m^{-2}$)	Material
90°	8	PP-Glass 2002 68tex
0°	274	TENAX J IMS60 E13 24K
+60°	6	PP-Glass 2002 68tex
-60°	6	PP-Glass 2002 68tex
Stitching	4	PES 4.9tex hf SC

Table 2.2 – Construction of the SAERTEX Unidirectional Fabric

The TENAX J IMS60 E13 24K fibre is an intermediate modulus, aerospace-grade carbon fiber produced by Toho Tenax in Japan for use in high performance composites reinforcements. These fibers are produced from poly-acrylonitrile (PAN) precursors and are surface treated to promote adhesion to organic matrix polymers (sizing). The epoxy-based sizing materials are designed to aid in handling. The following paragraph breaks down and explains the meaning of the carbon fibers item name.

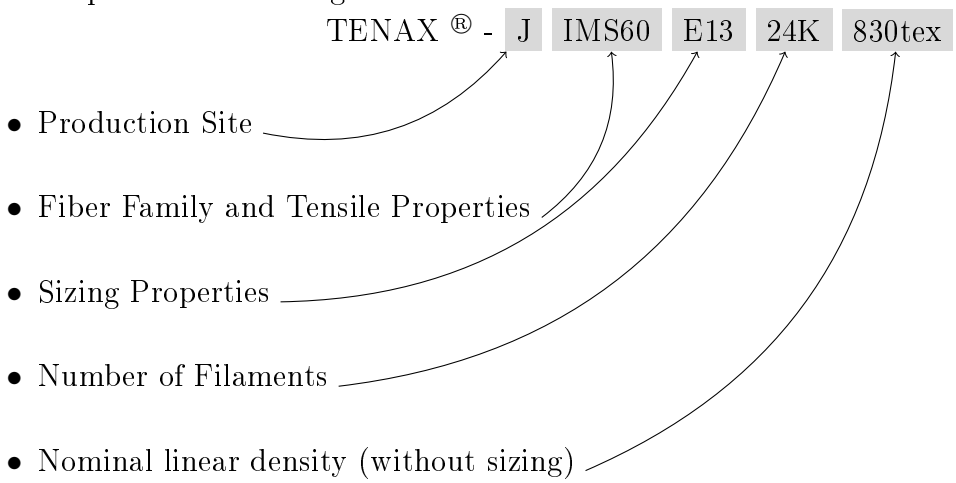

These TENAX fibers are produced in Japan (code J), are intermediate modulus fibers with a tensile strength around 6000 MPa (IMS60). The sizing is based on an epoxy polymer reaching a level of around 1.3 wt.% (E13). A single tow is made of 24000 fibers (24K) and reaches a linear density of 830 tex (ie. 830 $g.km^{-1}$). In addition, table 2.3 provides the key properties of the SAERTEX unidirectional fabric. Especially interesting is the electrical conductivity of the carbon fiber: measured lengthwise, it reaches a value of 6.90 $\times 10^4$ $S.m^{-1}$.

Property	Value	Unit
Filament Diameter	5	µm
Number of filaments	24000	
Linear density (with sizing)	840	$g.km^{-1}$ (tex)
Sizing level	1.25	wt.%
Density	1.79	$g.cm^{-3}$
Tensile Strength	5720	MPa
Tensile Modulus	290	GPa
Elongation at break	1.97	%
Electrical Conductivity	6.90×10^4	$S.m^{-1}$

Table 2.3 – Key properties of the SAERTEX Unidirectional Fabric

2.2.3 Carbon Nanotubes

The Carbon Nanotubes selected for this study are unfunctionalized Multi-Walled Carbon Nanotubes (MWCNTs) provided by Arkema (France). A masterbatch based on the MVR 444 resin from Cytec was prepared by Arkema using their Graphistrength C S1-25 MWCNTs as an additive. With this method the CNT masterbatch is based on the same resin than the one used to dilute to the final CNT concentration, and by thus ensuring perfect compatibility, having only two constituents in the MVR 444 / C S1-25 mixture. For health and safety reasons it was decided to work with carbon nanotubes already encapsulated in a polymeric material. The as-received degree of cure of this thermoset masterbatch containing 25 wt.% CNTs was determined to be $\alpha = 0.03$ (confirmed via calorimetry). The most important characteristics of the carbon nanotubes were determined by Arkema, and are summarized in Table 2.4.

Property	Value	Unit
Carbon Atoms Purity	> 90	%
Number of Walls (mean)	5 - 15	
Outer Diameter (mean)	10 - 15	nm
Length (mean)	0.1 - 10	µm
Density (powder)	0.05 - 0.15	$g.cm^{-3}$

Table 2.4 – Properties of the carbon nanotubes provided by Arkema [89]

Figure 2.4 presents two scanning electron microscope observations (described in 2.3.1) of the supplied C S1-25 as they appear as powder form before encapsulation in the epoxy masterbatch. It shows the characteristic bundles structure of the nanotubes here still in the form of agglomerates. It also enables us to confirm the order of magnitude of the dimensional properties provided by the manufacturer.

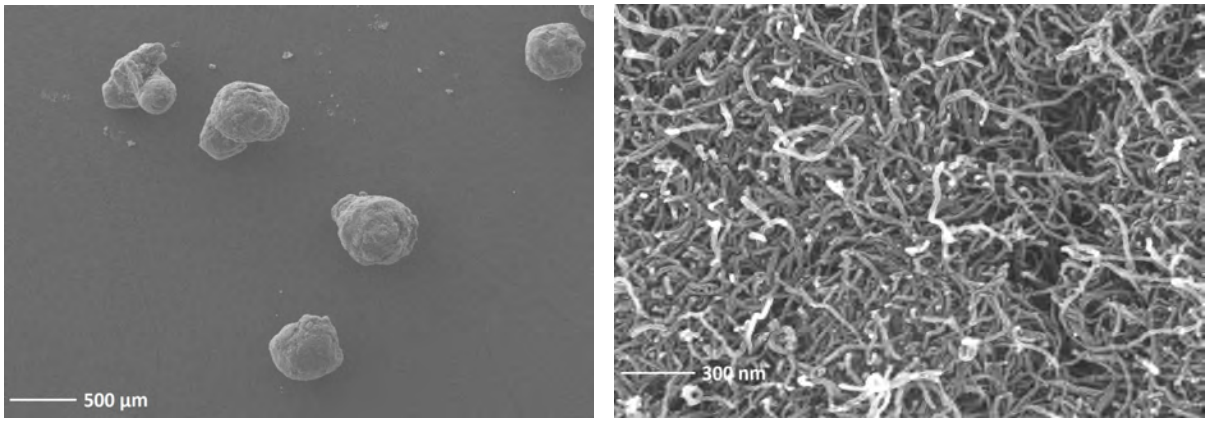

(a) CNT agglomerates (b) CNT bundles

Figure 2.4 – SEM observations of CNT aglomerates of Arkema's Graphistrentgh MWCNTs)

2.3 Analysis Methods

2.3.1 Microscopy

Optical Microscopy

Optical microscopy was performed on a Keyence VHX-500F microscope with Z20 (20x - 100x magnification) and Z1000 (100x - 1000x magnification) lenses in transmitted and reflected light modes. Representative samples were cut with a band saw and cold-mounted in 25 mm diameter molds by pouring room-temperature cured epoxy resin (EpoFix provided by Struers) around the sample. It was later polished with a polishing machines from the same company up to a grain size of 4000 before observation.

Scanning Electron Microscopy

SEM observations were made using a scanning electron microscope JSM 6360F from Jeol, Japan, for the observation of morphology of epoxy/CNT nanocomposite as well as for CFRP. In order to do so, the samples were cryo-fractured in liquid nitrogen for the nanocomposites or cut with a band saw for the observation of the fracture surface of CFRP samples. Both sample types were sputtered with a thin layer of platinum before observation.

2.3.2 Differential Thermal Analysis

Principle

Differential Thermal Analysis (DTA) is a thermoanalytical characterization technique, where a material sample and an inert reference undergo an identical thermal cycle, while the temperature difference between the two is measured. When a sample undergoes a phase transition (fusion, cure, crystallization, etc.) it releases (or absorbs) a different amount of heat compared to the reference where no transition occurs. The device transmits a constant amount of power to the samples, and thus the temperature difference can be measured.

Experimental Procedure

All DTA measurements have been performed using a TA Instruments Q2000 calorimeter. This calorimeter is a heat flux calorimeter, that is to say that both pans (one containing the sample, the other one the reference) are in one single oven, both placed on one metallic support plate. The changes in heat capacity cause a sensible temperature difference between the two pans. Measurements parameters such as sample mass, heating rate, temperature domain investigated and purge gas have to be carefully chosen. The calorimeter has to be carefully calibrated with chemical elements for which the various temperatures and enthalpies associated with its transitions are well known.

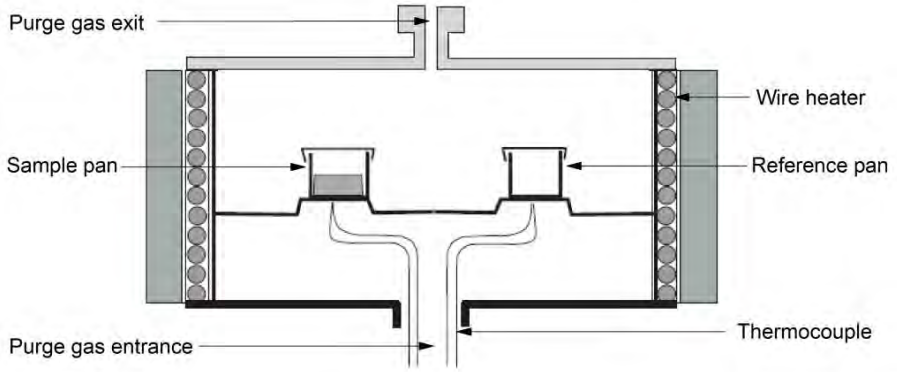

Figure 2.5 – Schematic representation of an heat flux calorimeter [90]

In order to perform the test, a few milligrams of the tested material are inserted in the pan placed then in the calorimeter. The measured heat is then plotted as a function of the temperature (or time). Figure 2.6 shows the cross-linking of the thermosetting matrix chosen (MVR 444 polyepoxy). The glass transition can be observed (T_g) as well as the peak corresponding to the formation of the three-dimensional network (with the corresponding enthalpy ΔH_{Total}).

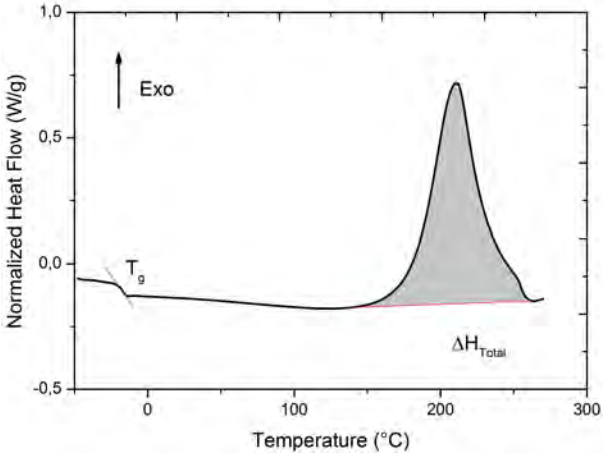

Figure 2.6 – Example of a thermogram - Cross-linking of a polyepoxy (MVR 444)

2.3.3 DC Conductivity Measurements

DC conductivity measurements have been performed with the help of a Keithley 2400 sourcemeter. The principle of the method is to inject an electrical direct current in the specimen while the voltage drop between the ends of the specimen is measured. To achieve a good contact between electrodes and the sample surface, a metallic coating shall be deposited on the edges of the specimen (silver paint coating in our case).

Airbus proposes with the standards Airbus Test Method (AITM) 2-0064 and AITM 2-0065 a principle of measurement of the electrical resistance for a composite laminate with carbon fibers, along the X or Y [91], or Z direction [92].

Because the resistances measured here are sometimes very small (less than 1 Ω), a classical two wires ohmmeter cannot be used, because the resistance of the wires would induce a too large error. Thus the voltage drop shall be measured through different wires than the ones used to inject the current. This method is called four points method or four probes method, as four distinctive probes are used to measure the voltage drop and inject the current.

Considering that the device can only measure resistances up to 200 MΩ, this measurement technique will be more suitable for high-conductivity materials (ie. CFRP), whereas the Dynamic Dielectric Spectroscopy (DDS) will be able to analyze both polymer/CNT nanocomposite and CFRP materials.

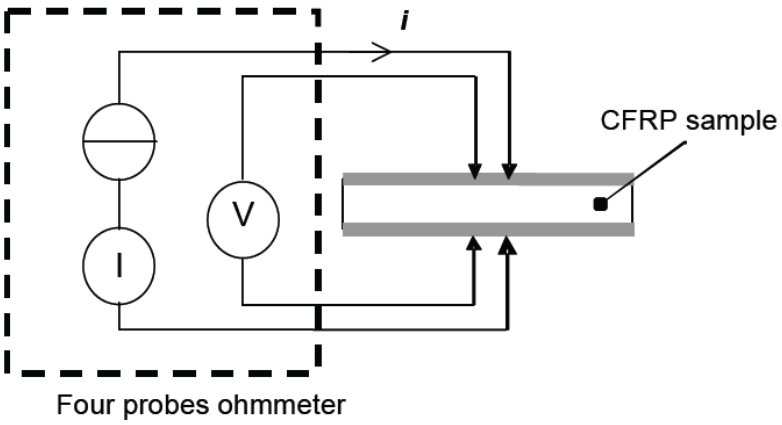

Figure 2.7 – Setup of a DC conductivity measurement [92]

2.3.4 Dynamic Dielectric Spectroscopy

Principle

Dynamic Dielectric Spectroscopy is a useful technique used to determine the dielectric properties of a material. The goal of the technique is to measure the complex impedance Z^* of the studied sample, placed between two electrodes between which a sinusoidal electrical tension $U^*(\omega)$ is applied as described in equation 2.1, where U_0 is the amplitude and ω the angular frequency of the applied voltage.

$$U^*(\omega) = U_0 \exp(i\omega t) \tag{2.1}$$

This electrical tension induces an alternating current in the material $I^*(\omega)$, which has the same angular frequency but is shifted in time from $\phi \neq \frac{\pi}{2}$ (as the material is not a perfectly dielectric material).

$$I^*(\omega) = I_0 \exp(i(\omega t + \phi)) \tag{2.2}$$

From equations 2.1 and 2.2 the complex impedance can be expressed as shown in equation 2.3

$$Z^*(\omega) = \frac{U^*(\omega)}{I^*(\omega)} \tag{2.3}$$

Z^* describes the dielectric response of the studied material and only depends on the

sample geometry (ie. thickness e and surface S) as well as on the dielectric properties of the material. The complex capacitance $C^*(\omega)$, the complex permitivity $\epsilon^*(\omega)$ and the complex conductivity $\sigma^*(\omega)$ can be written as a function of $Z^*(\omega)$, as in equation 2.4

$$C^*(\omega) = \frac{1}{i\omega Z^*(\omega)} \tag{2.4a}$$

$$\epsilon^*(\omega) = \frac{C^*(\omega)}{C_0} \; with \; C_0 = \frac{\epsilon_0 S}{e} \tag{2.4b}$$

$$\sigma^*(\omega) = i\,\omega\,\epsilon_0\,\epsilon^*(\omega) = \underbrace{i\omega\epsilon_0\epsilon^{'}}_{\sigma^{''}} + \underbrace{\omega\epsilon_0\epsilon^{''} + \sigma_{dc}}_{\sigma^{'}} \tag{2.4c}$$

Experimental Procedure

A broadband dielectric spectrometer Novocontrol BDS 4000 featuring a Solartron 1260 Impedance/Gain-Phase Analyzer was used, connected to a Broadband Dielectric Converter (the BDC allows to measure the impedance at high and low frequencies). The thermal regulation was ensured thanks to a Quatro cryo-system , enabling measurements in the range of -160°C to 400°C (with an accuracy of ± 0.01°C). The DDS enables the measurement of the dielectrical properties of materials exhibiting impedances in the range of 10 to 10^4 Ω and in a frequency domain from 10^{-2} to 10^6 Hz.

Dielectric Permittivity

A dielectric material is a material which can be polarized by an electric field. Because of the inertia in molecular polarization, a momentary delay called dielectric relaxation can be linked to the polarization. This relaxation is often described in terms of permittivity as a function of frequency and / or temperature.

This can, for ideal systems, be described by the Debye model [93]. In this model, the dielectric relaxation of an ideal, non-interacting number of dipoles to an alternating external electric field is described. It usually expresses the complex permittivity ϵ^* of a

medium as a function of the field's frequency ω.

$$\epsilon^*(\omega) = \epsilon^{'}(\omega) - i.\epsilon^{''}(\omega) = \epsilon_\infty + \frac{\Delta\epsilon}{1 + i\omega\tau} \tag{2.5}$$

where $\epsilon^{'}$ is the real part of the dielectric permittivity, $\epsilon^{''}$ the dielectric loss, τ the relaxation time of the medium and $\Delta\epsilon = \epsilon_S - \epsilon_\infty$ where ϵ_S is the static low frequency permittivity and ϵ_∞ the permittivity at high frequency.

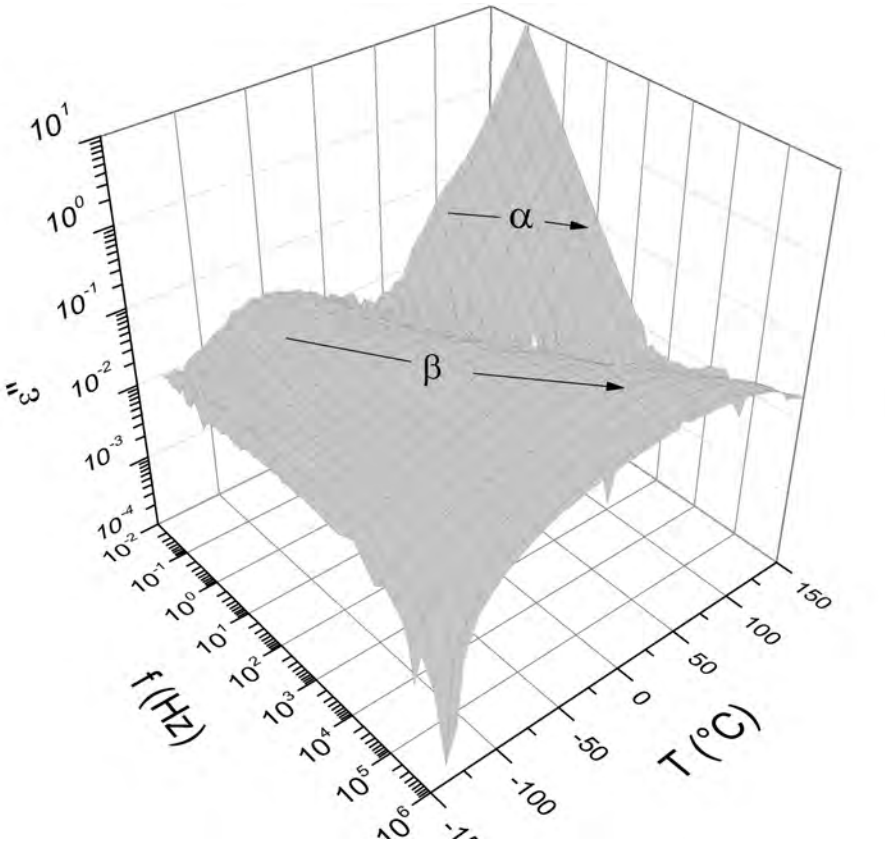

Figure 2.8 – Frequency and temperature dependance of the imaginary part of the complex permittivity

However, relaxation processes in polymers do no exhibit a unique relaxation time as presented in Debye's theory. The Havriliak-Negami relaxation model [94] is an phenomenological modification of the Debye relaxation model, accounting for the asymmetry and width of the relaxation phenomenon.

$$\epsilon^*(\omega) = \epsilon_\infty + \frac{\epsilon_S - \epsilon_\infty}{(1 + (i\omega\tau)^{\alpha_{HN}})^{\beta_{HN}}} \tag{2.6}$$

with α_{HN} and β_{HN} the broadness and asymmetry parameters (with α and β between

0 and 1). The Debye model can be found again taking $\alpha_{HN} = \beta_{HN} = 1$.

The three-dimensional representation of the imaginary part of the complex permittivity of the MVR444 polymer is presented in figure 2.8. Two relaxation modes can be observed. At high temperature and low-frequency, a relaxation called α is partially hidden by the high-temperature conductivity. This α relaxation is the manifestation of the glass transition. The secondary relaxation β visible at high frequency and high temperature, stretches out in a continuously front up to the low frequency - low temperature region. The β relaxation mode can be associated with the local mobility of the diphenylpropane and hydroxyether groups [95]. Other works [96, 97] report an intermediary relaxation ω in the high frequency region between the α and β peaks. This relaxation has not been observed for this particular material.

Universal Dielectric Response

In a disordered medium, the alternating current conductivity σ_{AC} increases with increasing frequency (figure 2.9). The real part $\sigma^{'}(\omega)$ of the complex conductivity $\sigma^{*}(\omega)$ can be written as in equation 2.7, where σ_{DC} is the direct current or static conductivity. $\sigma_{AC}(\omega)$ represents the dynamic conductivity. The change between conduction mechanism is observed for a critical frequency ω_c. For a frequency $\omega > \omega_c$, the conductivity is frequency dependent $\sigma^{'}(\omega) = \sigma_{AC}(\omega)$ while for $\omega < \omega_c$ the conductivity is frequency-independent following a plateau with $\sigma^{'}(\omega) = \sigma_{DC}$.

$$\sigma^{'}(\omega) = \sigma_{DC} + \sigma_{AC}(\omega) \tag{2.7}$$

For disordered materials, $\sigma_{AC}(\omega)$ follows a simple power law as a function of frequency: $\sigma_{AC}(\omega) = A\omega^{s}$ where A is a temperature dependent constant and s a temperature and frequency dependent exponent ($0 < s < 1$). As a consequence $\sigma^{'}(\omega)$ follows equation 2.8 proposed by Jonscher [98] as the Universal Dielectric Response (UDR).

$$\sigma^{'}(\omega) = \sigma_{DC} + A\omega^{s} \tag{2.8}$$

$\sigma^{'}(\omega)$ represents the charge transport mechanism as well as interactions between charge carriers when one investigates the relationship between $\sigma^{'}$ and the temperature

and frequency parameters. The main characteristics (figure 2.9) of a hopping conduction mechanism [99] in a disordered medium are:

1. $\sigma^{'}$ increases with increasing frequency and temperature
2. at high temperatures, $\sigma^{'}$ is constant at low frequency but increases after ω_c
3. ω_c is shifted to the lower frequencies when the temperature decreases
4. above ω_c $\sigma^{'}$ is proportional to ω^s with $0 \leq s \leq 1$
5. at low temperatures, $\sigma^{'}$ is proportional to ω^s with $s \simeq 1$

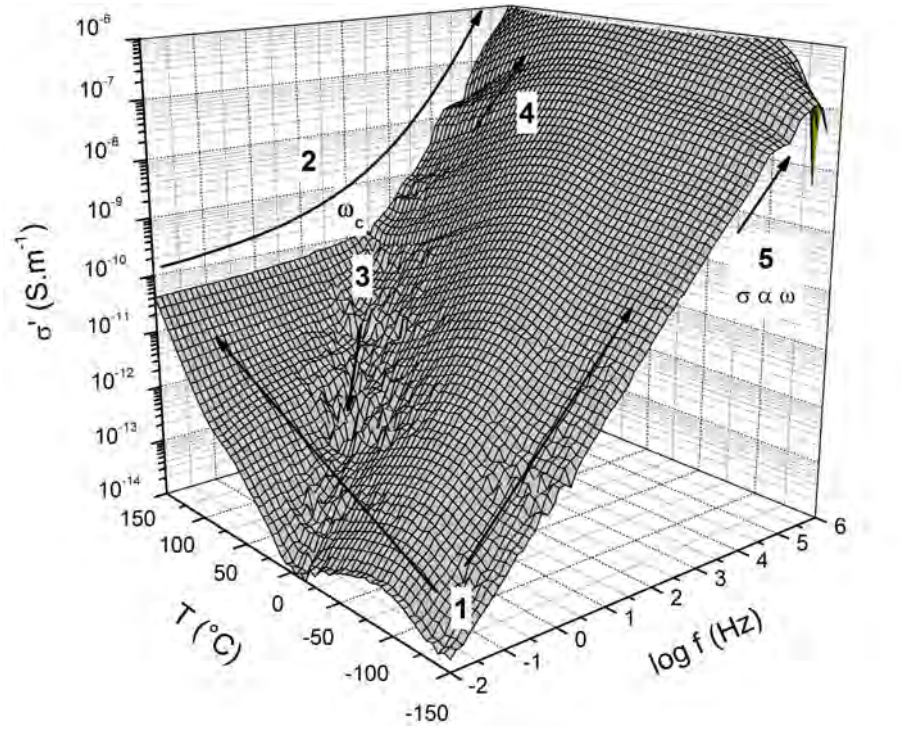

Figure 2.9 – Three-dimensional map presenting the conductivity of neat MVR 444 epoxy

The temperature and frequency dependency represents a continuous process:

- at lower frequencies, charge transport must extend over longer distances r compared to ξ the distance between two neighbor sites, and is limited by bottlenecks of poorly conducting regions
- when the frequency increases, the mean distance r traveled by charge carriers is lowered

- when $r \ll \xi$ the conductivity follows then a frequency proportional power law $\sigma^{'}(\omega) \propto \omega^{s}$ denoting a hopping conduction mechanism between sites.

2.3.5 Dynamical Mechanical Analysis

The Dynamic Mechanical Analysis (DMA) or Dynamic Mechanical Spectroscopy (DMS) is a technique widely used to characterize a material's properties as a function of temperature (DMA) or frequency (DMS).

Principle

During a dynamic mechanical analysis a sinusoidal force (strain γ, equation 2.9a) is applied to the sample and the resulting displacement (stress σ, equation 2.9b) is measured. This strain hold the same pulsation ω, but a phase lag δ will appear because of the viscoelastic nature of the polymer.

$$\gamma^{*}(\omega) = \gamma_0 \, exp\,(i\omega t) \tag{2.9a}$$

$$\sigma^{*}(\omega) = \sigma_0 \, exp\,(i\omega t + \delta) \tag{2.9b}$$

The complex mechanical modulus can be written as in equation 2.10

$$G^{*}_{\omega} = G^{'}(\omega) + iG^{''}(\omega) = \frac{\sigma^{*}(\omega)}{\gamma^{*}(\omega)} = \frac{\sigma_0}{\gamma_0} \, exp\,(i\,\delta(\omega)) \tag{2.10}$$

The real part of this complex is called storage modulus $G^{'}(\omega)$, it measures the stored energy. The imaginary part $G^{''}(\omega)$ is called the loss modulus and represents the dissipated energy.

Damping is the dissipation of energy in a material under cyclic load. It measures how well a material dissipates energy and is reported as the tangent of the phase angle (equation 2.11).

$$tan(\delta) = \frac{G^{''}(\omega)}{G^{'}(\omega)} \tag{2.11}$$

It quantifies the ability of a material to adsorb energy. It varies with the state of the material, its temperature and with the frequency.

Procedure

The measurements were performed using an ARES Rheometer from TA Instruments using a torsional beam geometry. A solid sample (width = 10mm ; length $\approx$ 40mm and thickness $\approx$ 3mm) was held in tension between the lower and upper fixtures. Axial sample torsional deformation was applied by the lower fixture linked to the motor, while a torque sensor (linked to the upper fixture) measured the resulting torsional moment the thermal regulation enabled a measurement between -50 and 300°C, and with a frequency of 1 Hz

For the Dynamical Mechanical Analysis at the suspension level, the rheological behavior of the unfilled and filled uncured epoxy polymer was studied using the same ARES Rheometer and will be presented in section 3.4. A so-called Couette test setup was used. The Couette geometry, as pictured on figure 2.10, used includes a cup containing the sample and applying the shear forces (lower part, linked to the motor) and an upper cylinder linked to the torque sensor (upper part). Parameters of the setup include a gap of 1 mm between the lower and upper part, the upper cylinder having a diameter of 32 mm and a fully immersed length of 34 mm. this specific test setup was chosen in order to achieve a larger surface of contact with the sample, which enables a more appropriate range of torsional moments to be measured by the torque sensor (the MVR 444 having a low viscosity at processing temperatures). Furthermore the amount of material being tested remains the same all along the measurements, which is not always the case with other geometries (for example with parallel plates where the fluid can exit the setup from the sides).

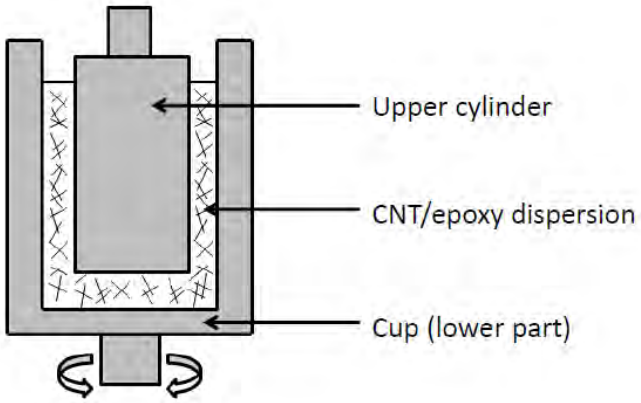

Figure 2.10 – Schematic representation of the Couette setup

Complex modulus in the epoxy polymer

On cured samples, the dynamic mechanical spectroscopy measurements are performed at low deformation rates (typically between 0.01 and 0.1 %), as to stay in the linear response domain. Figure 2.11 highlights the mechanical relaxations occurring in the pristine MVR444 polymer:

- a main relaxation α at high temperature
- a secondary relaxation β at low temperature
- and an intermediate relaxation ω

The main relaxation α ($T_\alpha = 200°C$) is associated with the mechanical manifestation of the glass transition of the material.

The β secondary relaxation is known to occur whatever the chemical nature of the epoxide or curing agent, it has been associated with the mobility of the O-CH_2-CHOH-CH_2 hydroxylpropylether units that are presents in these systems [100]. On figure 2.11 only the end of the β relaxation can be observed (as our device only allows measurements down to -50°C), we can nevertheless confidently assume that T_β = -50°C. This low-temperature peak is quite broad, indicating that a wide spectrum of mobility types and/or activation energies are involved in this relaxation.

The ω relaxation, located at a temperature of 100 - 130°C, is the less pronounced of the three observed. A few authors [101, 102] have found this ω relaxation to be correlated

with network homogeneity, for instance with moisture absorption inside the polymeric network. With a higher moisture absorption, they noticed this relaxation to happen at a lower temperature with a higher intensity and a broader base of the peak, This ω peak is therefore moisture-dependent, the water being absorbed preferentially in lowly cross-linked regions [103]. In our case the samples were dried to avoid any influence of the moisture. Other authors [104] have found this relaxation to be linked with the mobility of poorly cross-linked chain segments.

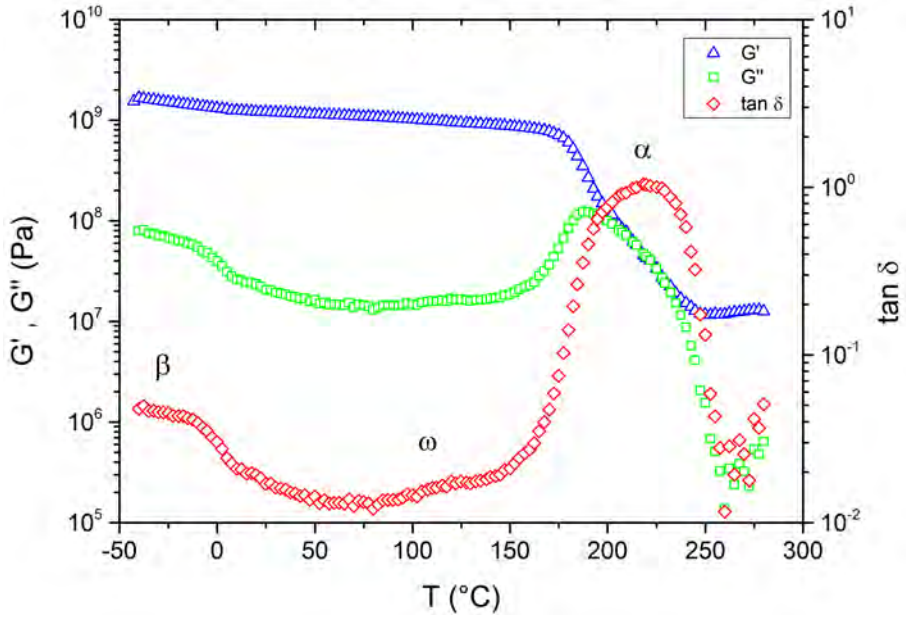

Figure 2.11 – Mechanical relaxations in pristine MVR444 as a function of temperature

2.3.6 Interlaminar Fracture Toughness

Laminated fiber-reinforced composites made of high strength fibers in a relatively weak matrix are susceptible to delamination (i.e. separation of the layers). The subsequent propagation of the crack will be controlled by the interlaminar fracture toughness of the composite material. This section specifies the principle and experimental procedure used to determine the interlaminar fracture toughness of carbon fiber composites manufactured [105].

Interlaminar fracture toughness of laminated composites is normally expressed as the critical energy release rate, represented by the denomination G_c. The critical energy release rate is the energy consumed to produce a unit length of crack growth through a

unit area at the interlaminar interface. It is commonly expressed in Joules per square meters ($J.m^{-2}$). It can be measured in three modes as presented in figure 2.12: mode I (opening), mode II (shear) and mode III (tearing). In isotropic materials, toughness values are usually only quoted for the mode I case. For theses materials the toughness is lowest in this mode, so that even if a crack is loaded to drive the growth in mode II or III, the crack will deviate and grow in a direction which will be pure mode I. In laminated materials (anisotropic materials), however, the delamination can be constrained to lie between the strong fiber layers, so that it is possible to have delamination in all the three modes showed in figure 2.12.

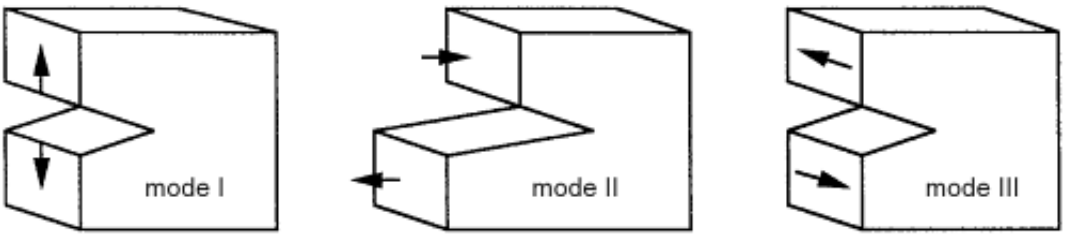

Figure 2.12 – Schematic representation of the crack opening modes [105]

For metals and polymers, fracture toughness is often expressed in terms of the critical stress intensity factor K_c. For linear elastic isotropic materials, K_{Ic} and G_{Ic} are related by equation 2.12, where E is the Young's modulus and ν the Poisson's ratio.

$$G_{Ic} = K_{Ic}^2 \frac{1-\nu^2}{E} \tag{2.12}$$

In the following section, the manufacture, test procedure and data processing for mode I and II interlaminar toughness are described following recommendations from the AITM1-0005 [106] and AITM1-0006 [107] norms. The method for measuring interlaminar fracture toughness involves a beam type specimen for application to unidirectional laminates, with the delamination growth in the direction of the fibers. These tests require measurement of the load and applied displacement at which a delamination of known length grows. For mode I and mode II, the tests uses respectively the double cantilever beam specimen show in figure 2.13a and the end-notched flexure specimen as shown in figure 2.13b.

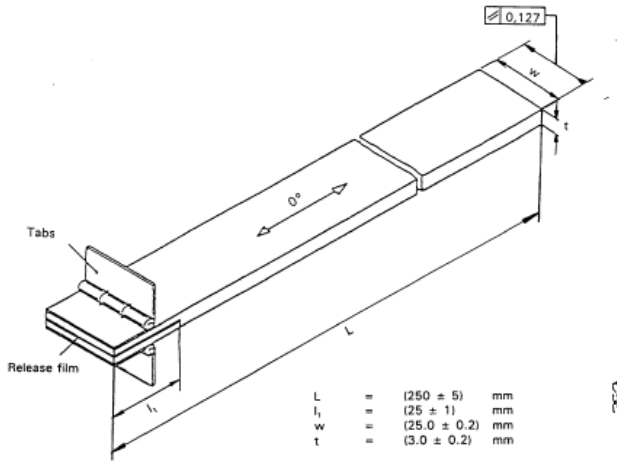

(a) Double cantilever beam geometry - mode I [106]

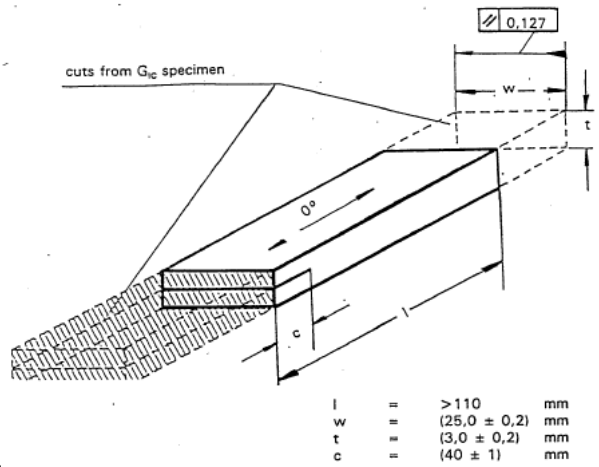

(b) End-notched flexure - mode II [107]

Figure 2.13 – Specimens used to determine the interlaminar fracture toughness

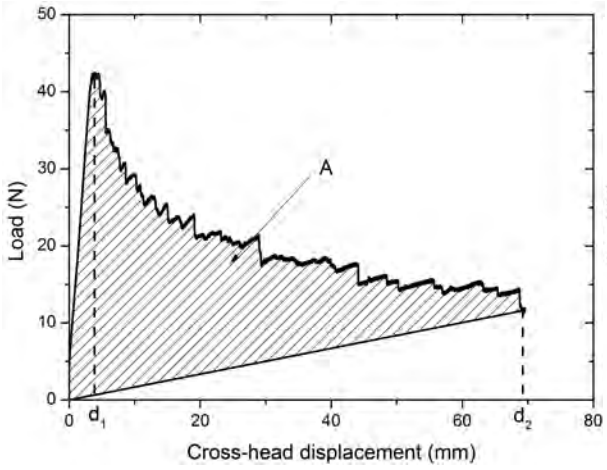

(a) Mode I

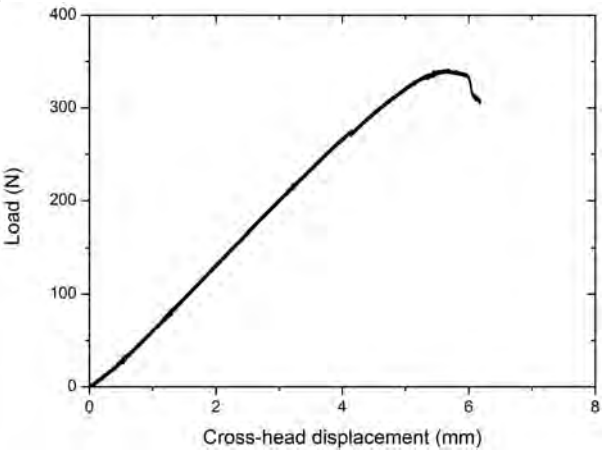

(b) Mode II

Figure 2.14 – Load - cross-head displacement diagramm of a carbon fiber / epoxy laminate

Figure 2.14 presents the typical load / cross-head displacement diagram of a carbon fiber / epoxy laminate in both mode I and II. The fracture toughness energy in mode I is determined using equation 2.13, where A is the energy to achieve the propagated crack length, a is the length of the propagated crack and w the specimen width. The energy A is determined by integration of the area under the load / cross head displacement curve.

$$G_{Ic} = \frac{A}{a \times w} 10^6 \tag{2.13}$$

The fracture toughness energy in mode II is determined using equation 2.14, where d is the crosshead displacement at crack delamination onset, P is the critical load to start the crack, a is the initial crack length, w is the width of the specimen and L is the span length.

$$G_{IIc} = \frac{9 \times P \times a^2 \times d \times 1000}{2 \times w \left(\frac{L^3}{4} + 3 \times a^3 \right)} \tag{2.14}$$

2.3.7 Interlaminar Shear Strength

Another popular test procedure which investigates the interlaminar properties of the material is the measurement of the ILSS by three-point flexure of a short beam. This test gives useful information about the quality of the resin-fiber relation. The span / depth ratio of the beam is chosen so that the beam should fail by interlaminar shear rather than tensile failure. In practice, failure is often a mix of both failure modes. Typical intermlaminar shear strength values for an epoxy / carbon fiber composite reach around 60 $.10^6$ N.m^{-2} (or MPa).

This method consists of the determination of the resistance to delamination under shear forces parallel to the layers of the laminate. For this determination, a specimen of rectangular cross section is tested in flexure on two supports. The load is applied at the centre of the specimen by means of a loading nose midway between the supports. The determination of the ILSS described here follows recommendations from the EN 2563 norm [108]. Figure 2.15 presents a load - cross-head displacement diagramm of a carbon fiber / epoxy laminate during ILSS testing.

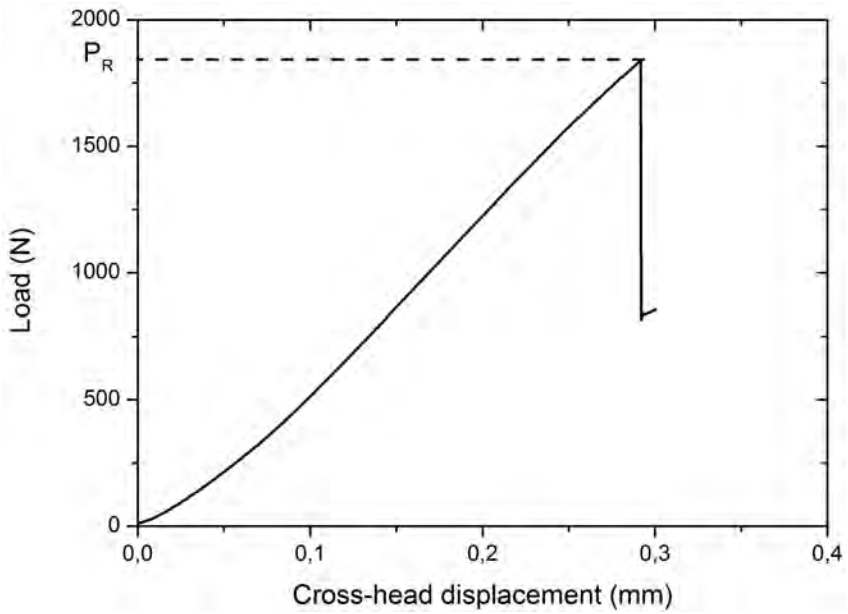

Figure 2.15 – Load - cross-head displacement diagramm of a carbon fiber / epoxy laminate during ILSS testing

The apparent interlaminar shear strength is calculated as in equation 2.15, where τ is the apparent interlaminar strength (in MPa), P_R the maximum load at the moment of first failure (N), b the width of the specimen (mm), h the thickness of the specimen (mm).

$$\tau = \frac{3\,P_R}{4\,b\,h} \tag{2.15}$$

Chapter 3

Thermal, Rheological and Electrical Analysis of MWCNTs/Epoxy Matrices

Contents

3.1 Introduction

In order to manufacture CNT-modified CFRP using state of the art infusion processes (Resin Transfer Molding, Resin Transfer Infusion, etc.) a few challenges have to be overcome. Indeed the change in thermoset resin properties due to the insertion of CNTs (high viscosity, CNTs filtration effect) makes it almost impossible to infiltrate. That is why alternative CFRP processing methods have to be developed. One of the alternatives could be to spray CNT/epoxy dispersions on the dry carbon fibres, followed by a controlled curing process. This will be developed in chapter 4. Manufacturing CNT doped CFRP with such a technique requires a good knowledge of the processing parameters involved, considering that the spray gun operates at higher processing temperatures and shear rates. In that sense a few questions have to be answered in order to be able to process CNT modified CFRP with this selected spraying process.

Firstly, it is important to determine the influence of the spraying process on the polymerization kinetic and the time available to spray the CNT/epoxy dispersions on the dry fibres. That is why, understanding the polymerization kinetics of CNT-epoxy dispersions from the monomer state up to the final cured CFRP is crucial. Secondly, we need to assess the influence of the spraying process on the rheological behavior of the CNT/epoxy dispersion and define if the CNT doped resin is spray-able from a rheological point of view. At last, these results (thermal and rheological analysis) need to be correlated with DC conductivity measurements, to find the best compromise between electrical performances and amount of CNTs inserted, which strongly influences the thermal and mechanical behavior.

3.2 Dispersion and Processing of MWCNTs / Epoxy Nanocomposites

In this section, the dispersion process of the CNTs within the epoxy matrix will be presented, as well as their corresponding parameters.

Carbon nanotubes dispersion was carried out using a three-roll mill (Exakt 80E, EXAKT GmbH, Germany). The masterbatch was first diluted with uncured epoxy resin to the desired CNT concentration and then calendered.

Figure 1.3a presents a schematic representation of the work principle of the three-roll mill. In complement, figure 3.1 presents impressions of the three-roll mill while being operated. The material is poured between the feed and center roll, then passes through the center and apron roll gap, before being collected by the knife in contact with the apron roll. The ratio of roll speeds is as following: feed/center/apron $\equiv$ 1/3/9 (i.e. the apron roll rotates 9 times faster than the feed roll). A calibration run was performed before starting the mixing procedure, so as to calibrate both roll speed and roll gaps (δ_1 and δ_2). A water cooling system was used to keep the resin temperature close to room temperature when poured between the rolls and counterbalance the increase in temperature due to the high shear forces applied (the cooling water typically reach a temperature between 30°C and 40°C).

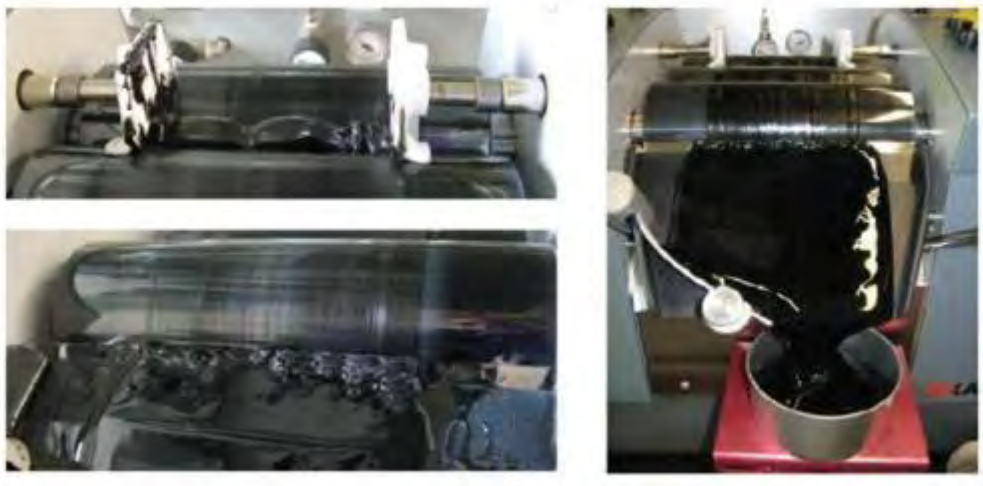

Figure 3.1 – Three-Roll Mill during calendering procedure

A calendering cycle developed in a previous work [109] was used. Table 3.1 presents

Step	δ_1 μm	δ_2 μm	ω_{apron} (rpm)
1	120	40	100
2	120	40	300
3	45	15	300
4	15	5	300
5	15	5	500
6	15	5	500
7	5	5	500
8	5	5	500
9	5	5	500

Table 3.1 – Calendering procedure used in this study [109]

the nine steps of the calendering process and their corresponding parameters. This program composed of nine successive runs with decreasing gap width and increasing roll velocity can be divided in three parts with following functions. The first two steps (1 and 2) are meant to break the solid pellets of the masterbatch into miscible powder. The intermediate part of the process (step 3 to 6) mixes the CNT masterbatch to the epoxy matrix, while during the last part of the process (steps 7 to 8) occurs the actual disentanglement of the nanotubes. The repetitive steps (see steps 5 - 6 and 8 - 9) are particularly useful to disperse into a large amount of material (for instance 2000 g, see below) the masterbatch pellets which contain a high concentration of nanotubes (25 wt%). An advantage of the calendering process which is often reported in the literature is the possibility for this method to be up-scaled. Quantities of CNT-modified epoxy between 100 and 2000 g were prepared. For a 100 g preparation, the total processing time usually averages 120 minutes.

The process effect on the cure kinetics was assessed. Calorimetric measurements performed before and after the complete process showed that the degree of cure of the dispersion after calendaring remains at a minor value of $\alpha = 0.03$. Mixtures were manufactured with a CNT weight content of 0.10 ; 0.25 ; 0.50 ; 0.75 and 1.00 wt.%.

This cycle was developed and optimized in order to give the best dispersion results. In parallel to this study, the percolation behavior of the nanocomposites was investigated in order to assess the carbon nanotubes state of dispersion in the polymer matrix (section 3.5).

3.3 Thermal Behavior - Cure Kinetics

The cure kinetics of both unfilled and 1.00 wt.% CNT-doped epoxy have been studied. This study focuses on these two concentrations (i.e. CNT weight percentages of 0 and 1.00 wt.%), as they represent the lower and upper limits of the CNT concentration domain investigated.

The polymerization of thermoset resin systems can be characterized by the recording of the residual enthalpy. Equation 3.1 correlates the heat flow dH/dt with the reaction rate dα/dt, where α is the degree of cure, H the enthalpy of the system and t the time.

$$\frac{d\alpha}{dt} = \frac{1}{\Delta H_{total}} \frac{dH}{dt} \tag{3.1}$$

For low reaction rates (long durations) the conversion rate can be determined via Equation 3.2. This method enables the calculation of a good approximation of the conversion rate.

$$\alpha_t = \frac{\Delta H_{total} - \Delta H_{residual}(t)}{\Delta H_{total}} \tag{3.2}$$

The process of the epoxy prepolymer and amine hardener reacting together to form the three-dimensional network can be as well characterized by an increase of the glass transition temperature. Equation 3.3a presents the relation between T_g and the polymerization rate proposed by DiBenedetto [110].

$$\frac{T_g - T_{g0}}{T_{g\infty} - T_{g0}} = \frac{\lambda\alpha}{1 - (1-\lambda)\alpha} \tag{3.3a}$$

$$\lambda = \frac{\Delta C_{p\infty}}{\Delta C_{p0}} \simeq \frac{T_{g0}}{T_{g\infty}} \tag{3.3b}$$

T_{g0} and $T_{g\infty}$ are the glass transition temperature of the uncured and fully cured epoxy resin (cured in this case: 2 hours at 180°C, as per recommendation of the resin manufacturer, as presented in 2.2 in chapter 2). This equation is based on the fact that

each chemical bond formed corresponds to one less chain-end and in that way increases the glass transition temperature.

In Equation 3.3b, ΔC_{p0} and $\Delta C_{p\infty}$ are the specific heat capacity step around T_g of the uncured and fully cured epoxy. $\Delta C_{pi} = (C_{pi})_l - (C_{pi})_g$ is the change in the isobaric heat capacity of the constituent ($i = 0\ or\ \infty$, either uncured or fully cured) between the liquid/amorphous and glassy states. Pascault and Williams [111] stated that λ should be considered as an adjustable parameter, but that its value could be approximated by the ratio between T_{g0} and $T_{g\infty}$, the product $\Delta C_p\,.\,T_g$ being approximately constant. It is shown in this paper that this estimate enables to predict, with reasonable accuracy this adjustable parameter. Figure 3.2 shows the general shape of the resulting curves (related to equations 3.3a and 3.3b). The relative increase of the glass transition temperature is greater at higher reaction extents, a fact that is consistent with the step increase in cross-linking density beyond the gel point. This explains why this approximation shows rough agreement with the experimental results. Six calorimetric runs were performed in order to determine T_{g0} and $T_{g\infty}$ for both neat and 1.00 wt.% CNT-doped epoxy. We obtained a value of $\lambda = 0.52 \pm 0.01$ for the neat resin and $\lambda = 0.53 \pm 0.01$ for the doped resin, which is coherent which values from the literature [111, 73].

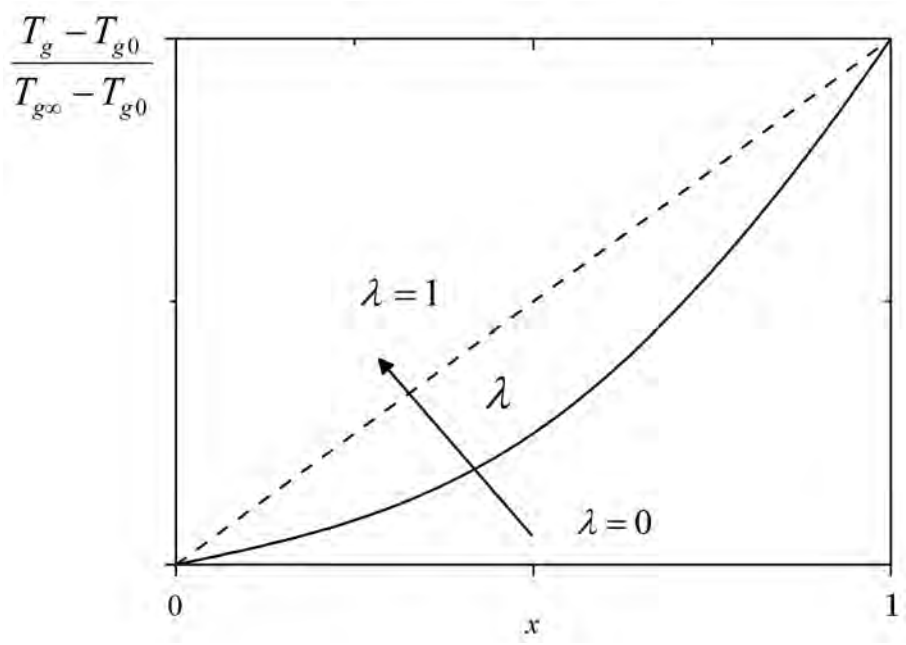

Figure 3.2 – Relationship between the glass transition temperature and the thermoset conversion for a λ value between 0 and 1 as presented by Pascault et al. [111]

First, temperature scanning measurements from -50°C to 320°C (with a heating rate of 5°C/min, under nitrogen atmosphere) have been performed in order to measure the total reaction enthalpy ΔH_{total} and the glass transition temperature of the uncured epoxy T_{g0}.

Secondly, different samples from both neat and 1.00 wt% doped epoxies were placed in an oven at isothermal conditions (60°C, 80°C and 100°C) for durations up to 175 hours. Those were selected in order to achieve the maximal curing rate for these temperatures (especially for T = 60°C).

Thirdly, temperature scanning measurements (-50°C to 320°C, with a heating rate of 5°C/min, under nitrogen atmosphere) were performed on small amounts of material sampled (3 mg) and placed in aluminum pans at regular time intervals to determine the residual enthalpy (ΔH_{total}) and glass transition temperature (T_g). Determining these two experimental parameters enabled the calculation of the conversion rate as a function of time through equation 3.2 and 3.3a.

In Figure 3.3, the thermograms obtained for various durations in isothermal conditions (60°C, 80°C and 100°C) are presented for both neat and 1.00 wt.% CNT-doped samples. A few graphs are overlayed representing durations from t=0 h to t=170 h (or 168 h respectively). Exothermal peaks can be observed for each sample analyzed. These are associated with the cross-linking level of the epoxy polymer. The peak area decreases as the time spent at the isothermal temperature increases. The area under these peaks corresponds to the residual enthalpy used to calculate the conversion rate (Equation 3.2). The results of these calculations are presented on Figure 3.5.

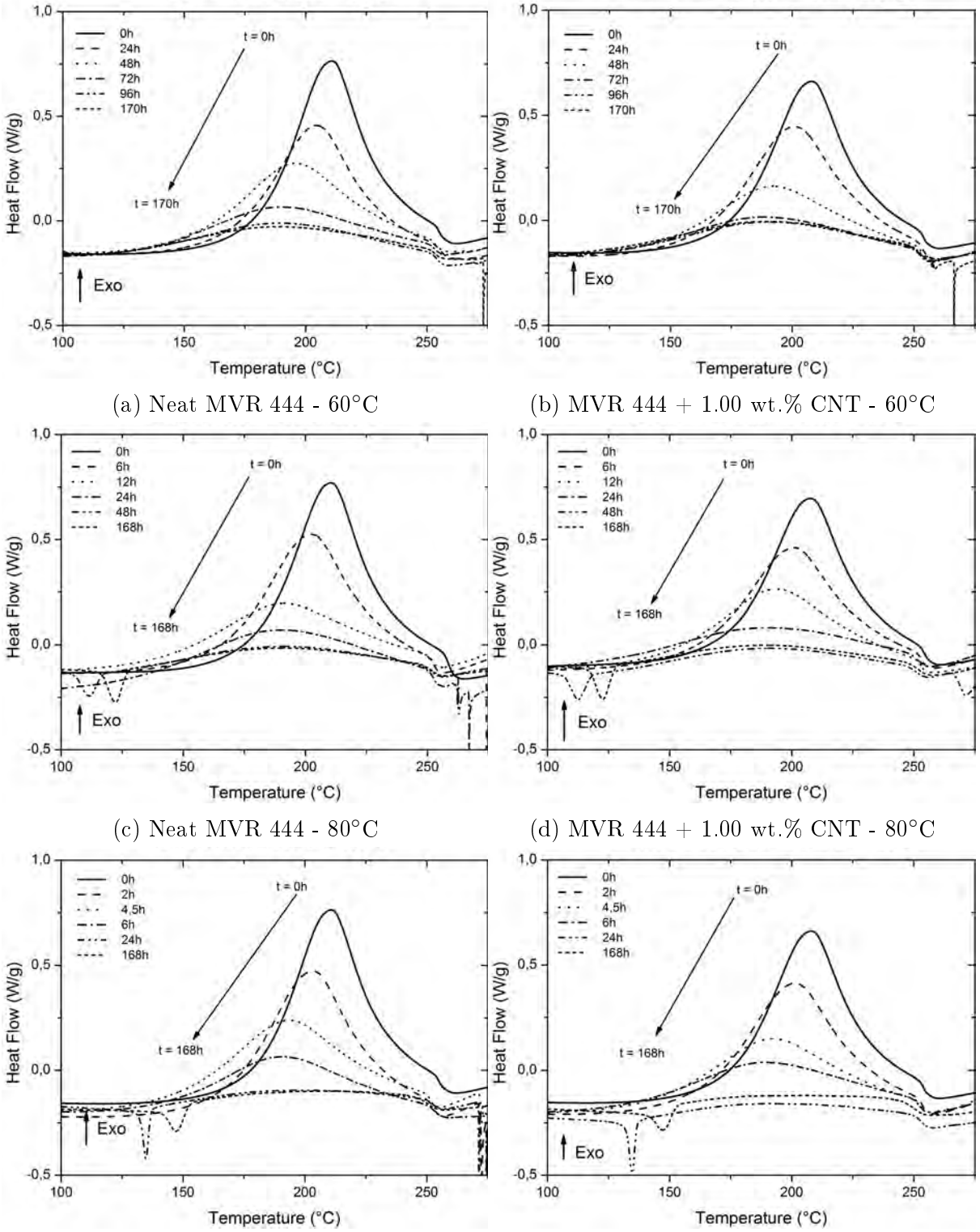

(a) Neat MVR 444 - 60°C

(b) MVR 444 + 1.00 wt.% CNT - 60°C

(c) Neat MVR 444 - 80°C

(d) MVR 444 + 1.00 wt.% CNT - 80°C

(e) Neat MVR 444 - 100°C

(f) MVR 444 + 1.00 wt.% CNT - 100°C

Figure 3.3 – Thermograms obtained for various durations in isothermal conditions (60°C, 80°C and 100°C) for both neat and 1.00 wt.% CNT-doped samples

The 3D cross-linking can, in the same way as with the residual enthalpy, be characterized by monitoring the changes in the glass transition temperature. Figure 3.4 shows the changes in T_g as a function of the time spent under isothermal conditions: at either 60°C, 80°C or 100°C, for both pristine and 1.00 wt.% CNT-doped epoxy. The boxed graphs inside the diagrams represents a zoom of the domain of interest.

On figure 3.4, two noticeable stages can be pointed out. First, for short times spent on the isotherm (i.e. up to 75h at 60°C, up to 25h at 80°C and up to 10h at 100 °C), we notice a strong and steady increase of T_g. This is directly related to the 3D cross-linking of the polymer. Indeed, in this first step, the amine and epoxy groups are free to react with on another. As the T_g continues to increase, it will eventually reach the point where it comes above the isothermal temperature ($T_g > T_{isotherm}$). We notice that as soon as it reaches this point, the increase in T_g is then slowed down. The polymer has then reached its vitrification state. In this state the molecular mobility is reduced and the chemical reactions are limited by the diffusion of the chemical species, which translates to a slower increase of the glass transition temperature. The results indicate a very similar curing behavior to other epoxy amine systems [39, 73, 112, 113]. Furthermore, we noticed that the CNT-doped dispersions show a slightly accelerated increase in T_g as far as the lowest curing temperature is concerned (60°C).

Figure 3.5 presents the conversion rate (α) obtained through the residual enthalpy ($\circ$ symbol on the graphs), and the monitoring of T_g ($\square$ symbol), for neat and 1.00 wt.% CNT-doped epoxy at 60°C, 80°C and 100°C isotherms. The boxed graphs inside the diagrams represent a zoom of the domain of interest.

We first notice that for medium to high conversion rates (above 0.3) both methods give coherent results. For low conversion rates (below 0.3), it seems that the monitoring of the T_g gives more reliable results than the recording of the residual enthalpy, particularly in the case of the neat resin at 60°C. On the diagrams, these results were fitted using a least-square fitting method (plain line for T_g and dashed line for $\Delta H_{residual}$). A comparison to an existing model can be found later in this work.

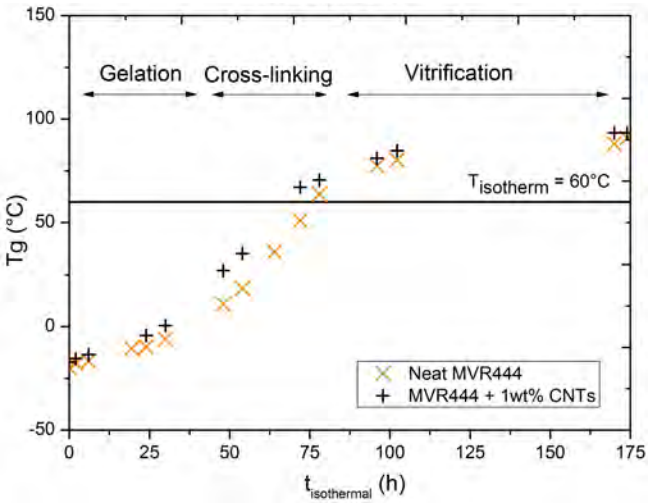

(a) Isotherm 60°C

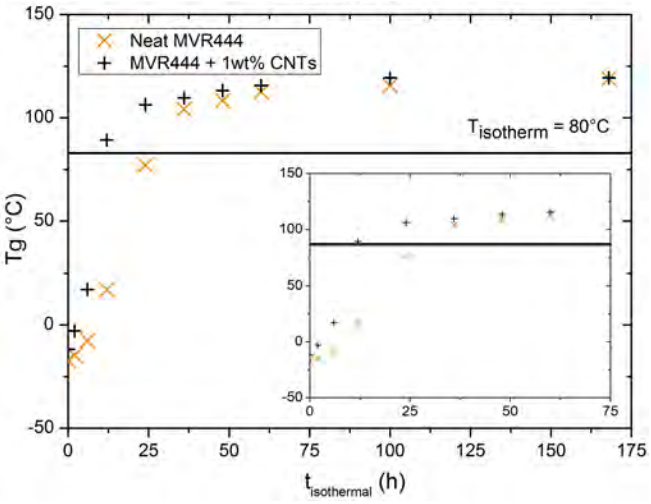

(b) Isotherm 80°C

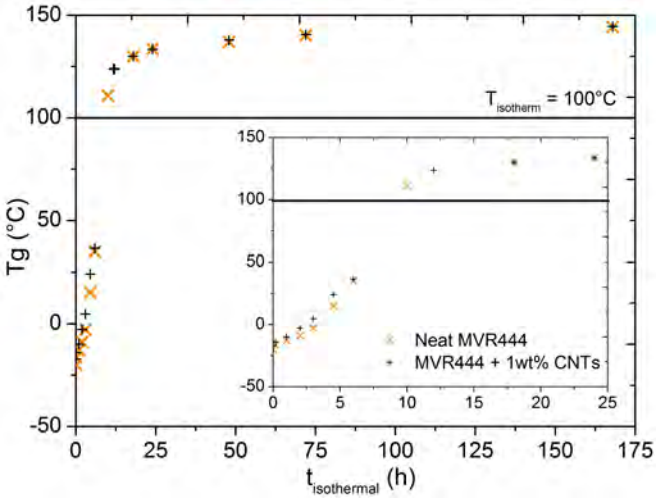

(c) Isotherm 100°C

Figure 3.4 – Glass transition temperature as a function of isothermal curing time (60°C, 80°C and 100°C) for both neat and 1.00 wt.% CNT-doped samples

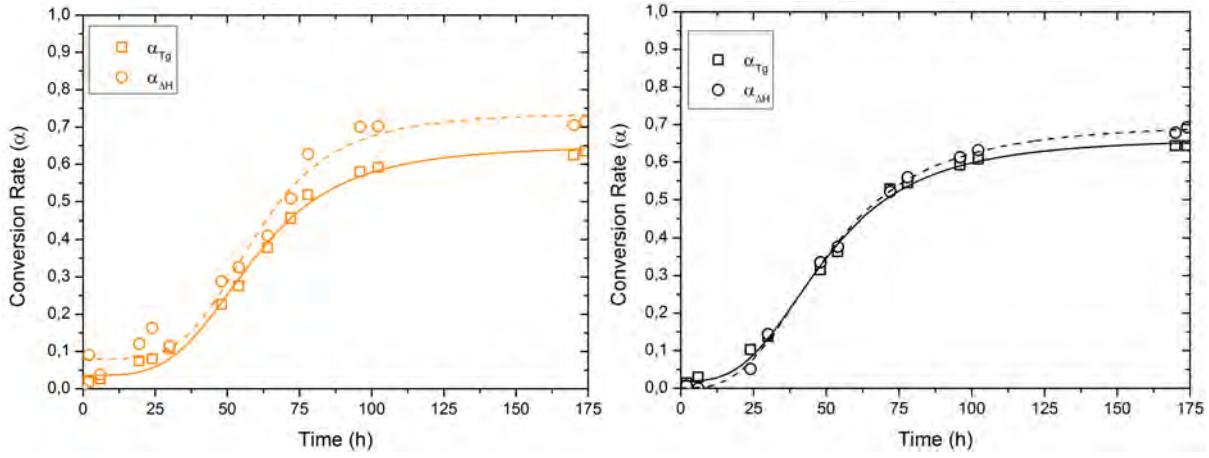

(a) Neat MVR 444 - 60°C

(b) MVR 444 + 1.00 wt.% CNT - 60°C

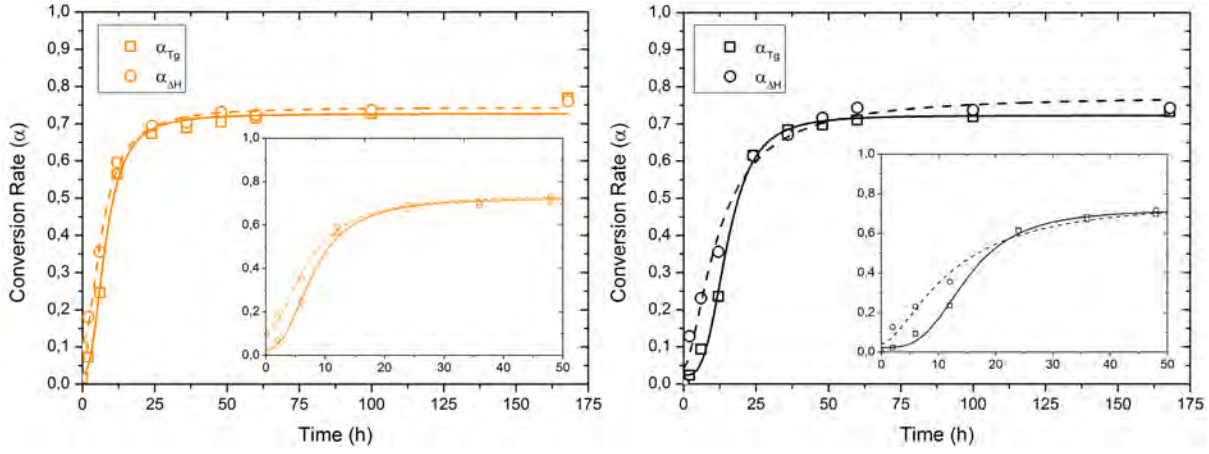

(c) Neat MVR 444 - 80°C

(d) MVR 444 + 1.00 wt.% CNT - 80°C

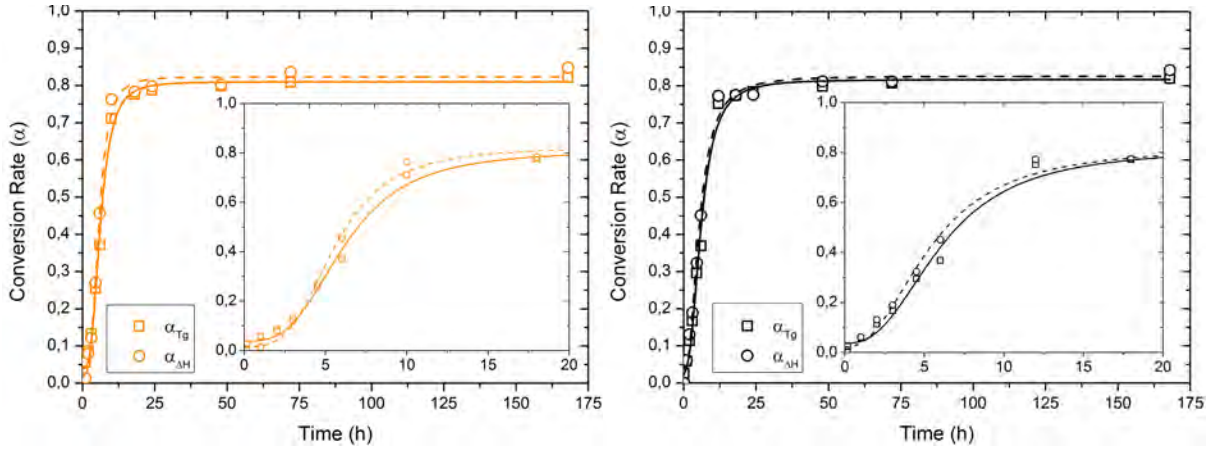

(e) Neat MVR 444 - 100°C

(f) MVR 444 + 1.00 wt.% CNT - 100°C

Figure 3.5 – Conversion rate as a function of polymerization time in isothermal conditions (60°C, 80°C and 100°C) for both neat and 1.00 wt.% CNT-doped samples

We notice a good agreement between results obtained following the two methods. The results obtained using the recording of $\Delta H_{residual}$ are coherent with those determined using T_g monitoring. They both exhibit the same two-stage behavior mentioned in the previous paragraph. In addition to the previous comments, we observed a non-linear increase of the conversion rate. First increasing slowly for the first part (gelation phenomenon), then achieving the highest reaction rates before T_g reaches the isothermal curing temperature at which point the reaction rate decrease to very low values (the conversion rate reaches its asymptotic value), the reaction being limited by the diffusion of the chemical species due to the vitrification of the polymer). It finally stabilizes to a plateau, a final maximal degree of cure being reached ($\alpha_{max,60°C} = 0.65$, $\alpha_{max,80°C} = 0.75$ and $\alpha_{max,100°C} = 0.80$).

Even though the MWCNTs used are chemically inert (no chemical functionalization), it can be expected that the thermal conductivity of the epoxy matrix is increased by the presence of MWCNTs. Indeed and for instance, a 1 vol. % CNT / epoxy nanocomposite (i.e 0.10 wt.% CNT, with $\rho_{MWCNT} = 0.10\ g.cm^{-3}$ and $\rho_{epoxy\ ,\ uncured} = 1.11\ g.cm^{-3}$) more than doubles the thermal conductivity of the base polymer [114]. This increase in thermal conductivity could lead to a faster polymerization when the resin is doped with CNTs [115, 116]. It was noticed experimentally that, for the lowest investigated curing temperature (60°C) and at a given time, the CNT-doped dispersion exhibit a slightly higher degree of cure compared to the pristine MVR 444. At 80°C and 100°C, the changes in the degree of cure are similar for both materials, no influence of the MWCNTs could be noticed.

From figure 3.5, we can also deduce the time available to process the resin without interfering with its chemical state. At 60°C this processing window has a duration of 20 h, at 80°C of 5 h and at 100°C of 2 h. It is essential to perform the rheological analysis inside this window in order to only observe molecular mobility induced phenomena and no chemically induced one such as gelation or vitrification.

The cure kinetics of epoxy resins can be modeled by a few catalytic and autocatalytic models. The cure kinetics model developed by M.R. Kamal and S. Sourour [117, 118] is based upon both catalytic and autocatalytic mechanisms, and is the most widely used in the literature for epoxy systems [112]. This model was therefore chosen in order to model

the curing kinetics of the MVR 444. It is expressed by equation 3.4

$$\frac{d\alpha}{dt} = (k_1 + k_2\alpha^m)(1-\alpha)^n \tag{3.4}$$

In equation 3.4 α is the degree of cure, $d\alpha/dt$ the curing rate. k_1 is the parameter describing the rate constant of the reaction with the partial order m and k_2 is the parameter corresponding to the autocatalytic reaction with the partial order n. In our study, the four parameters of the Kamal and Sourour model have to be determined: m, n, k_1 and k_2. The reaction rate constants k_i are thermally activated and described by an Arrhenius equation (Equation 3.5).

$$k_i(T) = A_i exp(-\frac{E_i}{RT}) \tag{3.5}$$

In equation 3.5, E_i is the activation energy and A_i is a pre-exponential factor.

As indicated by equation 3.4, the consistency with the Kamal and Sourour model can be observed by plotting the reaction rate $d\alpha/dt$ as a function of the degree of polymerization α. A non-linear regression of these two series of data is subsequently performed. These results are presented on Figure 3.6. A least-square fitting algorithm using the Kamal-Sourour equation was used on these sets of data. The identification was performed for each isothermal curing.

We observed that the Kamal-Sourour equation fits the experimental data very well. The four parameters of the model determined using this method are summarized in table 3.2. The reaction orders of the m and n are in good agreement with the literature concerning epoxies [119, 58]. We notice that these orders of the curing reaction are not influenced by the curing temperature nor by the addition of CNTs.

Table 3.2 reveals that the value of k_2 steadily increases as the temperature rises. The reaction rate constant k_2 (corresponding to the partial order n) is associated with the autocatalytic reaction of the secondary amine with another epoxy group to form a tertiary amine. Looking at the values of k_2, it can therefore be assumed that this second reaction is thermally activated. Furthermore, for the same temperature similar values of k_2 were obtained, excluding a possible influence of the CNTs on this parameter.

If we now turn to k_1 which is the parameter describing the rate constant of the

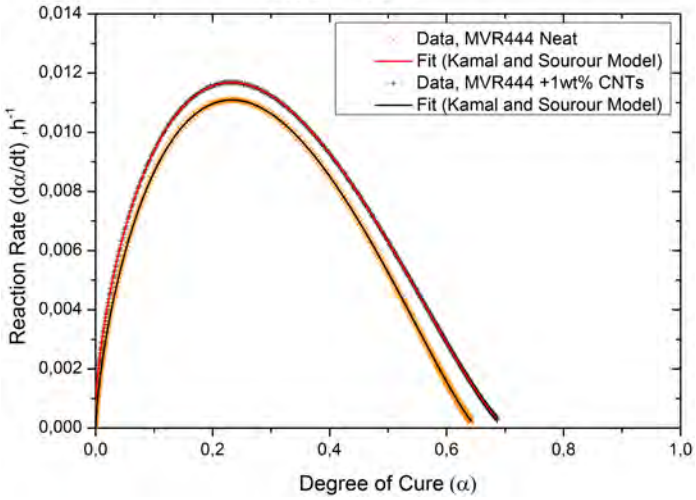

(a) Isotherm 60°C

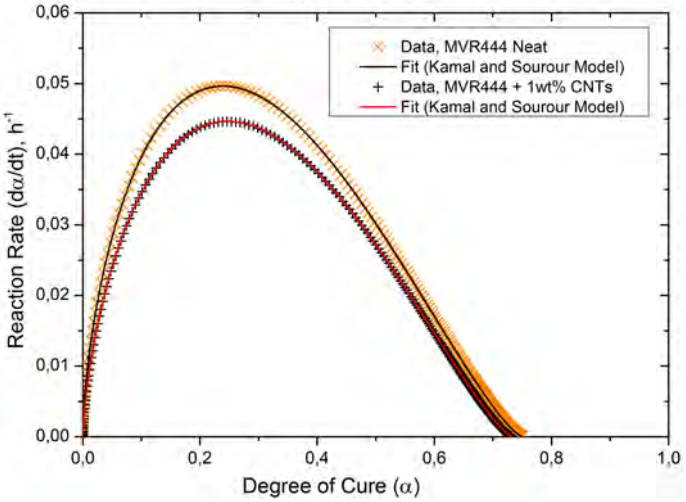

(b) Isotherm 80°C

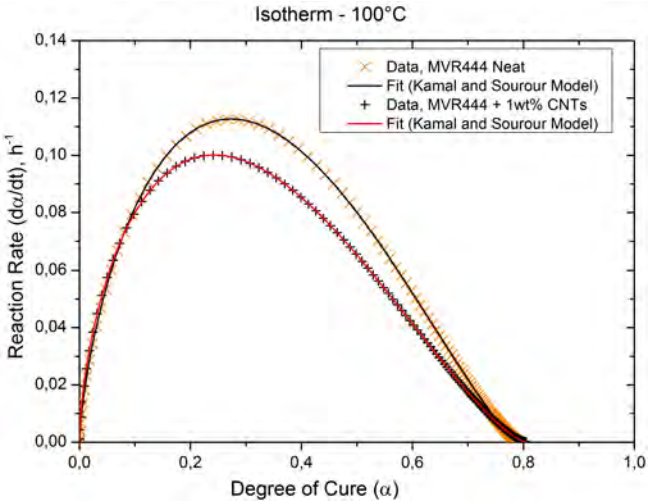

(c) Isotherm 100°C

Figure 3.6 – Reaction rate $d\alpha/dt$ as a function of the degree of cure α

Temperature	Sample	m	n	k_1	k_2
60°C	Neat	0.71	1.28	$2.20.10^{-6}$	$9.43.10^{-2}$
	1 wt.% CNT	0.70	1.36	$1.24.10^{-3}$	$8.57.10^{-2}$
80°C	Neat	0.63	1.35	$1.05.10^{-4}$	$3.03.10^{-1}$
	1 wt.% CNT	0.67	1.31	$1.00.10^{-4}$	$2.94.10^{-1}$
100°C	Neat	0.70	1.34	$1.00.10^{-18}$	$6.72.10^{-1}$
	1 wt.% CNT	0.62	1.43	$1.00.10^{-18}$	$5.49.10^{-1}$

Table 3.2 – Cure kinetics parameters for neat and 1 wt.% doped MVR 444

reaction with the partial order m, the results of this study did not show any significant trend related to the temperature behavior. It can nevertheless be noticed that for the curing at 100°C, k_1 is almost equal to zero for both neat and CNT-doped epoxy. This means that the associated reaction (the reaction of an epoxide with a primary amine producing a secondary amine) is discriminated compared to the reaction represented by k_2 (with the partial order n). Interestingly, we notice that at 60°C, k_1 is increased by the addition of CNTs confirming their acceleration effect on the curing kinetics at this temperature, having an acceleration effect on this first reaction only, as no effect of the nanotubes on k_2 could be noticed.

3.4 Rheological Behavior - Influence of the MWCNTs

In this section, the rheological behavior of the uncured epoxy is studied at three temperatures inside the processing range of the spray gun (60°C, 80°C and 100°C) both for pristine and CNT-modified resin. The duration of the tests does not exceed the time intervals determined in the previous sections. The testing duration has been limited to 1h, remaining far from the 2h gelation-free window in the case of an isotherm at the maximal temperature of 100°C. It can be therefore assumed that $d\alpha/dt \approx 0$ (and $\alpha = 0$) during the measurement. After defining the domain of linear response, the influence of the temperature and MWCNTs on the shear viscosity will be presented.

3.4.1 Determination of the Linear Response Domain

First of all, the linear response domain of the material as a function of the applied strain had to be experimentally determined for each temperature considered. In order to do so, strain sweeps were performed at the above mentioned isothermal temperatures in a range of strains from 10^{-2} to 8.10^2 %. These measurements were performed each time for a few selected shearing frequencies: 10^{-2}; 5.10^{-2}; 10^{-1}; 1; 10; 80 Hz. It was chosen to record only the torsional moment (Torque) as this is the only raw data not being processed by the rheometer software. The aim was here to determine the frequency and strain domains, for which the material exhibits a linear response to the stress applied: i.e. a requirement to define the complex viscosity $\eta^*(\omega)$. As for the thermal analysis we chose to focus on the lower and upper limits of the CNT concentration domain (pristine epoxy and 1.00 wt.% CNT doped epoxy.

Figure 3.7 shows the strain sweeps (from 10^{-2} up to 8.10^2 % strain) performed at the selected isothermal temperatures, each time for the selected shearing frequencies. The vertical dashed lines are reading guides representing the two strain levels later considered: 10 % and 100 %.

It can be noticed that for each given frequency and temperature, the torsional moment increases with the increase in frequency. It can be noticed as well, that the torsional

moment decreases with increasing temperature for both neat and CNT-doped epoxy. Indeed in the range of temperature considered (60°C - 100°C), the viscosity decreases with the increase of temperature. The rheological behavior as a function of the applied strain can be divided in two parts. For the lower strain levels (low torsional moments measured), the response of the material is erratic and does not follow any linear trend. On the other hand, as soon as a critical strain level is achieved, the material follows a linear trend, characterizing the linear response of the material.

The determination of the linear response domain can be done via a detailed analysis of figure 3.7.

For the undoped epoxy resin (Figures 3.7a, 3.7c and 3.7e), and for values above the critical strain rate above-mentioned, the torque increases following a linear trend with increasing frequencies (straight line with constant slope). Therefore, the material presents a linear response for the shearing frequencies from 5.10^{-2} to 80 Hz for both 10 % and 100 % strain and for all three isothermal temperatures.

For the 1.00 wt.% doped resin, two cases have to be distinguished. First, at 60°C (Figure 3.7b), the doped polymer exhibits the same type of response as observed for the neat resin. Here again, the material presents a linear response for the shearing frequencies from 5.10^{-2} to 80 Hz for both 10 % and 100 % strain and for all three isotherms considered. However, when testing at 80°C (Figure 3.7d) and 100°C (Figure 3.7f), a different behavior is observed. For low shearing frequencies (80°C: 10^{-2} to 1 Hz; 100°C: 10^{-2} to 10 Hz), experimental points are not aligned and cannot be interpolated (with respect to strain level) by a linear function. A change in its slope and a curved form of the graphs with CNTs is observed. We are in the case of a non-linear response of the material. This non-linear response observed can be a manifestation of either the heterogeneity of the material or an homogeneous material but exhibiting a complex mechanical response. In any case, as having a linear response of the material is required in order to define the viscosity function η^*, one can only determine and represent $\eta^{'}$ for temperatures and shear rates where a linear response is observed.

For the second part of the study, it has been decided to work inside the linear response domain by choosing not to investigate the behavior at 100% strain and 100°C (all other temperature and strain combinations being inside the linear domain).

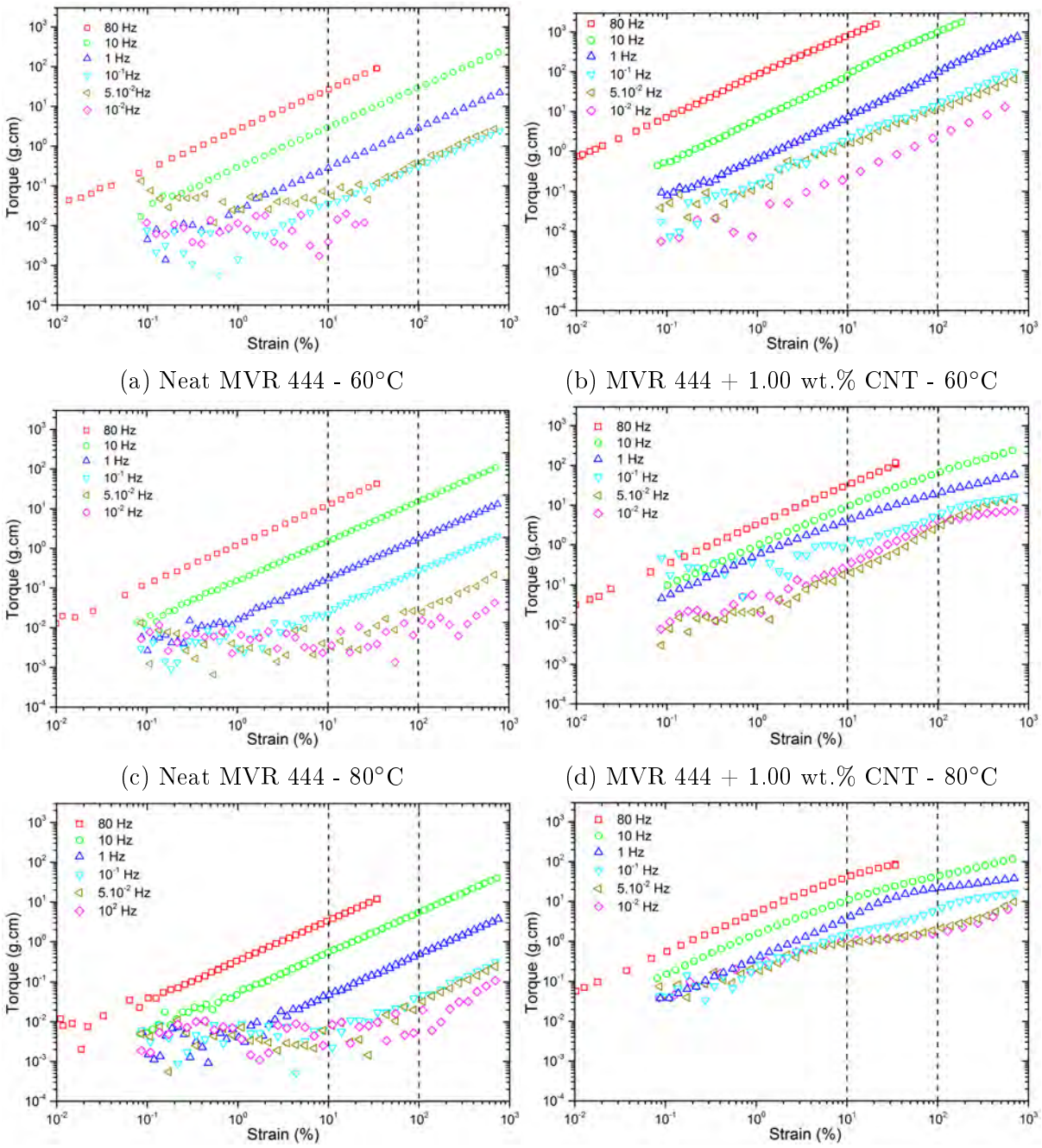

(a) Neat MVR 444 - 60°C

(b) MVR 444 + 1.00 wt.% CNT - 60°C

(c) Neat MVR 444 - 80°C

(d) MVR 444 + 1.00 wt.% CNT - 80°C

(e) Neat MVR 444 - 100°C

(f) MVR 444 + 1.00 wt.% CNT - 100°C

Figure 3.7 – Torsonial moment as a function of the applied strain

3.4.2 Rheological Behavior as a Function of Shear Frequency

In a second time, the rheological behavior was investigated as a function of the shear frequency. Frequency sweeps were performed at the three selected isothermal temperatures for the selected strains and frequency domain, determined to ensure a measurement inside the linear response domain of the material (section 3.4.1). In this second part, all the CNT content range (from 0 to 1.00 wt.%) was investigated. On figures 3.8 and 3.9 is presented the real part of the complex viscosity $\eta^{'}$ as a function of the shearing frequency f. The graph representing the frequency sweep at 100 % strain and 100°C is not presented on figure 3.9 as the 1.00 wt.% doped epoxy does not exhibit a linear response to the strain applied as presented in figure 3.7.

From figures 3.8 and 3.9 it can be noticed that the behavior observed is different depending on the testing temperature. At 60°C and for CNT contents ranging from 0 to 0.75 wt.% (figures 3.8a and 3.9a) the polymer exhibits a Newtonian or quasi-Newtonian behavior, as the value of the real part of the complex viscosity remains almost the same for all the range of frequencies investigated. Only the epoxy dispersion containing 1.00 wt.% CNTs undergoes a decrease in the $\eta^{'}$ value with increasing frequency, characterizing a shear-thinning behavior. At 80°C, a different trend can be noticed. For CNT weight fractions from 0 to 0.25 wt.% the behavior is still Newtonian as at 60°C, though for higher CNT contents the shear-thinning behavior is more pronounced. Indeed the shear-thinning effect is already present from 0.50 wt.% and up to 1.00 wt.%. As for T = 60°C, the value of the strain applied does not seem to influence the results obtained. At last for the results at T = 100°C, the same Newtonian behavior is observed for concentrations from 0 to 0.25 wt.% CNTs and shear-thinning behavior from 0.50 wt.% to 1.00 wt.%. Although the same shear-thinning behavior is observed here, the trend followed by the shape of the curve is different compared to the one observed at 80°C. A deviation in the decreasing trend is observed as a sort of "bump" appears along the graph. When comparing the experiments for strains of 10% (figures 3.8a, 3.8b and 3.8c) and 100% (figures 3.9a and 3.9b), we notice that the value of the strain applied does not influence the results obtained (almost stackable curves).

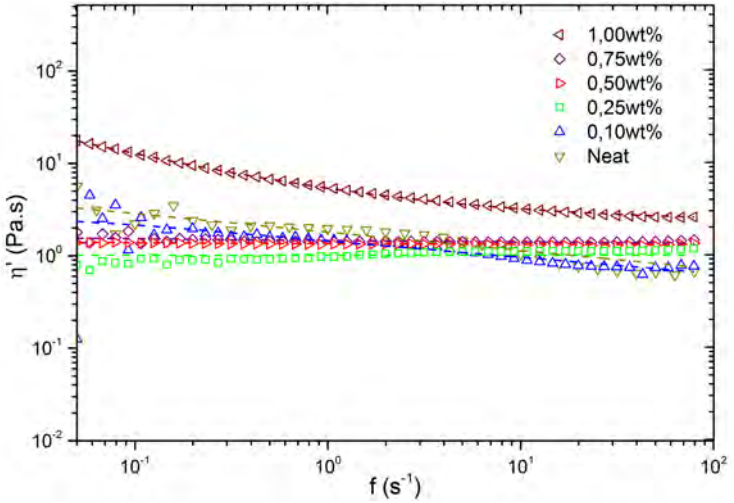

(a) Strain = 10% ; T = 60°C

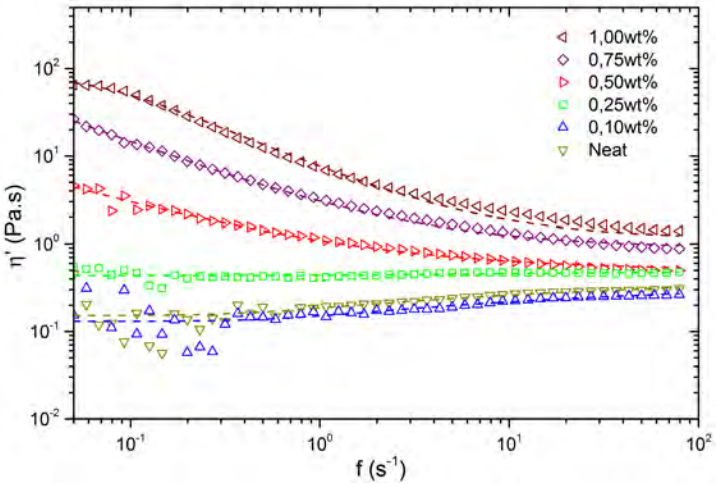

(b) Strain = 10% ; T = 80°C

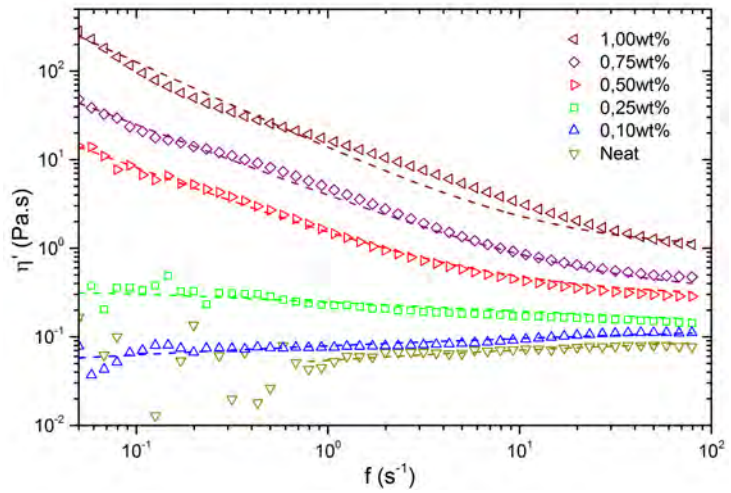

(c) Strain = 10% ; T = 100°C

Figure 3.8 – Logarithmic frequency sweeps for neat and CNT doped epoxy at 10% strain

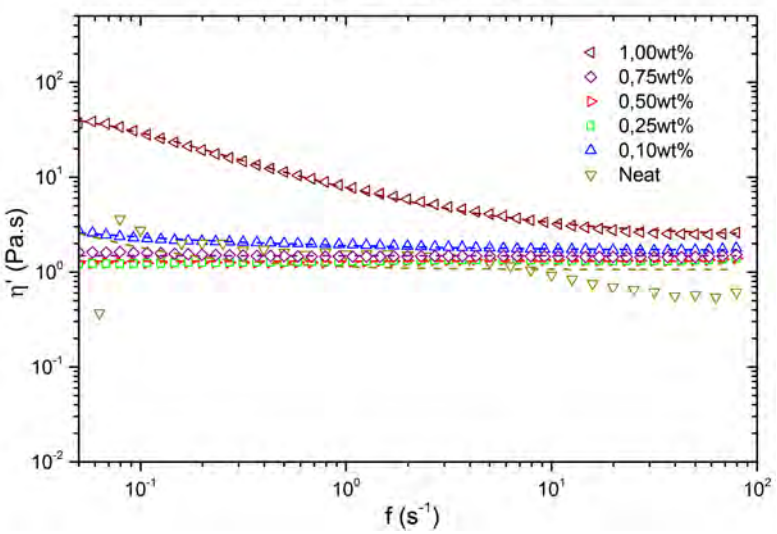

(a) Strain = 100% ; T = 60°C

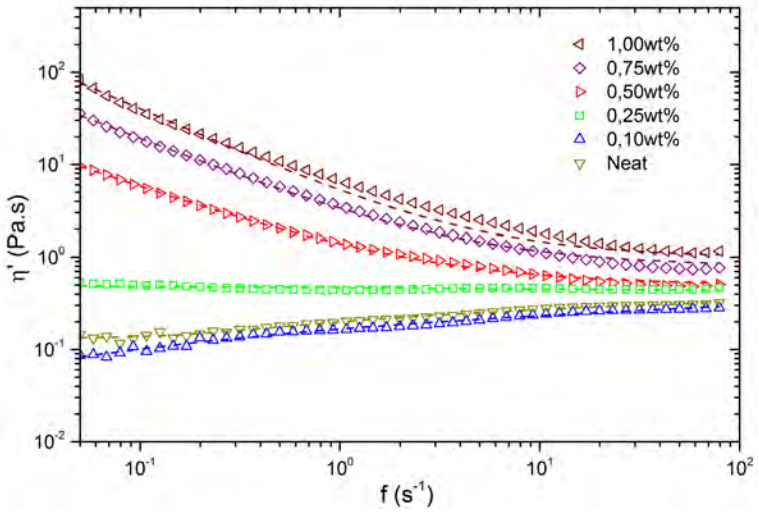

(b) Strain = 100% ; T = 80°C

Figure 3.9 – Logarithmic frequency sweeps for neat and CNT doped epoxy at 100% strain

To further investigate this shear-thinning behavior, the Carreau-Yasuda rheological model [120, 121] (equation 3.6) was used to fit the obtained experimental results.

$$\frac{\eta - \eta_0}{\eta_0 - \eta_\infty} = (1 + (\tau f^2))^{\frac{n-1}{2}} \tag{3.6}$$

In equation 3.6, η_0 and η_∞ are respectively the viscosity values at very low and very high shearing rates, n is the shear-thinning index, characterizing the degree of shear-thinning compared to a Newtonian behavior (where $n = 1$), and τ is a characteristic time of the shear-thinning behavior. For all temperatures and strain values studied, the data was fitted with this equation (dashed lines on figures 3.8 and 3.9). In most cases a very good correlation of the experimental values with the Carreau-Yasuda model is obtained. Only the experimental results at 100°C and 10 % strain seem to deviate from the theoretical model for the epoxy doped with 0.75 wt.% and 1.00 wt.% CNTs. For these two dispersions, as mentioned in the previous paragraph, a small "bump" can be noticed along the graph, where the experimental results deviate from the model.

When examining the zero shear viscosity (i.e. the viscosity at low shearing rates η_0) of the MWCNT doped epoxy on figures 3.8 and 3.9, a temperature and CNT amount dependency can be noticed. In order to make easier the investigation of this parameter, figure 3.10a presents the evolution of η_0 as a function of the temperature (the dashed lines represent the linear trends followed by the experimental data). The zero shear viscosity η_0 seems to follow a different trends whether the CNT amount is below or above a critical loading (between 0.25 and 0.50 wt.%). It shows a linear dependency of η_0 with the temperature T, however two different trends have been noticed. On one hand, for CNT concentrations from 0 to 0.25 wt.%, η_0 decreases linearly while the temperature increases. On the other hand, for CNT concentrations higher or equal to 0.50 wt.%, η_0 increases while the temperature increases. This is well highlighted in figure 3.10b which presents the slopes of the linear regressions performed on the data presented in figure 3.10a, as a function of the CNT weight percentage. A doted line reminds of the position of the electrical percolation threshold at 0.25 wt.% CNT. On this graph, a jump in the slopes values can be observed above a certain threshold, this jump is marked by the dashed lines which serve as guide for the eye.

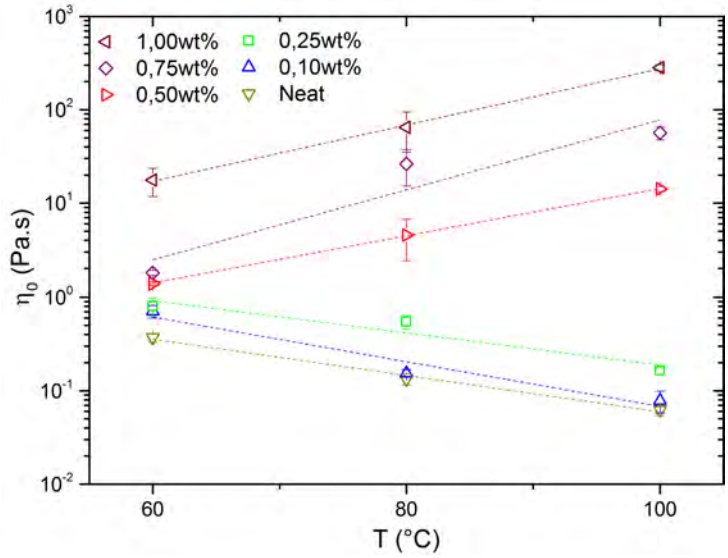

(a) Influence of the temperature on the viscosity at low shearing rates η_0

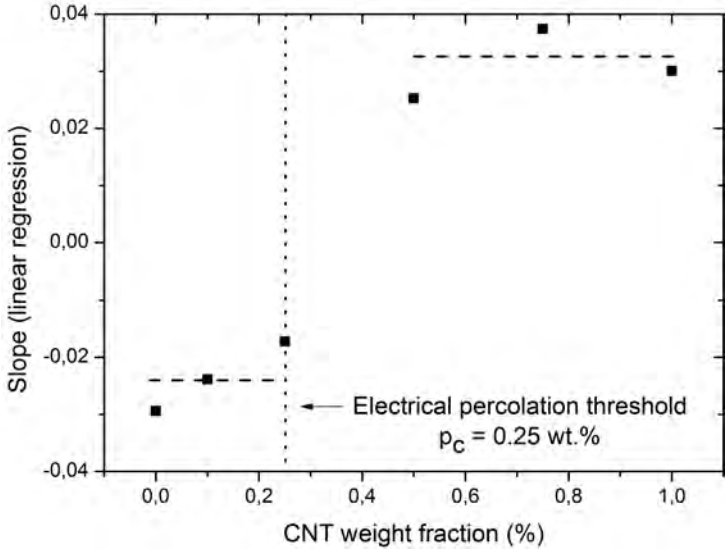

(b) Slopes of the linear regression of η=f(T) data

Figure 3.10 – Mechanical characterization of the electrical percolation phenomenon

Earlier works [122, 123, 124, 125, 126] have reported that the viscoelastic properties observed are strongly dependent on the dispersion state and interactions of the nanofillers inside the polymer matrix. Pötschke and McClory [122, 124] suggested that the rheological behavior can be used in order to identify the electrical percolation threshold of CNT / polycarbonate composites. They observed that the resistivity threshold occurred in the same concentration range as the increase in melt viscosity found at low frequencies. Starting from a CNT loading of 2 wt.%, the frequency dependence of the viscosity curves changed significantly and a step increase in viscosity was observed at low frequencies. In

this study the electrical percolation threshold was found at 2 wt.% as well. Furthermore, Sumfleth et al. [125] also discussed the different percolation phenomena found in the electrical behavior of the cured epoxy/CNT nanocomposites as well as in the rheological properties of the CNT-filled suspensions. This comparison gave a comprehensive insight in the network forming process. The electrical percolation threshold of the cured samples was found to occur at lower CNT content than the jump in storage modulus values of the uncured suspension (one order of magnitude: 0.025 vs. 0.2 wt.%). This was linked to the re-agglomeration process occurring during curing, which is usually promoted by high-shear forces and elevated temperature.

Based on figure 3.10a and these observations from the relevant literature, we presume that there might be a relation between the formation of the electrical percolation network and the mechanical behavior of the CNT / epoxy suspension. In the uncured suspension, polymer chain interactions might be found (although negligible), the introduced CNT-monomer interaction and especially CNT-CNT interactions dominate and are responsible for the increase of η at low shear rates [122]. With the increase in nanofiller loading, an inter-connected network structure is formed above a critical particle loading, this dense network prevents polymer chain and monomer mobility which might be the explanation of the increase in zero-shear viscosity with temperature (figure 3.10a). On the other hand, below this critical particle loading, increasing temperature decreases the zero-shear viscosity as the thermal agitation promotes monomer mobility in an environment where they are free to move (no CNT network obstruction). At last, in this study, a lower percolation onset in suspension could not be observed, as in Sumfleth et al. [125], which might be a manifestation of a re-agglomeration process occurring in the uncured suspensions at high CNT contents and temperature.

3.4.3 Influence of the Spraying Process on the Rheological Properties of the MWCNTs/Epoxy Suspension

In complement of the investigations performed previously, where the rheological behavior before performing the spray process was analyzed, this section evaluates the influence of the spraying process on the rheological properties of the MWCNTs / epoxy dispersion. The spray process (which will be presented in detail in chapter 4) submits the sprayed material to high shear forces when operating. A short review of the literature available showed that shear levels of $10^3 - 10^4\ s^{-1}$ may be reached [127, 128]. This is why it is important to analyze such an effect on the CNT / epoxy dispersion.

In order to evaluate the influence of the spray process on the viscosity, the spray deposition technique was used in the same way and with the same parameters presented in section 4.2.2. The spray gun was used to deposit the adequate amount of material (5 g) directly inside the cup part of the Couette setup (see also figure 2.10). Before proceeding to the rheological analysis, the curing degree of the samples was determined via calorimetry and reached $\alpha = 0.06 \pm 0.01$. In section 3.3, it was shown, through measurements performed after the calendering process (and thus before spraying) that the degree of cure after this step reached $\alpha = 0.03 \pm 0.01$. These two measurements indicate that the spray process has a slight influence on the curing degree of the sprayed material. Thanks to the analysis of the cure kinetics performed previously and summarized in figure 3.5, it can be noted that the samples are then on the beginning of the gelation step, which starts around curing degrees of approximately 0.10 .

After spraying into the Couette setup, the samples were stored under nitrogen atmosphere in polyethylene sealed bags before being conserved at -18°C. It was found that without nitrogen atmosphere storage, the water pick-up was too important and led to non-reliable measurements. In the same way as previously, frequency sweeps were performed at two selected isothermal temperatures (60°C and 100°C, as they represent the limits of the investigated domain), for a strain of 10 % and frequencies from 5.10^{-2} to 80 Hz (to remain inside the linear response domain) on pristine and 0.75 wt.% doped epoxy samples (as they are the two types of materials having been sprayed).

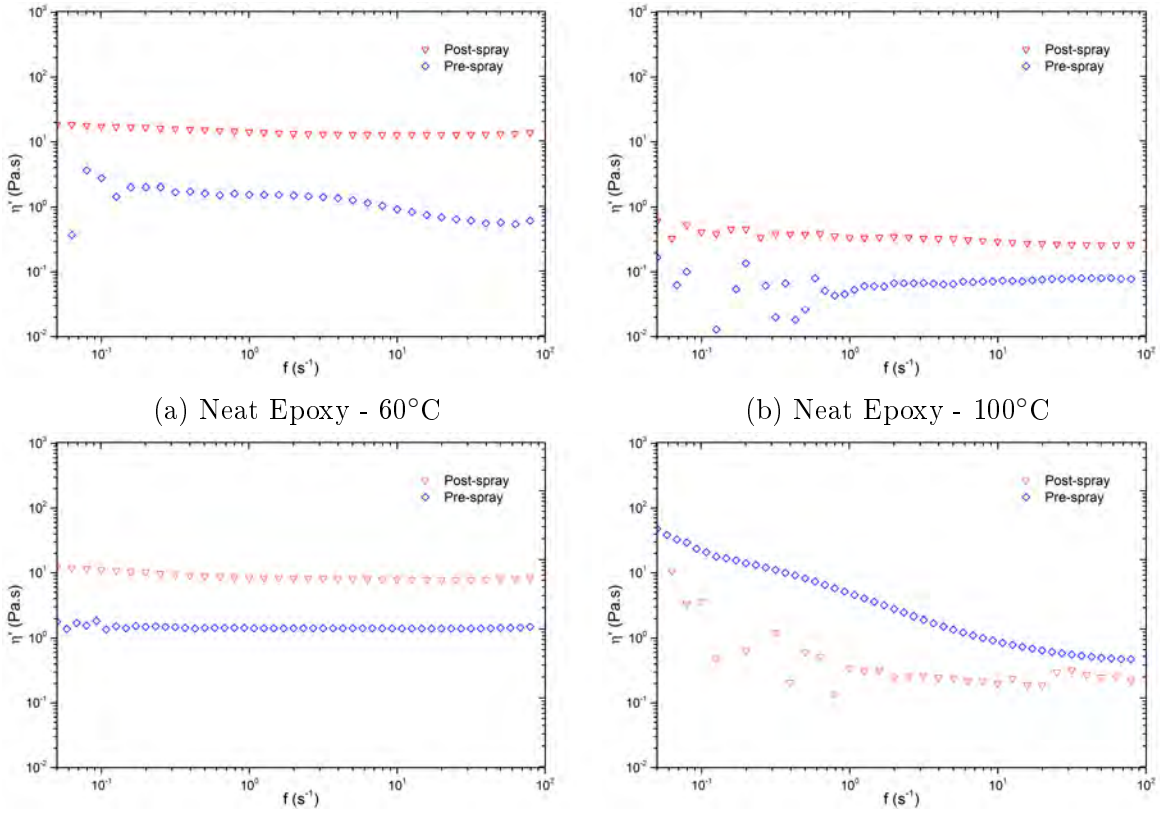

(a) Neat Epoxy - 60°C

(b) Neat Epoxy - 100°C

(c) 0.75 wt.% doped Epoxy - 60°C

(d) 0.75 wt.% doped Epoxy - 100°C

Figure 3.11 – Influence of the spraying process on the rheological properties

Figure 3.11 presents the results of these measurements. On these graphs, the real part of the complex viscosity is presented for the range of frequency, the two materials and temperatures investigated. Both pre- and post-spray values are reported on the same graphs for comparison. Pre-spray values are taken from the measurements performed in section 3.4.2.

Figure 3.11a and 3.11b present the frequency sweeps for the pristine epoxy. As it can be seen, the post-spray samples (downward facing red triangles) at both 60°C and 100°C exhibit a newtonian behavior, similarly to the pre-spray samples (blue diamond-shaped symbols). It can also be noticed that the η' values are one order of magnitude higher in comparison to the pre-spray values. This can be attributed to the higher polymerization degree, the samples being in an early gelation state and thus exhibiting a higher viscosity value.

On figure 3.11c, it can be seen that at 60°C, the 0.75 wt.% doped sample presents a newtonian behavior as well, in accordance with the pre-spray experiments where a

similar behavior was reported. Likewise, an increase in viscosity values by one order of magnitude was noticed. This increase can, as for the undoped samples, be attributed to the increase in curing degree.

On figure 3.11d, it can be observed that, at 100°C, the 0.75 wt.% doped samples exhibit a different behavior. Analogously to the pre-sprayed samples, these samples exhibited a shear thinning behavior, with a viscosity decreasing with increasing shearing frequency. However, it was found for this particular type of material, that the post-spray η' values where slightly lower than the pre-spray values. This could be explained by a better dispersion of the nanoparticules by the spray gun leading to lower viscosity values. Additional experiments have to be performed to improve the understanding of this phenomenon.

3.4.4 Thermorheological Behavior

A thermorheological analysis of the CNT-doped suspensions was performed. It was chosen to submit the samples to a linear temperature ramp of 2 K.min^{-1} from room temperature to 150°C (to avoid curing of the polymer in the Couette setup). A frequency of 1 Hz and a strain of 100 % were chosen.

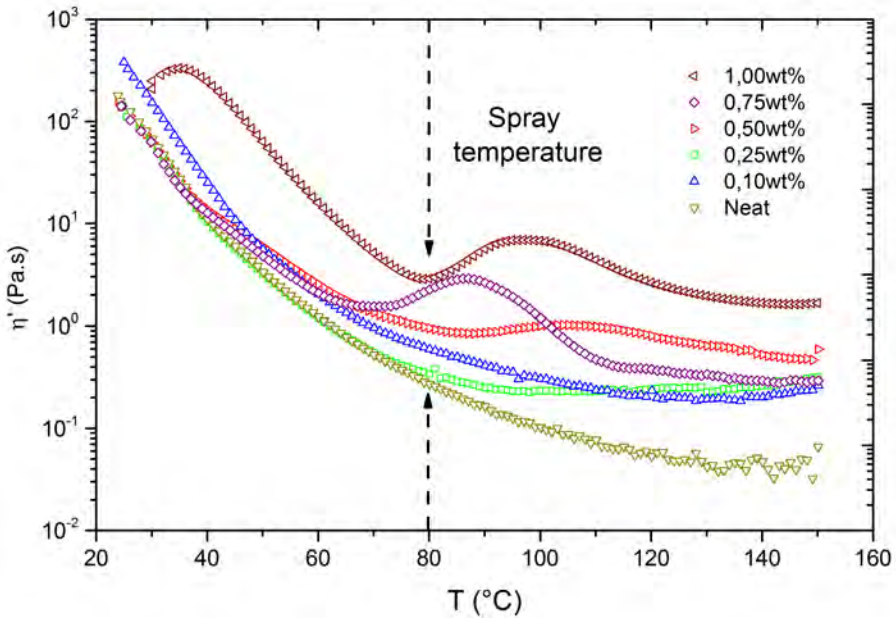

Figure 3.12 – Linear temperature sweeps for neat and CNT-doped MVR444

Figure 3.12 presents the results of these ramps for both pristine and CNT-doped epoxy

(up to 1wt.% CNT). It can be first noted, that the increase in temperature has a thinning effect on all samples (neat and CNT-doped). As seen previously on the frequencies sweeps, it can here also be noted that the CNT-doped suspension exhibit a higher viscosity. This effect is particularly noticeable at high temperature: at 140°C an important viscosity gradient $\Delta\eta$ can be observed between the different CNT value fractions. Furthermore we notice that this gradient increase with increasing temperature.

A second interesting phenomenon can be noted on this graph. It was noticed that for the 0.5, 0.75, and 1 wt.% suspension, a "bump" can be noted along the graph (in the range of 90 to 120°C for 0.50 wt.% CNT, 70 to 110°C for 0.75 wt.% and 80 to 120°C for 1.00 wt.% CNT). Further experiments were performed to analyze this behavior and suggest a plausible explanation. It was first thought, that this effect might be due to a change in the chemical composition (rupture of the isochemical state) of the sample. This hypothesis was ruled out by performing the same temperature ramp on a sample submitted to differential thermal analysis and noticing that no significant change in the conversion rate could be observed. It was in a second time assumed, that this phenomenon could be a mechanically activated reorganization of the nano-particle network caused by the strain applied on the suspension (re-agglomeration). To investigate this hypothesis, it was decided to submit a 0.75 wt.% doped sample to an hysteresis loop. This loop was composed of a ramp "up" (similar as on figure 3.12, 2 $K.min^{-1}$ from room temperature to 125°C), a stabilization plateau at 125°C for one minute, and a ramp "down" to room temperature at $2°K.min^{-1}$. It was chosen to limit the investigated domain to 125°C, to remain in an isochemical state (no polymerization occurring, confirmed with DTA). These trials were performed at a strain of 100 % and a frequency of 10 Hz in the same way as the experiments presented on figure 3.12.

On the dozen of hysteresis experiments performed, and although the ramp up was performed with the exact same materials and testing parameters no trace of the previously observed "bumps" (observed as well on a substantial number of tests) could be found. This invalidates the hypothesis of a thermo-mechanically activated phenomenon. Additional experiments are needed to shed light on this "bump" phenomenon.

3.5 Electrical Behavior - Influence of the MWCNTs

Figure 3.13 shows the measured DC conductivity at room temperature of the MWCNTs/epoxy nanocomposites as a function of the CNT weight fraction. It can be observed that the nanocomposite exhibits a transition between an insulating and a conductive state separated by 11 orders of magnitude. The percolation threshold was found to be around $p_c = 0.25$ wt.% CNTs and the maximal conductivity which was already achieved for a CNT weight content of 0.75 wt.% is $\sigma_{DC}(max) = 6.10^{-3}\, S.m^{-1}$.

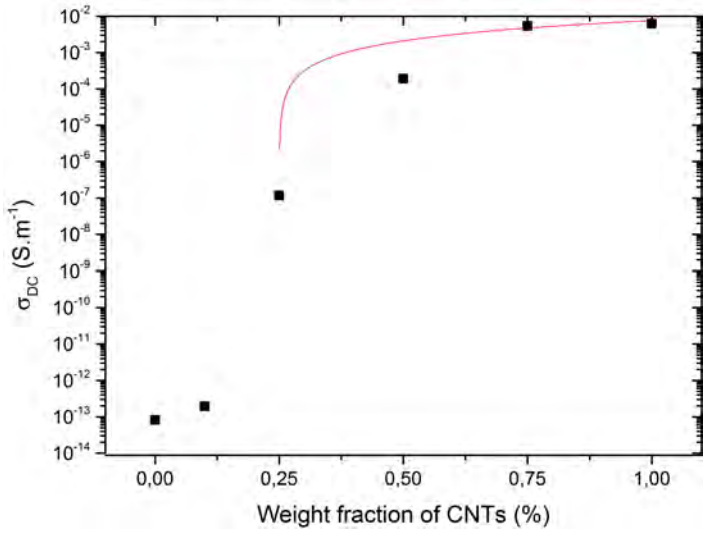

Figure 3.13 – Dependance of the DC conductivity on the CNTs weight fraction of MWCNTs/epoxy

The existence of a percolation threshold indicates the presence of a percolation path for the electrical charges to travel through the material. Above this CNT loading the conduction phenomenon is due to the formation of a connecting path thanks to the CNT bundles network inside the epoxy matrix. In the percolation theory [129], Stauffer defines the insulator-conductor transition and the corresponding percolation threshold achieved as presented in equation 3.7, where σ_0 is a constant, p is the CNT weight fraction corresponding to the percolation threshold and t the critical exponent. On figure 3.13, the data post percolation ($\geq 0.25\, wt.\%$ CNTs) is fitted with equation 3.7 (solid line). The interpolation of the experimental values leads to the determination of the

above-mentioned parameters summarized in table 3.3.

$$\sigma = \sigma_0 (p - p_c)^t \; with \; p > p_c \tag{3.7}$$

Parameter	Value	Unit
p_c	0.25	wt. %
σ_0	$1.07 \; . \; 10^{-2}$	$S.m^{-1}$
t	1.18	

Table 3.3 – Parameters obtained by fitting the experimental data to the percolation theory

The high aspect ratio of the nanotubes makes the percolation possible at a very low CNT concentration, here $p_c = 0.25\, wt.\ \%$. Furthermore, we observe that the maximal DC conductivity is already achieved around 0.75 wt% nanotubes. This concentration appears to be the best compromise between increase in electrical conductivity and processability from a rheological point of view in order to limit the increase in resin viscosity (figures 3.8 and 3.9). The state of dispersion of the nanotubes inside the epoxy matrix can be accessed via the measure of the DC conductivity of the nanocomposite [61]. A low percolation threshold signifies the presence of a homogeneous dispersion state, with few to no CNT bundles. Our percolation threshold obtained is similar to what is reported in the literature [25, 73] for mechanically dispersed nanotubes, indicating a very homogeneous, well dispersed three-dimensional nanotube network.

Furthermore, figure 3.14 presents $\sigma^{'}$, the real part of the complex conductivity of a 0.75 wt.% CNT-doped sample for a few isotherms (from -150 to +150°C). It can first be noticed that for all the temperature spectrum and below a critical frequency (here between 10^3 and 10^4 Hz) the conductivity does not depend on the frequency. Above this critical frequency, the conductivity increases linearly with the frequency. This is a typical behavior for conductive nanocomposites [96, 58]. A temperature-dependence of the low frequency part of the conductivity can also be noticed. The σ_{DC} conductivity increases slightly with an increasing temperature. We propose to study this evolution thanks to the VRH model.

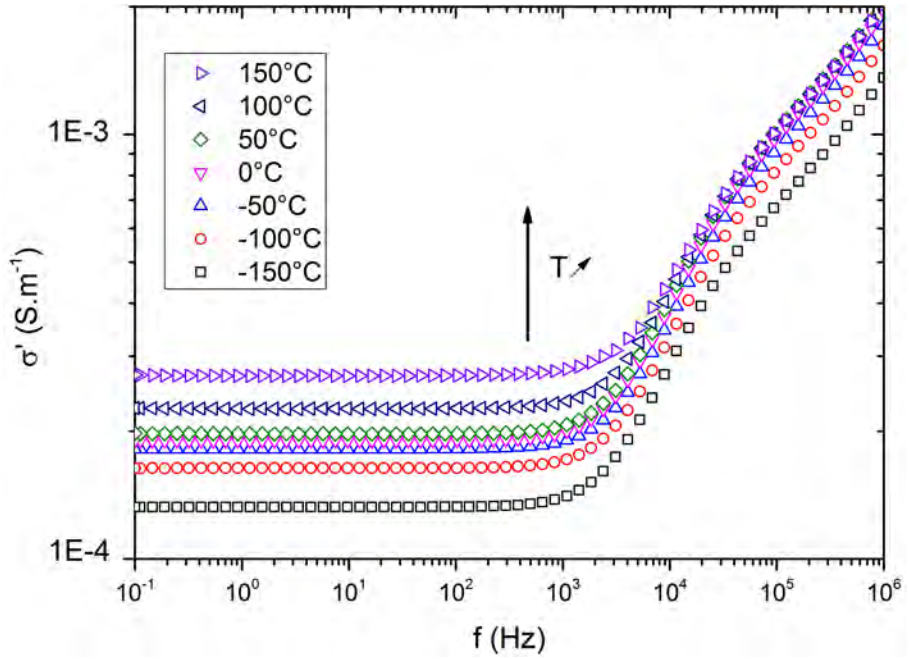

Figure 3.14 – Temperature behaviour of the real part of the complex conductivity of a 0.75wt.% doped epoxy

Variable-range hopping (VRH) (or Mott variable range hopping) is a model describing low-temperature conduction in strongly disordered systems presenting localized charge-carrier states, as presented by N.F. Mott [130]. Mott showed that the probability of hopping from a state i (having an energy E_i) to a state j (E_j) separated by a distance R_{ij} can be written as:

$$P \sim exp\left(-2 \times \frac{R_{ij}}{\xi} - \frac{\Delta E_{ij}}{k_B \times T}\right) \tag{3.8}$$

where k_B is the Boltzmann constant, and ξ the localization length.

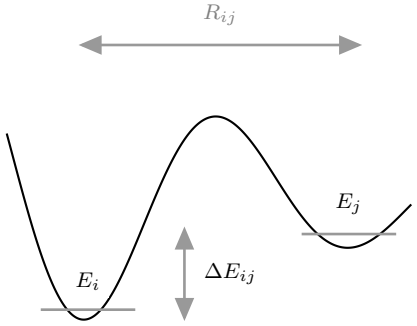

Figure 3.15 – Schematic representation of hopping conduction from a state i to j

In order for the electron hopping to happen, this probability must reach a maximum value, in other words the argument of the exponential function must reach a minimum:

$$\frac{\partial}{\partial R}\left[-2\times\frac{R_{ij}}{\xi}-\frac{\Delta E_{ij}}{k_B\times T}\right]=0 \tag{3.9a}$$

giving:

$$R_{ij}=\left(\frac{T_0}{T}\right)^{1/4} \tag{3.9b}$$

Mott considers then that the conductivity σ is proportional to the maximum value of the probability P:

$$\sigma=\sigma_0 exp\left[-\left(\frac{T_0}{T}\right)^{1/4}\right] \tag{3.9c}$$

Where σ_0 is a constant, which depends on the localization length ξ and n_{E_F} the density of electronic states at the Fermi level. T_0 is called Mott's temperature. T_0 is linked to the "height" of the energy barrier encountered by the charge carrier during the hopping transport mechanism.

In order to study the transport phenomena in the nanocomposites, figure 3.16 presents the σ_{DC} conductivity as a function of $\frac{1}{T^{1/4}}$ for the conductive samples (above the percolation threshold).

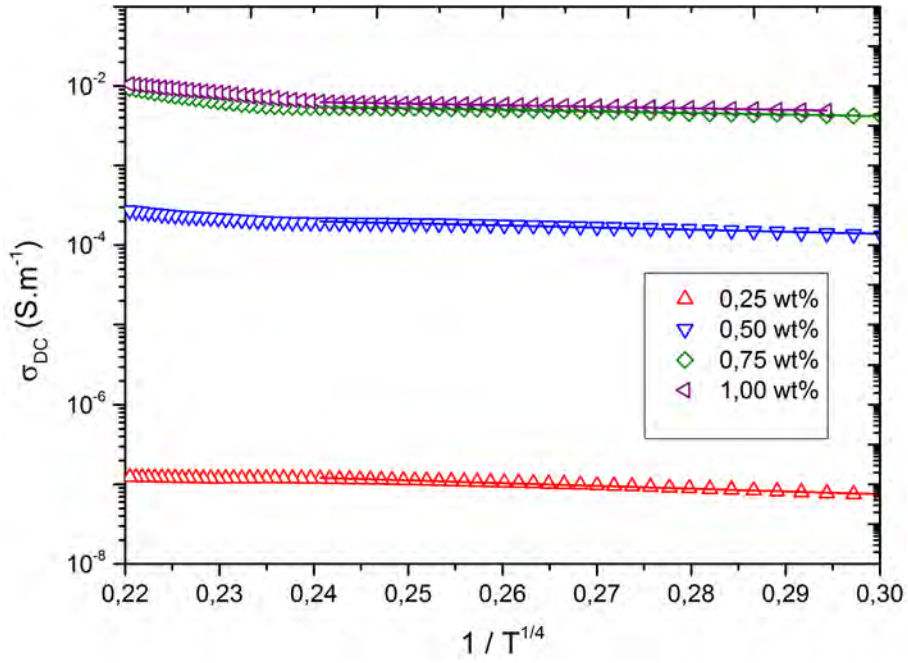

Figure 3.16 – σ_{DC} as a function of temperature for the samples above the percolation threshold

Our experimental results are fitted with the VRH model (equation 3.9c) for temperatures up to 50°C (as the VRH model is adequate for rather low temperatures). For temperatures above 50°C, a thermal activation of the conduction phenomenon can take place (the data exhibit a slope change at this point). Furthermore, the relaxation phenomena in the material can influence the conduction behavior as well, but, in this case, the testing temperature stays far below T_α, the temperature of the mechanical manifestation of the glass transition temperature ($T_\alpha \approx 210°C$ as seen further in chapter 4). Table 3.4 presents the values of T_0 as a function of the CNT weight percentage.

CNT weight percentage	T_0 (K)
0.25	144.8
0.50	48.4
0.75	15.0
1.00	14.1

Table 3.4 – T_0 as a function of CNT weight percentage

T_0 decreases with increasing CNT weight percentage. As presented in the VRH theory,

T_0 can be written as :

$$T_0 = \frac{\beta}{k_B \times \xi^3 \times n_{E_F}} \tag{3.10}$$

with n_{E_F} the density of electronic states at the Fermi level and β a constant which depends on the type of phonon-phonon interactions involved [131]. The decrease in T_0, can origin either from an increase in ξ (localization length) or n_{E_F}. Furthermore, it was shown that the localization length ξ is not influenced by the CNT weight fraction [132]. The decrease in T_0 can thus be associated with a higher density of electronic states at the Fermi level. In other words, a higher density of conductive paths can be found in the doped nanocomposites.

Chapter 4

Processing and Characterization of CNT-modified CFRP

Contents

4.1 Introduction

After having investigated the cure kinetics, rheological and electrical behaviors of the CNT-modified epoxy polymer in chapter 3, this present chapter will focus on the manufacturing and characterization of CNT-doped CFRP.

As seen in chapter 1, the manufacturing of multiscale composites faces three main challenges: nanotube dispersion, nanotube filtration and increased resin viscosity. The first issue (nanotubes dispersion) has been addressed in section 3.2 by the selection of the three-roll mill as dispersion tool, followed by an analysis of the dispersion state of the CNTs inside the cured epoxy matrix. The two issues remaining (filtration and increase in viscosity) prohibit the use of traditional liquid resin molding techniques. That is why an innovative manufacturing process has to be developed, in the form of a spraying technique enabling the high-viscosity CNT / epoxy dispersion to be introduced directly at the interlayer between the carbon fiber plies.

After having manufactured reference and CNT-modified CFRP samples, a second section will present the analysis of those materials. First, it will be ensured that the level of quality reached is sufficient and can be compared to state-of-the art CFRP materials. Even though the improvement of the electrical conductivity is the main driver of this work, an additional interest towards the assessment of the damage tolerance of such innovative materials will be presented as well. The assessment of the direct current conductivity and dynamic dielectric spectroscopy will be performed in order to investigate the electrical properties of the manufactured CFRP. A last section will be dedicated to the analysis of a few key mechanical properties: dynamic mechanical analysis, interlaminar shear strength and interlaminar fracture toughness. These three tests have been selected because they investigate mostly matrix - dominated properties, as in this work, the choice was made to follow the matrix modification approach (see also figure 1.8).

4.2 Processing of CNT-modified CFRP

4.2.1 Manufacturing of reference samples

In order to differentiate a potential influence of carbon nanotubes from one coming from the spraying process on the electrical and mechanical properties of composites, reference samples have to be produced. In order to do so, Vacuum Assisted Resin Infusion (VARI) was selected.

The Vacuum Assisted Process (VAP) was developed at Airbus Group Innovations (formerly EADS Innovation Works) and granted a patent in 2003 [133]. In the same way as for a VARI process, a vacuum bag is used to create a depression in order to infuse the liquid resin inside the dry fibers. The added value of the VAP is the use of a semi-permeable membrane to divide the infusion chamber from the vacuum chamber. This membrane is only gas-permeable, hence, during the infusion, the resin cannot escape the infusion chamber, while continuous degassing of the infiltrated preform lowers the void content in the final composite. Figure 4.1 presents a cutaway diagram of the vacuum assisted process.

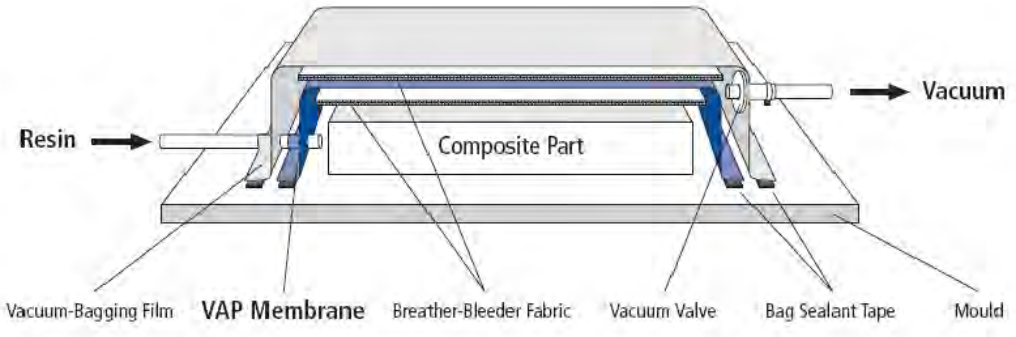

Figure 4.1 – Cutaway diagram of the vacuum assisted process [134]

This process has been used to manufacture two reference laminates: the first one made of 8 layers of unidirectional plies (UD) for electrical conductivity analysis and the second one made of 12 UD plies for mechanical testing. The laminates were cured as presented on the polymerization cycle in figure 2.2 and under a vacuum of P=10^{-2}mbar. A table summarizing the materials produced can be found respectively in appendix A.

4.2.2 Spraying of CNT-doped epoxy

As mentioned in section 1.3.1, the use of state of the art infiltration processes is not possible with CNT-doped resins, as this faces the issues of filtration and viscosity increase. That is why an alternative process has to be used. Maillot [21] developed a process where a limited amount of CNT modified resin was sprayed on the dry fiber plies, followed by an infiltration of the remaining resin (undoped) required to achieve the desired fiber volume fraction. While this might be a relevant approach to improve interlaminar mechanical properties, it was chosen in this work to attempt to manufacture a CNT-doped material where the entire amount of matrix would come exclusively from the spraying deposition process (no post-infiltration needed). This further development comes with two advantages. First, having the entire matrix modified with carbon nanotubes can be seen has a prerequisite to achieve the through-thickness bridging effect, in order to increase the transverse electrical conductivity. Second, without the previously required post-infiltration step, the risk of CNT migrating inside the preform is reduced and the matrix homogeneity is promoted.

The spraying equipment is presented in figure 4.2. It was delivered by the company Viseco GmbH and is composed of three main parts: a spray gun (figure 4.2a) and two control units, a first one regulating the pressurized air temperature and pressure (figure 4.2b) and a second one controlling the temperature of the spray gun itself (figure 4.2c). Thanks to these control units, the whole spraying gun can be heated (body, cup and nozzle), as well as the pressurized air flowing through the gun. Two separate air streams flow through the spraying gun: the first one through the handle up to the spray nozzle (standard feature of the equipment) and the second one through the cup down to the spray nozzle (added feature) to be able to work with higher viscosity products by applying pressure on the materials to be sprayed from the top of the container.

The spraying activities were carried out in an enclosed spray booth featuring exhaust fans, powerful lights and sufficient working space (figure 4.3a). Air flows in through the filtered entry, passes through the working area, and into the filtered exhaust wall located in the rear of the booth. This filtered exhaust air is drawn through the exhaust circuit and discharged into the atmosphere through the exhaust stack. As recommended by the conclusions of the European project Nanosafe [135], conventional personal protec-

tive equipment such as respirators featuring fibrous filters, full-body protective clothing, protective goggles and gloves were used.

As seen on picture 4.3b, a piece of cardboard protected by a non-adhesive foil is placed on the scale, a piece of peel ply used for composite production is then placed on top. After being pre-heated the epoxy resin is placed inside the gun container. By pulling the trigger the stream of epoxy is released. The parameters summarized in table 4.1 proved to lead to a regular and reproducible stream of released material. In order to spray as uniformly as possible a grid spraying pattern was adopted. It turned out to be a reproducible and homogeneous method to cover the whole carbon fiber ply (although remaining a manual process). Each carbon fiber layer is then sprayed with the relevant amount of resin as well as the lower and upper surface of the preform (by spraying on the peel ply for the lower surface, and on top of the last carbon fiber ply for the upper surface). It was experimentally determined that a resin amount of 134 ± 8 g.m^{-2} had to be sprayed to achieve a fiber volume fraction of 60 % in the case of a 298 g.m^{-2} unidirectional carbon fiber ply (a scale was used to gauge the mass deposited while spraying).

Parameters	Value	Unit
Air temperature	80	°C
Gun temperature	60	°C
Air Pressure	2	bar
Nozzle diameter	2	mm

Table 4.1 – Key parameters of the spraying process

The gun temperature was carefully chosen to avoid premature curing of the resin (see also section 3.3), and to achieve a viscosity as low as possible. This temperature was determined by performing linear temperature rheological sweeps for pristine and CNT-doped epoxy. These linear temperature sweeps were performed in the same conditions as for the frequency sweeps obtained in chapter 3. By looking at figure 3.12, it can be seen that the dispersion containing 0.75wt.% of carbon nanotubes reaches a local minimum around 60°C, making this a suitable temperature to use during the spraying process.

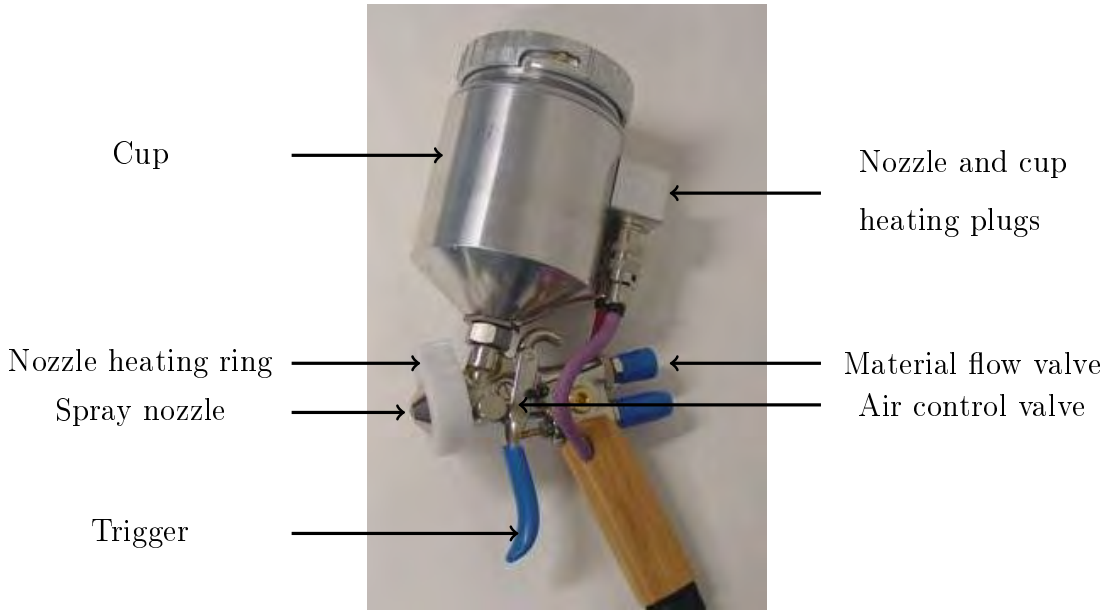

(a) Spray gun used to deposit the CNT/epoxy dispersion

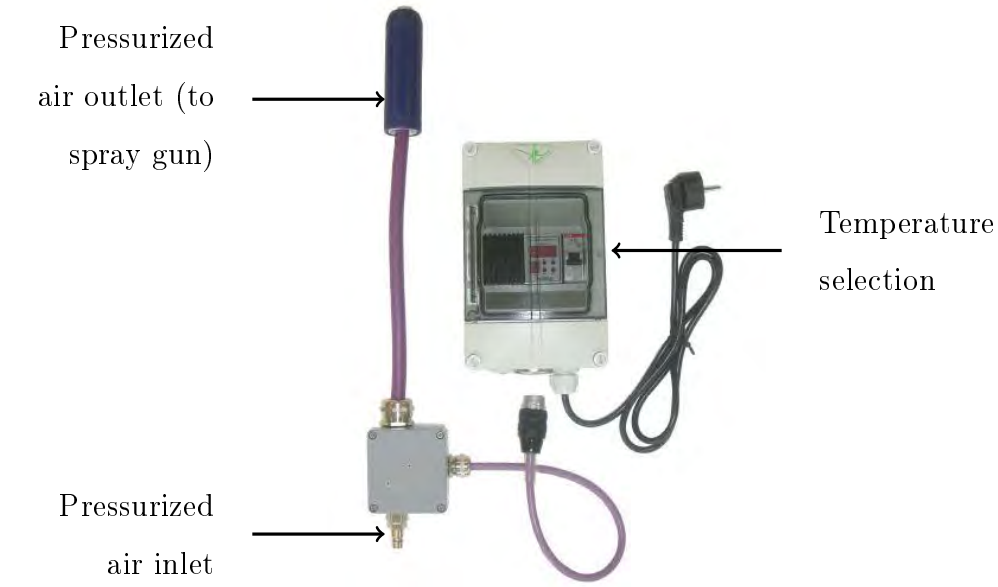

(b) Pressurized air control unit

(c) Gun temperature control unit

Figure 4.2 – Spray deposition equipment

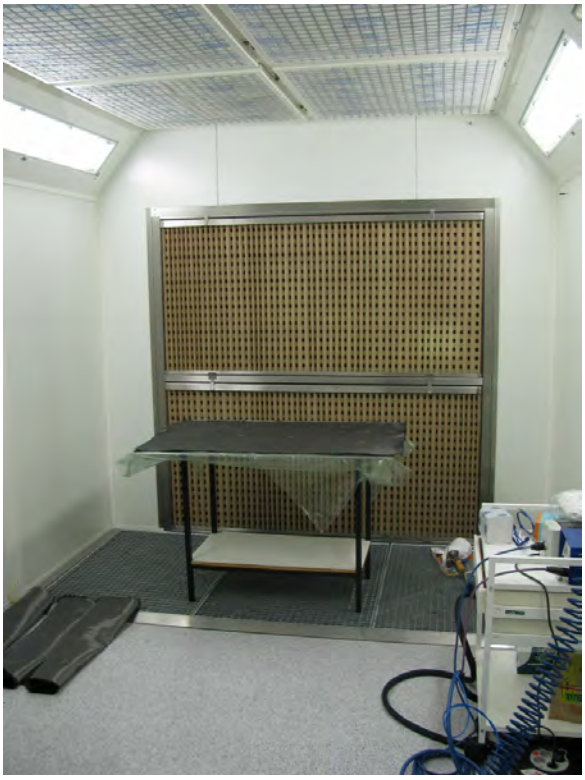

(a) Spraying booth

(b) Spraying setup

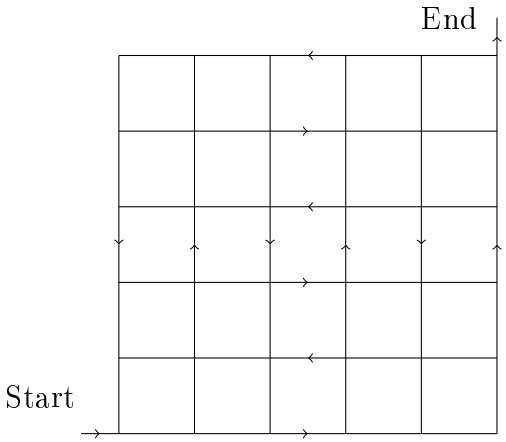

(c) Spraying pattern

Figure 4.3 – Spraying process

4.2.3 Curing of the sprayed preform

After having sprayed the CNT-doped material on the carbon fiber preform and placed a second layer of peel ply on top of the preform, the pre-impregnated preform is ready to be cured. The two main objectives of the curing phase are first to evacuate the air trapped in the preform during the spraying to avoid the formation of porosity, and

second to obtain a homogeneously and reproducibly cured composite laminate with a curing degree higher than 98%.

To this effect, a few concepts have been tried (autoclave, press curing...) with little to no success. One of the major problems was the resin flowing out of the preform, either because of too high pressure applied by the hot-press, or the suction from the vacuum. Nevertheless a curing process adapted from the VAP was used and proved to be successful.

The setup of this process is similar to the one presented in figure 4.1, the only difference being the absence of resin infiltration tube and flow medium. The pre-impregnated preform (between two peel plies) is placed on the oven's table protected by a non-adhesive, temperature resistant film. A membrane is placed on top to enclose the pre-impregnated material in a resin-tight chamber. A layer of breather material is positioned on top to apply the vacuum homogeneously. A second chamber is created by sealing the layout with a vacuum bag. The airtightness of the assembly was checked by stopping the vacuum pump for 1 minute and making sure that a vacuum drop of 5 mbar was not exceeded.

Great care must be taken in order to evacuate the trapped air thanks to the vacuum connection, but not let the resin flow out of the preform. By looking at the viscosity profile on figure 3.12, it has been decided to make use of a first phase at lower temperature to evacuate the pre-impregnated material. In this phase, the assembly is heated to 80°C (to limit the viscosity drop and thus resin fluidity) and evacuated down to a pressure of 10^{-2}mbar continuously for 30 min. The vacuum suction line is then clamped to let the setup under vacuum but cease to apply a continuous pulling force on the resin before increasing the temperature and so further decreasing the resin viscosity.

In a second step, the polymer is cured as presented in chapter 2 on figure 2.2. It was chosen, in order for the sprayed laminates to be comparable to the non-sprayed samples (manufactured using VAP) to keep a step of 1 hour at 120°C (which is normally used in the VAP to let the resin flow in each and every part of the preform and remove porosity). The polymer is then cured in a second step of 2 hours at 180°C. The analysis of the curing degree of the laminates will be investigated in section 4.3.1 of this chapter.

4.3 Characterization of CNT-modified CFRP

4.3.1 Quality Assessment

The purpose of this section is to ensure that the materials manufactured using this non-conventional manufacturing method reach the required level of material quality to produce reliable testing results. As this manufacturing process goes beyond the established state-of-the-art, it is crucial to carefully study its influence on the quality of the produced material. Another goal is to obtain relevant information on the material's internal structure (through microscopy or C-Scan), physical properties such as fiber volume content, or chemical properties such as curing degree, in order to contribute to the understanding of the material behavior.

This relevant material knowledge can be obtained through two main investigations routes: destructive or non-destructive methods. As this work focuses on investigations at coupon scale, most of these techniques will be destructive methods as a portion of the laminates can be reserved for this purpose. In composite production, non-destructive testing is often favored as this protects the part's integrity and saves cost. Nevertheless, ultrasonic testing will be used as well as this non-destructive testing technique holds the potential to provide for large area defect mapping images.

Optical Microscopy

Optical microscopy provides an insight inside the laminates manufactured. Figure 4.4 presents six images of the three materials, selected from those obtained during the optical microscope observations. Laminates made of 8 layers of UD carbon fiber plies were observed in both X (0°) and Y (90°) directions. Those laminates were the ones which were later on used for electrical conductivity testing. A slight waviness of the carbon fiber plies can be observed, especially for the laminates manufactured through spraying. This can be explained by the fact that handling is made harder in the case of pre-impregnated carbon plies (increased tackiness), although waviness is bound to happen as soon as hand

layup is involved.

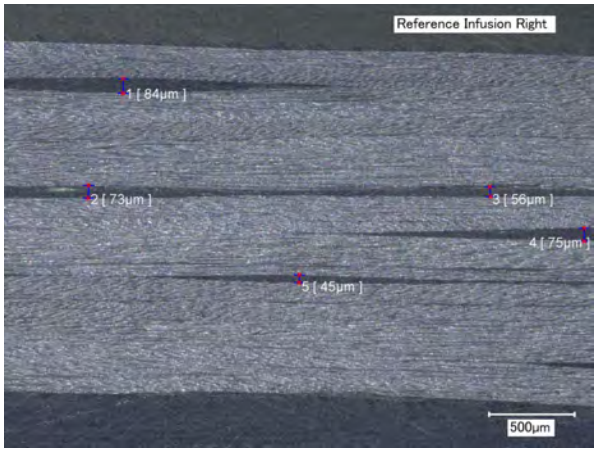

(a) Reference Infusion - 90° view

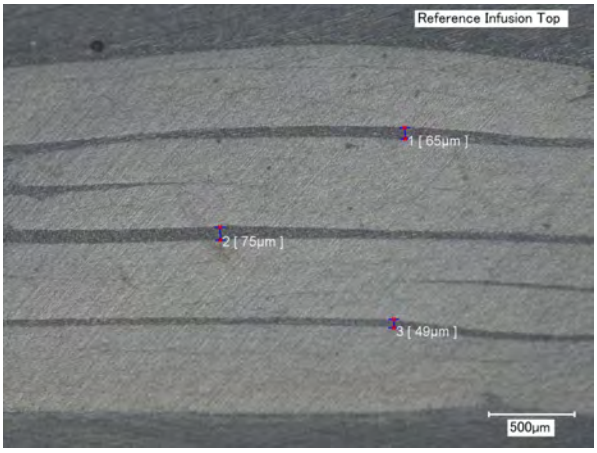

(b) Reference Infusion - 0° view

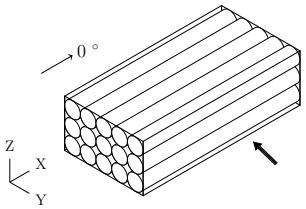

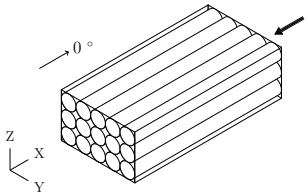

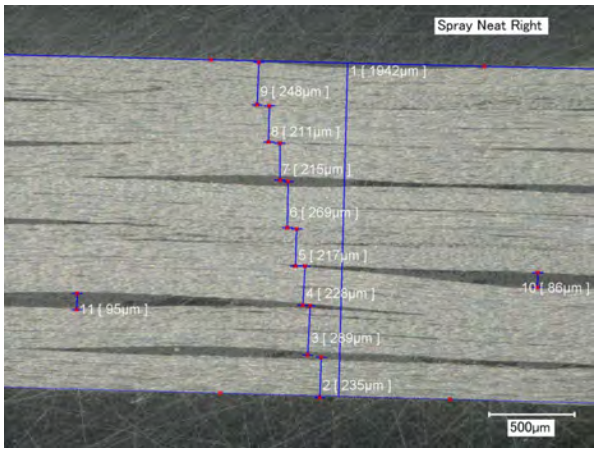

(c) Spray Neat - 90° view

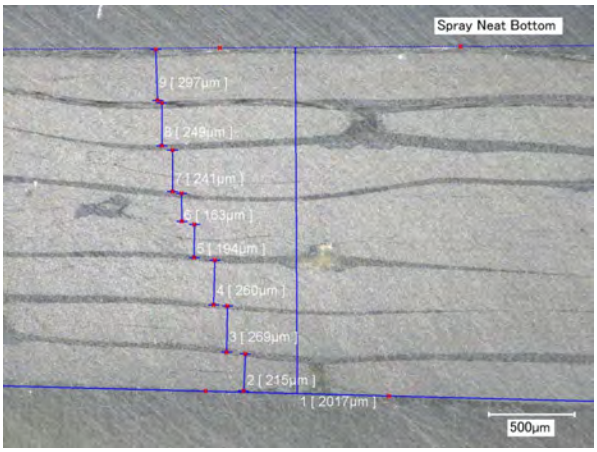

(d) Spray Neat - 0° view

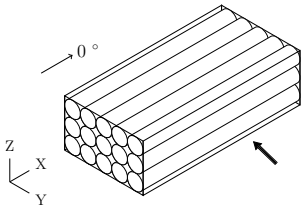

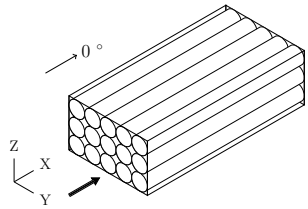

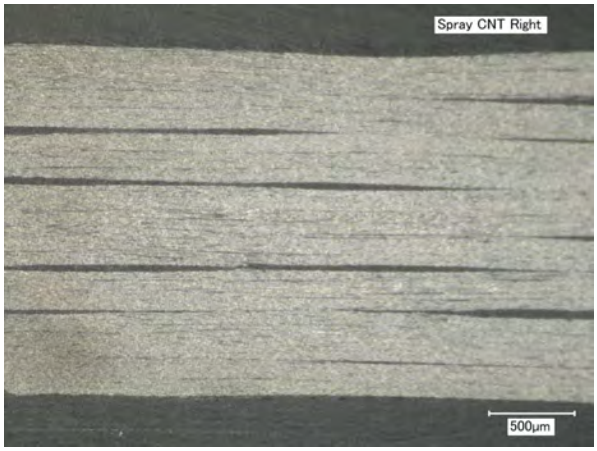

(e) Spray CNT - 90° view

(f) Spray CNT - 0° view

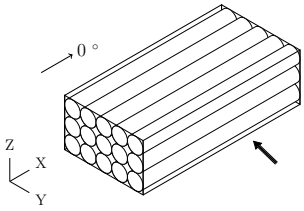

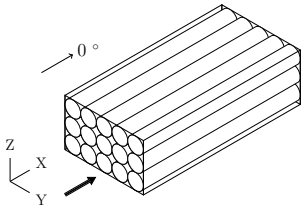

Figure 4.4 – Micrographs of the three types of produced materials

Porosity was found to be almost nonexistent: a very limited amount of voids could be detected through optical microscopy. A quantitative evaluation of the void content will be performed with the help of acid digestion and presented in section 4.3.1. As seen on the photographs, thin dark layers can be observed at the interface between carbon fiber plies. A close analysis of these regions showed that these are epoxy-rich layers caused by the glass-reinforced polypropylene (PPG) threads stabilizing the carbon fibers at $\pm$ 60° angles. These threads (see also figure 2.3 and table 2.2) create gaps between the plies which are neither compressible nor soluble in the matrix. The gaps are filled with epoxy matrix during infiltration or spraying. It can be assumed that these PPG threads have a negative influence on the transverse electrical conductivity of this state-of-the-art carbon fiber semi-finished material. Table 4.2 presents the results of the picture analysis, by reporting the mean values of the consolidated ply thickness (ratio between thickness of the cured laminate and the number of plies) and the mean thickness of the observed resin-rich interlayers. It should be mentioned that the mean value of the resin interlayer thickness, only takes into account the case where such an resin-rich interlayer is actually observed and that not all interlayers present such a layer.

Sample	Consolidated ply thickness (μm)	Interlayer thickness (μm)
Reference sample (VAP)	279 ± 6	72 ± 15
Neat sprayed resin	278 ± 7	91 ± 5
CNT-doped sprayed resin	276 ± 5	89 ± 10

Table 4.2 – Consolidated ply and interlayer thickness of manufactured materials

No influence of the spray manufacturing process and / or addition of carbon nanotubes on the consolidated ply thickness and / or laminate thickness and occurrence of resin interlayers could be observed. These two parameters are crucial to evaluate as they critically influence the transverse electrical conductivity and the interlaminar mechanical properties, investigated further in this work. As no influence on these sample parameters could be observed, comparative analysis between the three materials can be performed.

It was also tried to observe CFRP cross-section with a scanning electron microscope, unfortunately the depth of field of the samples was too low to obtain satisfying observations. Nevertheless, SEM observation of CFRP fracture surface are reported in section 4.3.3.

Ultrasonic Inspection

Among the many non-destructive inspection techniques beyond visual inspection, ultrasonic testing provides a way of evaluating the quality of the material being inspected. It uses ultrasonic waves to diagnose the condition of a composite material laminate. Anomalies adsorb or deflect the emitted waves, which are then detected as changes in the portion of the waves being reflected. It can detect holes, delamination, voids, damages as well as resin-rich or resin-poor areas.

C-scan is one of the ultrasonic inspection technique providing a two-dimensional graphical representation, in which the waves echoes are displayed in a top-view of the test surface. This method was here applied as reflected (or pulse-echo) transmission mode (wave emitter and detector are localized on the same side of the tested part). No indicator of defect depth can be given as this requires a time of flight evaluation.

Figure 4.5 presents three of the ultrasonic scans (C-Scan) performed for the three types of materials manufactured (reference using VAP, sprayed neat resin, sprayed CNT-doped resin). The color scale displays the percentage of signal directly reflected by the material. The darkest colors correspond to a low level of signal reflected, while the brightest colors correspond to a high level of reflected signal. As mentioned above, anomalies and defects adsorb or deflect the emitted waves, meaning that darker zones appearing on the scans can be identified as such.

On figure 4.5a, the quality level as achieved using the VAP process can be observed. Except for a few small defects, the quality of this type of panel is satisfactory. A few anomalies can be noticed on the scan, mostly small areas with a slight resin starvation (dark dots) and some fibers overlaps (dark lines). The same quality state can be observed for a sample manufactured by spraying neat resin (figure 4.5b), where only a few resin-poor areas and fiber overlaps can be observed. This is already a first evidence showing that the spraying method is an adequate method for producing high-quality composites. On the last of the three pictures (figure 4.5c), it can be seen that the CNT-doped panel presents a zone (see center of the scan) where the quality is not as high as on the rest of the panel and as observed on previously mentioned laminates. This center zone seems have a higher density of resin-poor areas. The fiber volume fraction of this particular region should be specifically investigated to determine the extent of this resin deficit (see also section 4.3.1). In any case, this zone should and will be avoided when sampling specimens for further testing.

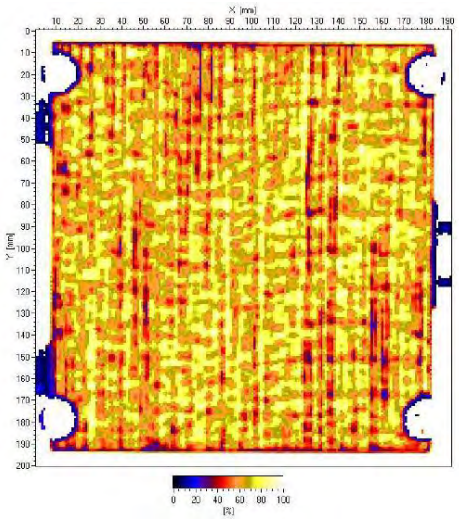

(a) Reference sample manufactured using VAP

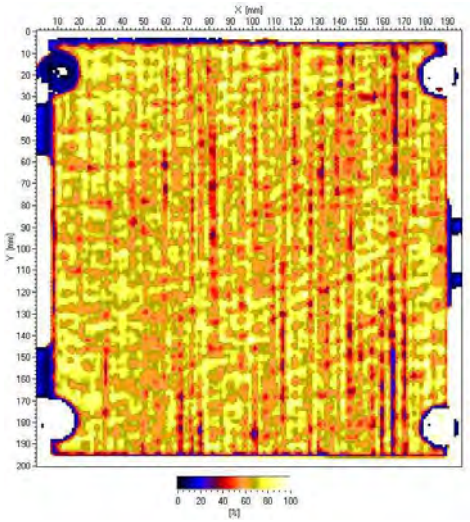

(b) Sample manufactured using neat sprayed resin

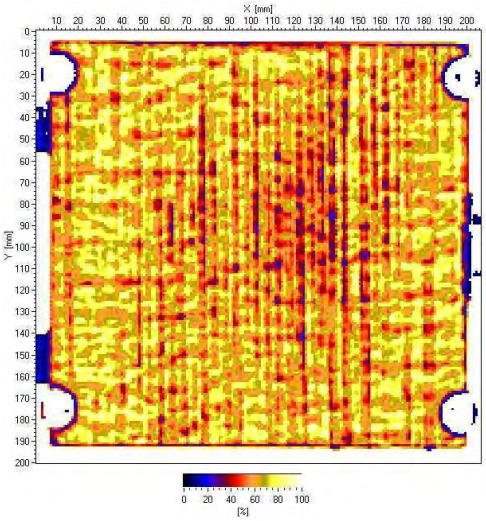

(c) Sample manufactured using CNT-doped sprayed resin

Figure 4.5 – Ultrasonic scans (C-Scan) of the three types of materials produced

Fiber Volume Content and Curing Degree

Fiber Volume Content

Fiber volume content (or Fiber Volume Fraction (FVF)) in the produced composites is an important parameter to be quantified to ensure laminate quality and reliable testing results. Both mechanical and electrical properties of CFRP depend on their fiber volume content. Equation 4.1 presents the fiber volume ratio V_f (or fiber content, expressed in percent), with v_f being the volume of fibers and v_c the total volume of the composite.

$$V_f = \frac{v_f}{v_c} \tag{4.1}$$

Two approaches exist which may be used to determine the ratios of constituents inside the composite material. The first method calculates reinforcement or matrix content based on the measured thickness of the laminate as presented in equation 4.2 (this method assumes that the fiber areal weight of the reinforcement is known). The thickness of a composite laminate depends on the amount of reinforcement and the relative amount of resin which has been included. For a given quantity of reinforcement, a laminate with a high fiber volume fraction will be thinner than one with a lower fiber volume fraction, since it will contain less resin. This first option is not applicable to the measurement of void volume.

$$V_f = \frac{n.A_w}{t.\rho_f} \tag{4.2}$$

With n the number of carbon fiber plies, A_w their areal weight, t the thickness of the laminate and ρ_f the density of the carbon fibers.

The second method (described by the EN 2564 standard [136]) physically removes the matrix by acid digestion (or in some other cases ignition), leaving the reinforcement essentially unaffected and thus allowing calculation of reinforcement or matrix content (by weight or sometimes volume) as well as percent void volume. These test methods are primarily intended for two-part composite material systems. However, these test methods can be extended to filled material systems with more than two constituents, as the volume fraction of the filler is here very low compared to the two other (in our case < 0.5 vol.%). To this date it is still unclear whether the carbon nanotubes are retained

by the filter used in this acid digestion method or not. The pore size of the used cellulose filter allow particles down to 12 - 15 μm to be filtrated, which is not sufficient to filtrate single CNTs but could be filtering larger CNT agglomerates.

Table 4.3 presents the measured fiber volume fractions and void contents for the three types of materials manufactured. A good agreement between the two testing methods can be observed, though a trend towards higher fiber volume fractions for acid digestion can be noticed. This means that following the thickness measurement method, more conservative results are obtained. Results obtained on multiple samples coming from different panels proved to be reproducible. No process influence or influence of the carbon nanotubes on the determined value could be obtained, all measurement being in the range of 60 $vol.\%$ which is the desired fiber volume content in the case of CFRP for aeronautical structural applications. Furthermore it can be noted that the void content remains low for the three materials produced ($\leq 1\% vol.$))

Sample	Fiber Volume Fraction (vol.%)		Void Content (vol.%)
	(via thickness)	(via acid digestion)	(via acid digestion)
Reference sample (VAP)	59.1	61.1	1.0
Neat sprayed resin	59.4	62.2	0.8
CNT-doped sprayed resin	59.8	61.9	0.4

Table 4.3 – Fiber volume fractions of manufactured materials

Determination of Curing Degree

As an insufficiently cured matrix could have an influence on the properties investigated (mostly interlaminar mechanical properties), it is crucial to ensure that the epoxy polymer is properly cross-linked when following the cured cycle presented above. In order to do so the extent of cure was determined by differential scanning calorimetry as similarly presented in section 3.3 and as normalized in the AITM 3-0008 [137]. Namely, temperature scanning measurements from room temperature to 320°C were performed with a heating rate of 5 K.min^{-1} to determine the residual enthalpy. Ten samples per material were tested on the laminates dedicated to the analysis of the electrical properties. No significant influence of the CNT or the modified manufacturing process could be

noticed. Furthermore, the curing degrees achieved are far above 98 %, proving that the laminates are sufficiently cured.

Sample	Curing Degree (%)
Reference sample (VAP)	98.5 ± 0.1
Neat sprayed resin	98.5 ± 0.1
CNT-doped sprayed resin	98.8 ± 0.2

Table 4.4 – Curing degree of manufactured materials

4.3.2 Electrical Characterization

DC Conductivity Measurements

Direct Current (DC) conductivity measurements were performed following the experimental protocol presented in section 2.3.3. The detailed sample preparation is presented in annex B. A direct current (I = 100 mA, V = 2.1 V) was injected in the sample, and the resistance of the sample was measured. The direct current electrical conductivity σ_{DC} was calculated as a first approximation using the following equation 4.3:

$$\sigma_{DC} = \frac{t}{l_1 \, l_2 \, R} \tag{4.3}$$

Where R is the resistance of the specimen (Ohm); t the distance between the two electrodes (m) ; l_1 and l_2 the two other side lengths of the specimen (m).

Z-direction

Figure 4.6a presents the testing configuration in the case of a transverse conductivity testing (along the Z axis). The hatched surfaces represent the location of the testing electrodes. All laminates tested were composed of 8 layers of unidirectional fiber plies $[0]_8$. Figure 4.6b presents the DC electrical conductivity in the transverse direction (Z-axis) for the three types of manufactured materials. It can first be noticed, that all results exhibit a low standard deviation, indicating that the data points tend to be very close to the mean and therefore that the amount of variation or dispersion of the data is very low. This proves the reproducibility of the measurement and indicates a good homogeneity of the material.

For the material used as baseline and manufactured through infusion a σ_{DC} value of 0.9 ± 0.1 S.m^{-1} was measured. A slight decrease in DC conductivity was noticed for the sprayed reference to 0.6 ± 0.1 S.m^{-1}. Whereas for the CNT-doped material a significant increase to 1.6 ± 0.2 S.m^{-1} was measured. These results seem to show an influence of the carbon nanotubes on the transverse conductivity of the laminate. Specifically that the CNTs increase as expected the conductivity of the CFRP material, but at a limited level. Furthermore, in this configuration, the influence of the spraying process on the conductivity is still unclear.

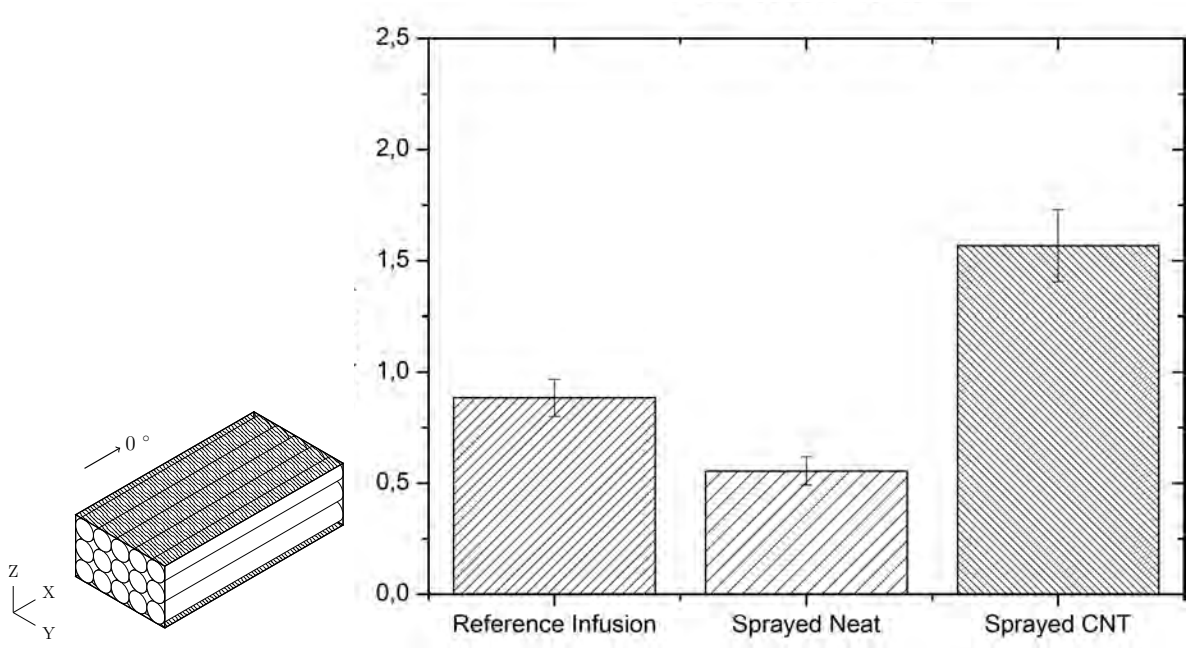

(a) Testing Configuration (b) DC Conductivity Measurements

Figure 4.6 – DC Conductivity in the Z-direction

Y-direction

Figure 4.7a presents the testing configuration in the case of a DC conductivity testing along the Y axis. As previously, all laminates tested were composed of 8 layers of unidirectional fiber plies $[0]_8$. Figure 4.7b presents the DC electrical conductivity in the Y-direction for the three types of materials manufactured. It can first be noticed, that again all results exhibit a low standard deviation, indicating a good reproducibility of the measurement and homogeneity of the materials.

For the baseline infused material a σ_{DC} value of 9.3 $\pm$ 0.3 S.m^{-1} was measured. A slight decrease in DC conductivity was noticed for the reference sprayed with unmodified epoxy to 8.0 $\pm$ 0.4 S.m^{-1}. Whereas for the CNT-doped material a noticeable increase to 13.8 $\pm$ 0.8 S.m^{-1} was measured. These results seem to show again an influence of the carbon nanotubes on the Y-conductivity of the laminate. Specifically that the CNTs increase as expected the conductivity of the CFRP material. Furthermore, in the same way as for the Z-direction, the influence of the spraying process on the conductivity seems to be low to negligible.

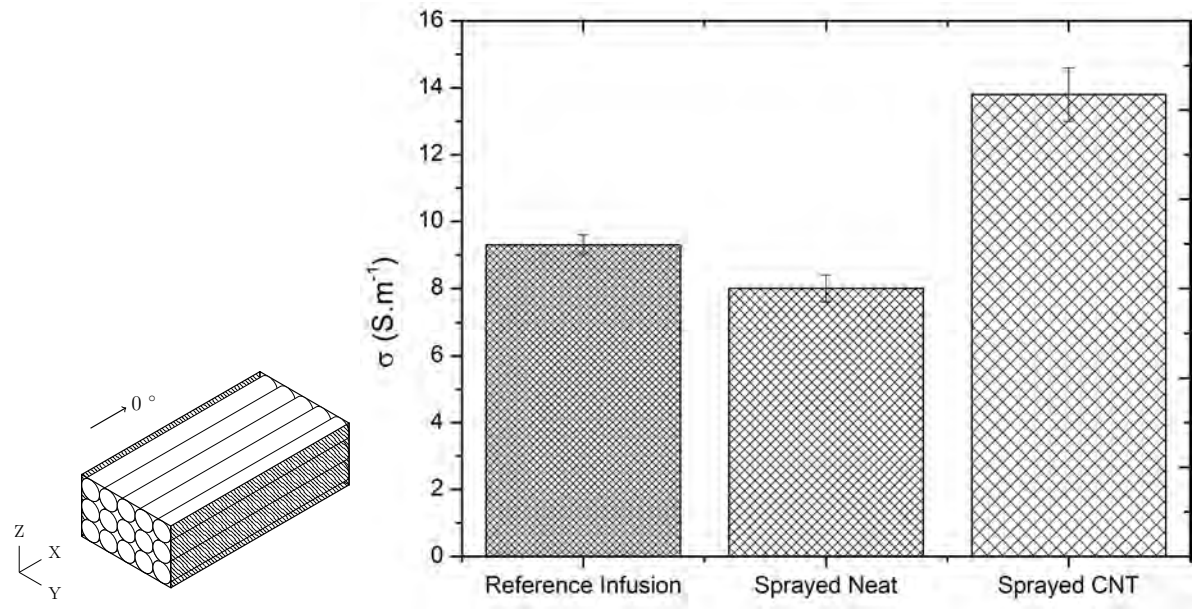

(a) Testing Configuration (b) DC Conductivity Measurements

Figure 4.7 – DC Conductivity Measurements in the Y-direction

For both Z and Y directions a modest but noticeable increase of the electrical conductivity was noticed. In these both directions, the matrix plays an important role in the conductivity behavior. Indeed, for the Z direction a thin matrix interlayer is found between the carbon fiber plies (see also section 4.3.1). For the Y direction, the carbon fiber bundles are fitted closer together (higher density of contacts between carbon fibers which explains a higher baseline conductivity) but a continuous carbon fiber path (as for the X direction, see below) can not be found. It seems that the insertion of conductive carbon nanotubes inside the matrix filling up the interstices between carbon fibers leads to a higher density of electrical contacts and thus a higher electrical conductivity. This still needs to be confirmed by the dielectric dynamic analysis as presented in the next section.

X-direction

Measurements of the X-conductivity (along the fiber direction) were performed on the same materials following the testing configuration presented on figure 4.8. It was noticed during the experiments that the resistance values measured were far lower than for the Y and Z direction (because of the high conductivity of the carbon fibers). In that case it was observed that the samples resistance was in the same order of magnitude

as the contact resistance. It was not possible with the available equipment and surface preparation method to come with an accurate electrical conductivity measurement. Nevertheless, it was possible to determine that the order of magnitude for these sample was $\sigma_{DC} \approx 10^4$ S.m^{-1}. At last, an influence of the CNT is not expected (and could not be observed) in the case of the X-direction, the conductivity being, in that particular configuration, driven by the much higher conductivity of the carbon fibers, which provide a continuous conductive path along the length of the sample.

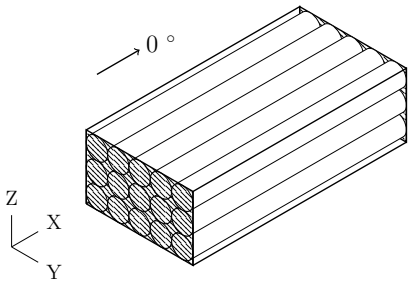

Figure 4.8 – X-Conductivity - Testing Configuration

Dielectric Spectroscopy

In the section, the influence of carbon nanotubes on the electrical properties of the CFRP are studied with the help of the dynamic dielectric spectroscopy (presented in section 2.3.4). The measurements were performed in the transverse direction (Z-direction, see also figure 4.6a) on the same laminates as previously (8 layers of unidirectional fiber plies $[0]_8$). The conductivity spectra for the three materials are presented in appendix C. We propose to study the dielectric behavior of the produced CFRP material, and for that purpose, the real part of the complex conductivity for the sprayed reference is reported in figure 4.9. In this graph, the real part of the complex conductivity $\sigma^{'}$ is presented for frequencies from 10^{-1} to 10^6 Hz. The influence of the temperature was studied from -150 to 150°C, a few selected isotherms are presented on the graph. On this figure, σ_{DC} can be deduced from the value of $\sigma^{'}$ at low frequency (10^{-1} Hz), as summarized on figure 4.10 for the three types of material.

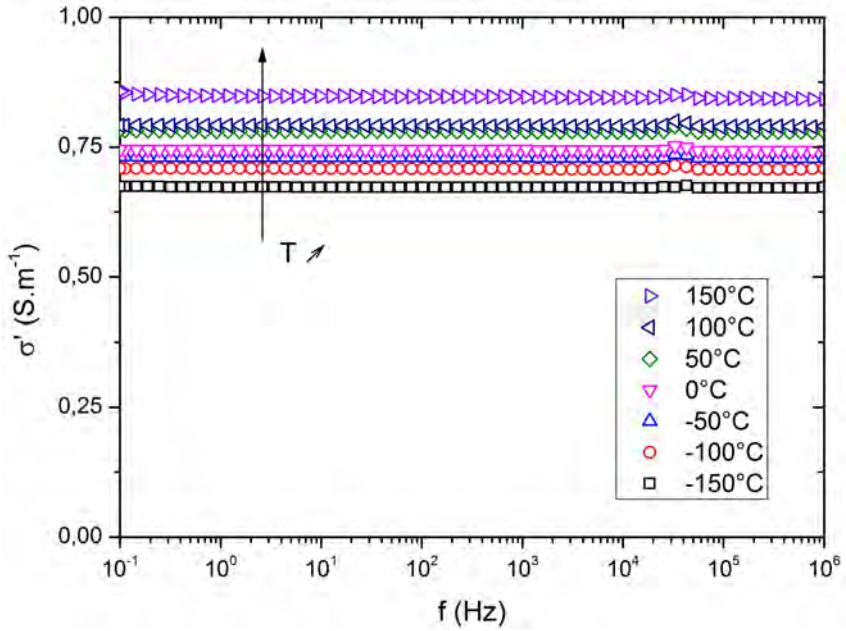

Figure 4.9 – Real part of the complex conductivity for the Sprayed Reference material produced

Three main observations can be made from looking at these results. The first one is related to the frequency-dependency of the electrical conductivity. By examining figure 4.9, it can be seen that the electrical conductivity $\sigma^{'}$ is constant all over the frequency domain (for the three materials as seen on appendix C, no dependence of the conductivity on the frequency can be observed. This behavior is typical for conductive materials above the percolation threshold [138], where a percolating network of carbon fibers already exists in the CFRP material.

A temperature dependency can be noticed as well. The real part of the complex conductivity increases with increasing temperature. The electrical conductivity is in this case temperature-activated. Although this increase in conductivity remains relatively low, this behavior is different from metallic conductivity, where the electrical conductivity decreases with increasing temperatures.

In addition, figure 4.10 presents the mean values of σ_{DC} obtained from the above-mentioned frequency spectra. The DC conductivity values (measured through DDS) obtained were respectively: 0.8 $\pm$ 0.1 S.m^{-1} for the infused reference; 0.6 $\pm$ 0.2 S.m^{-1} for the sprayed reference and 2.1 $\pm$ 0.1 S.m^{-1} for the sprayed CNT-doped laminate. The σ_{DC} value for the 0.75 wt.% doped matrix is also reported for comparison. By comparing

these values with those obtained through DC conductivity measurement and presented in figure 4.6b, a very good agreement between those methods can be noted.

From these observations obtained through two different analysis techniques, an influence of the CNTs on the transverse electrical conductivity of the CFRP can be presented. A significant increase (the transverse electrical conductivity of CNT doped CFRP is doubled compared to the reference material). It should moreover be noted that increasing the electrical conductivity above the percolation threshold is a substantial challenge. Furthermore, thanks to the results achieved in this work, the volume conductivity of the CFRP is more homogeneous.

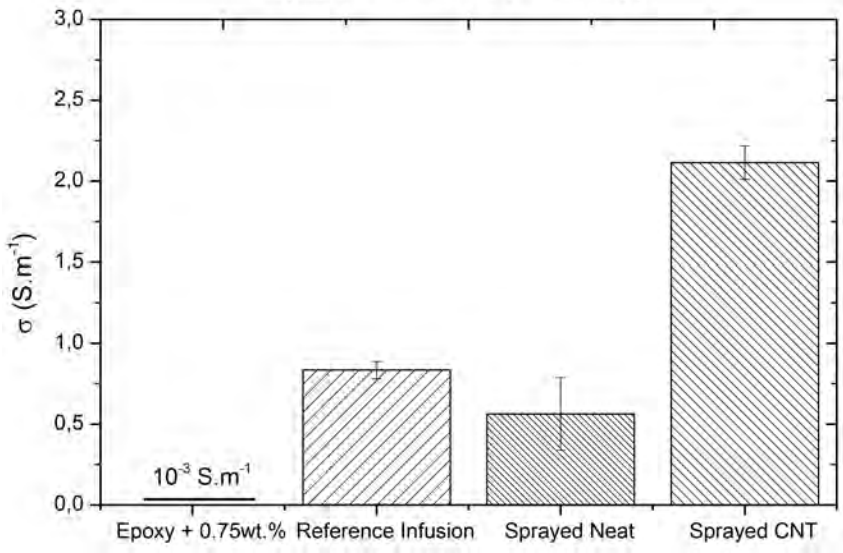

Figure 4.10 – DC Conductivity measured at 25°C via DDS

Figure 4.11 presents the DC conductivity as a function of $\frac{1}{T^{1/4}}$, for the three CFRP materials manufactured. The behavior of the 0.75 wt.% CNT-doped matrix is also reported for comparison. This figure shows as well an increase of the σ_{DC} conductivity for CNT-doped samples compared to the samples without nanotubes. In order to study the transport phenomena in the composites, the results are fitted with the VRH model (equation 3.9c) for temperatures up to 50°C (as the VRH model is adequate for rather low temperatures).

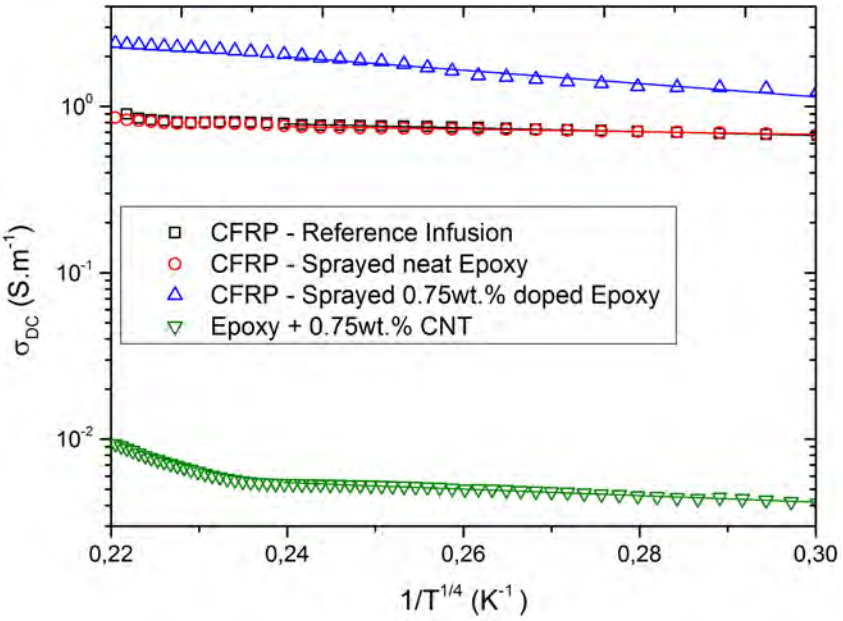

Figure 4.11 – σ_{DC} as a function of temperature for the CFRP samples

Table 4.5 presents the values of T_0 obtained through linear fitting of the data as a function of the CNT weight percentage. This temperature which is inversely correlated with the localization length (see equation 3.10) has been found to decrease with the addition of CNTs (see the works of El-Sawi [58] and Lonjon [139]). This was explained by the fact that adding CNTs to the matrix increased the number of charge-conducting paths inside the laminate.

Material	T_0 (K)
Spray CNT	255.8
Spray Neat	1.7
Reference Infusion	0.4
MVR444 doped with 0.75wt.% CNT	15.0

Table 4.5 – T_0 as a function of CNT weight percentage

In this work, this effect was indeed observed for the CNT-doped epoxy matrix (see section 3.5). But, although the addition of CNTs to the CFRP increased the number of charge conducting paths inside the laminate (confirmed by the increase in transverse electrical conductivity and later on by scanning electron microscopy), we do not observe

a decrease in T_0 for CNT-doped CFRP material.

The high value of electrical conductivity achieved (two orders of magnitude higher than for El-Sawi for instance), and the purely conductive behavior of the samples (no frequency-dependency, as see on figure 4.9) put the use of Mott's model into question. It probably reaches its limit.

.

4.3.3 Mechanical Characterization

The introduction of carbon nanotubes inside CFRP seems to have a noticeable effect on the electrical conductivity in the Z and Y direction. In this second part of the chapter, the influence of CNTs on the CFRP mechanical properties are investigated through three mechanical analysis techniques.

Dynamical Mechanical Analysis

First, the behavior of the manufactured materials is investigated under dynamical mechanical spectroscopy (see also section 2.3.5). The tests were performed at a low strain (0.05%), for a frequency of 1 Hz, and from room temperature to 280°C with a heating rate of 5 K.min^{-1}. These DMA measurements are performed at a low strain rate in order to take place in the linear response domain of the material. For each material a dozen of test has been performed on different samples, in figure 4.12 one representative sample per material is reported.

The influence of carbon nanotubes on the storage modulus G$'$ for the three manufactured materials is presented in figure 4.12a. A good superimposition of the three samples results can be observed, indicating that no influence of the CNT on the storage modulus could be noticed. The first column of table 4.6 presents a summary of the mean values of T_α reported from the loss modulus curves G$''$. Again, these results do not suggest an influence of the CNTs on the loss modulus.

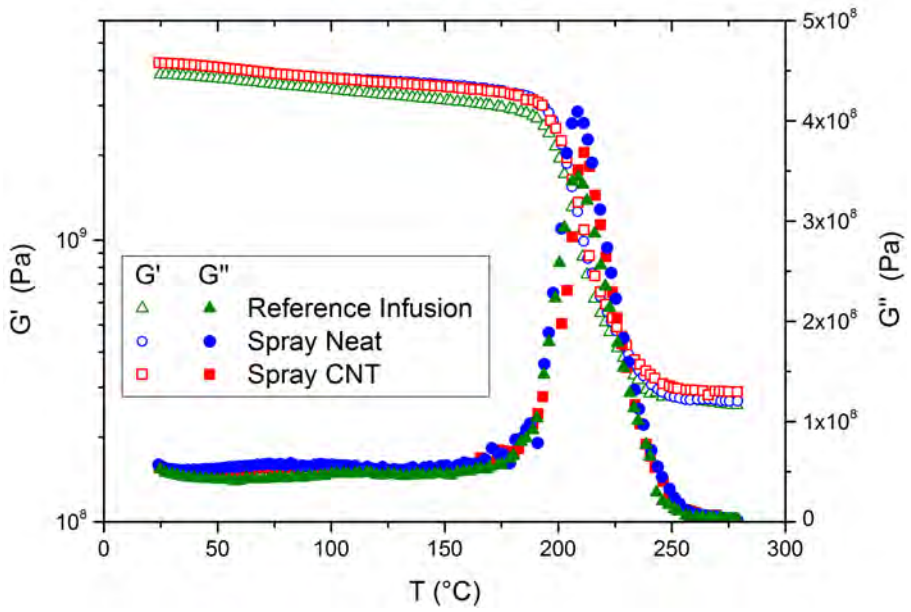

(a) Storage and Loss Modulus

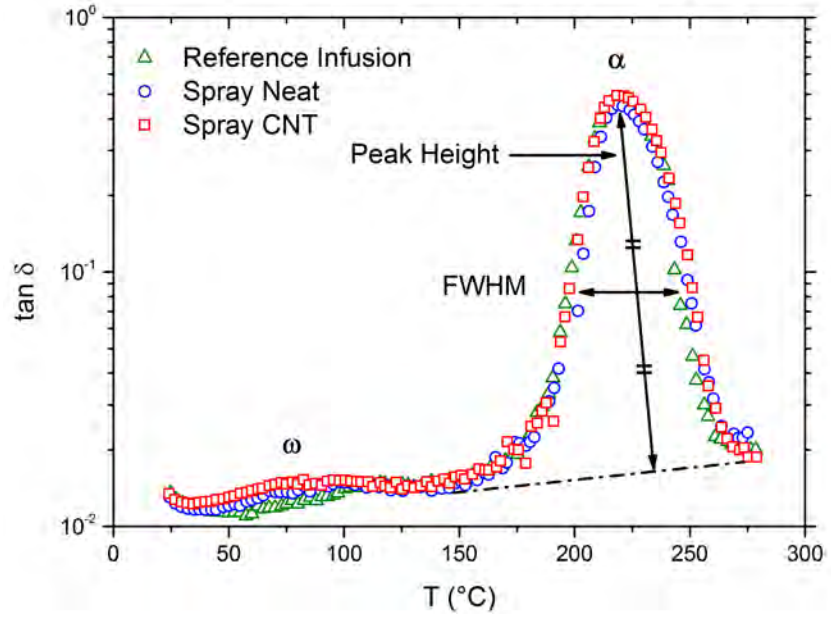

(b) Dissipation Factor

Figure 4.12 – Dynamical Mechanical Analysis of the three types of materials produced

The dissipation factor tan δ highlights the mechanical relaxation phenomena inside the epoxy polymer (see figure 4.12b). Two mechanical relaxations can be observed in the polymer matrix. A principal relaxation α can be observed at high temperature and an intermediary relaxation ω observed at lower temperature. It should be noted that a secondary relaxation β can also be observed at low temperature (around -50°C, see also

figure 2.11), but the range of temperature investigated in that case is too high for this relaxation to be observed.

The α mechanical relaxation is associated with the anelastic manifestation of the glass transition. It matches the delocalized segment chains mobility occurring in the polymer network. For a given polymer sample, the tan δ main relaxation peak represents the ratio of dissipated energy to the stored energy per cycle of sample deformation. The height and width of the tan δ peak can give a good idea of the state of the polymer network. In order to do so, the Full Width at Half Maximum (FWHM) and peak height (see figure 4.12b) were determined for each tested sample. The mean values of FWHM and peak height are summarized in table 4.6, as well as the T_α values taken from the maximal value of the loss modulus G″. These values of FWHM and peak height do not considerably change for sprayed and / or CNT-doped materials. These results do not indicate any influence of the CNTs on the polymer network homogeneity.

	T_α	FWHM	Peak Height
Reference Infusion	208.8 ± 1.8	33.4 ± 2.2	0.46 ± 0.03
Sprayed Neat Epoxy	208.5 ± 1.3	33.1 ± 0.9	0.47 ± 0.04
Sprayed CNT-doped Epoxy	211.1 ± 1.4	30.8 ± 0.8	0.44 ± 0.01

Table 4.6 – T_α, FWHM and peak height of the tan δ peak

Interlaminar Shear Strength

The present section focuses on the determination of the ILSS of the produced materials. Unique characteristic of laminated CFRP, the presence of interlaminar shear stresses in the composite often leads to delamination. This test gives useful information about the quality of the matrix / fiber interface.

Measurements of the ILSS were performed through three-point bending tests on CFRP laminates composed of 12 layers of unidirectional carbon fiber plies $[0]_{12}$. Testing was performed as described in section 2.3.7 and following the EN 2563 norm [108]. 20 samples per material were tested. A cross-head speed of 1 mm.min^{-1} was used. Figure 4.13 presents a load / cross-head displacement diagram where one representative sample of each tested material is represented.

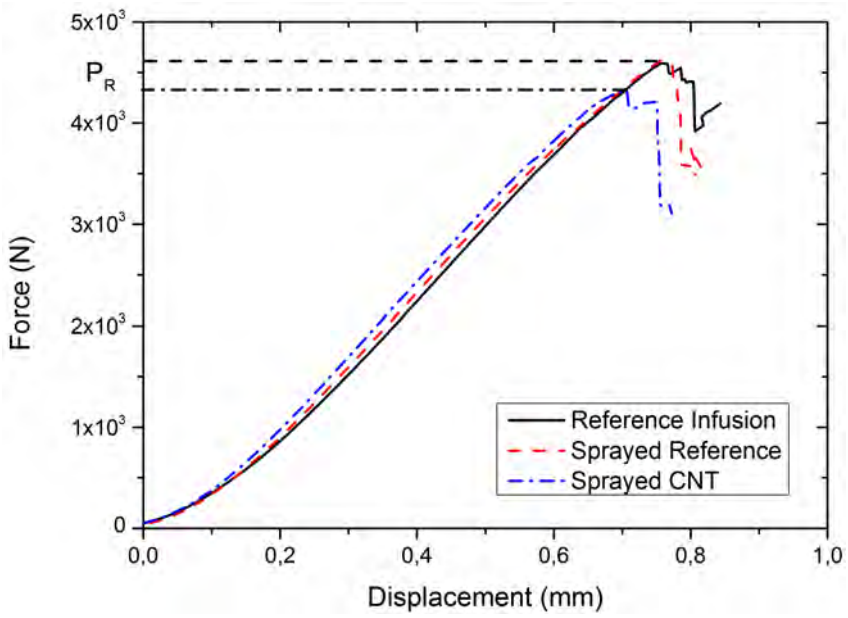

Figure 4.13 – Force - Displacement diagram of the interlaminar shear strength testing

On these diagrams it can be seen that the materials exhibit a short non-linear behavior for low loads. Whereas for higher loads the materials exhibit a linear response to the applied force until abrupt failure (presence sometimes of a sawtooth outline, which is a distinctive feature of a shear failure in multiple plane inside the laminated material). The apparent interlaminar shear strength was calculated following equation 2.15 using the maximum load (P_R) measured on the curves. The mean values and standard deviation of the ILSS are listed in table 4.7 and represented on graph 4.14.

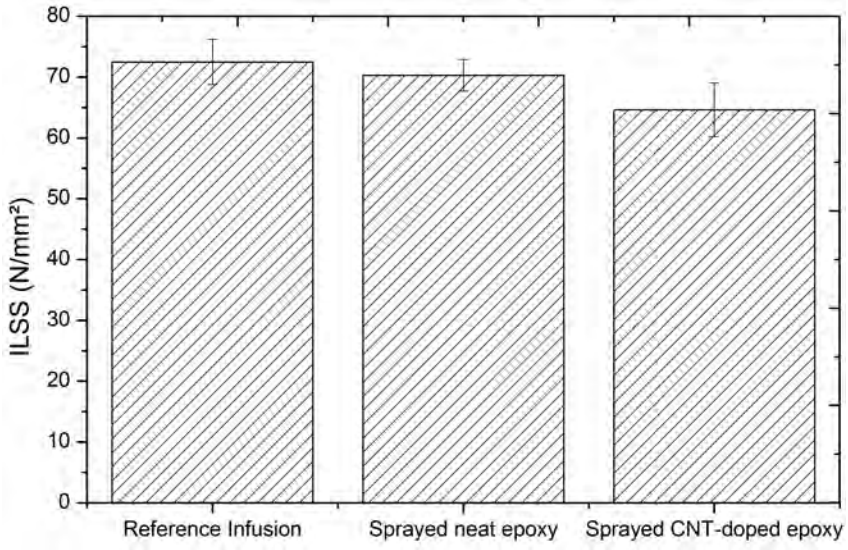

Figure 4.14 – ILSS of the three types of produced materials

	ILSS $(N.m^{-2})$
Reference Infusion	72.5 ± 3.7
Sprayed Neat Epoxy	70.3 ± 2.6
Sprayed CNT-doped Epoxy	64.6 ± 4.4

Table 4.7 – ILSS of the three types of produced materials

The reference samples achieve a mean interlaminar shear strength value of 72 N.m^{-2}. This value is in the range of what is typically achieved for carbon fiber / epoxy composites [140]. It can also be noticed that the standard deviation for all three series tested amounts to a few Newtons per square meter, which is typical for such a test. The ILSS of laminates sprayed with neat resin stays in the same range reaching 70 N.m^{-2}. It can already be stated that the spraying process seems to have no significant influence on the ILSS values, with sprayed samples performing as good as reference samples. The mean value of CNT-doped materials decreases slightly to 65 N.m^{-2}. This minor decrease could be explained by a less homogeneous composite laminates, which the CNTs acting as starting points for interlaminar crack initiation. Nevertheless, taking into account the variance of the results, it can be assumed that neither the spraying process nor the CNTs have a substantial influence on the interlaminar shear strength of our CFRP materials.

Figure 4.15 presents for each material two pictures depicting the fracture profile of various tested ILSS samples (perpendicular to the fiber direction). A close analysis of each fracture profile showed that the failures exclusively took place in interlayer planes (black and white arrows). As the specimens all failed in shear approximately at the neutral fiber axis, the interlaminar shear strength can be calculated in accordance with the formula 2.15. Should a specimen fail in flexure or by plastic deformation, the result obtained by this formula is not a true shear strength at failure.

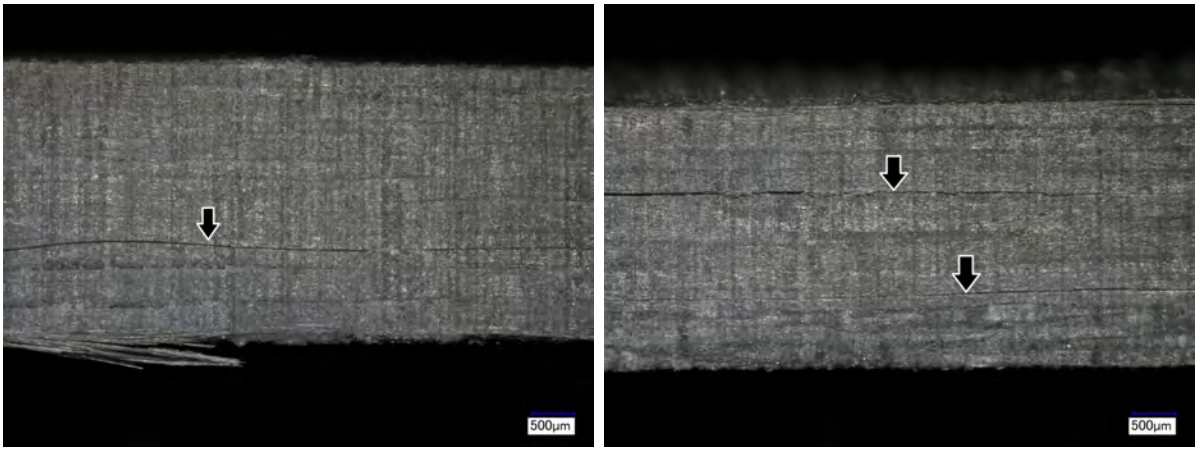

(a) Reference Infusion

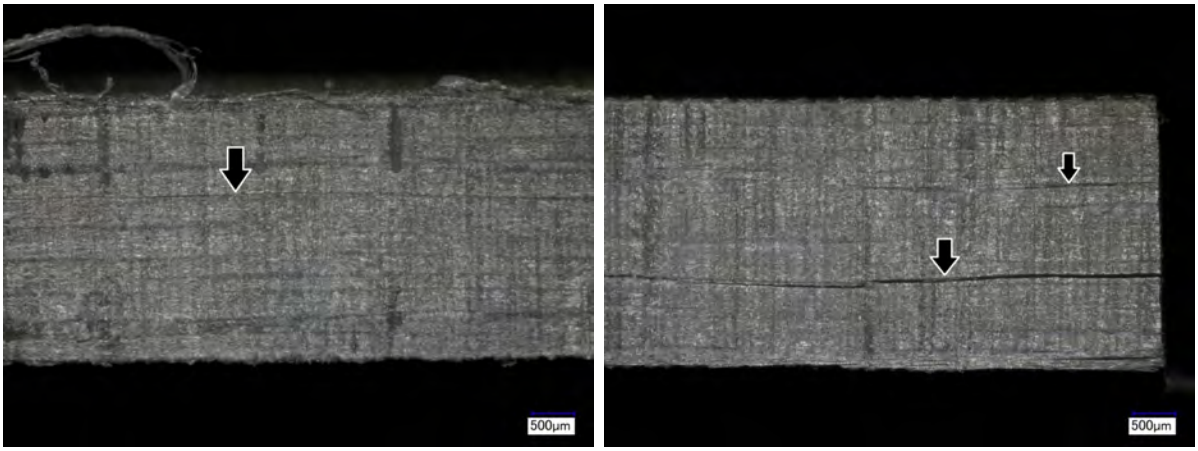

(b) Spray Neat

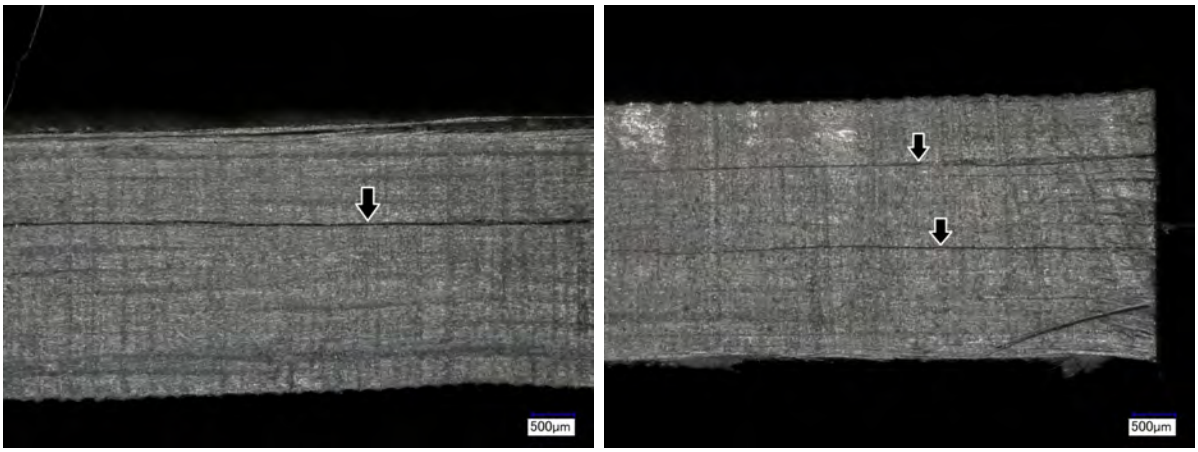

(c) Spray CNT

Figure 4.15 – Failure surface of tested ILSS samples

Interlaminar Fracture Toughness

Experimental procedure

At last, the influence of the spray deposition technique and the addition of carbon nanotubes on the Interlaminar Fracture Toughness in mode I (GI) was investigated. These tests have been performed on samples having a $[0]_{12}$ configuration, a symmetrical unidirectional layup was chosen in order for the crack to stay inside the mid-plane. A preexisting crack was generated by inserting a non-stick PTFE film at the laminates mid-plane thus enabling a $0°/0°$ interface to be tested. As presented on figure 4.16 the samples were drilled in order to place the two stirrups linked to the testing machine. This drilling enables the free rotation of the stirrups, avoiding the generation of a flexural moment opposing the one generated while opening the sample. Measurements were performed on samples having the geometry presented on figure 2.13a in chapter 2. Figure 4.17 presents the load / displacement of the arms of the testing machine curves obtained during mode I testing of one representative sample selected for the three materials manufactured. On each sample 10 opening / closing cycles were performed, with an opening speed of 2 mm/min. After each cycle the crack propagation length was measured on both sides (painted with white paint for easier measurements) and a mean value was calculated for further analysis. Between 6 and 8 samples were tested for each material.

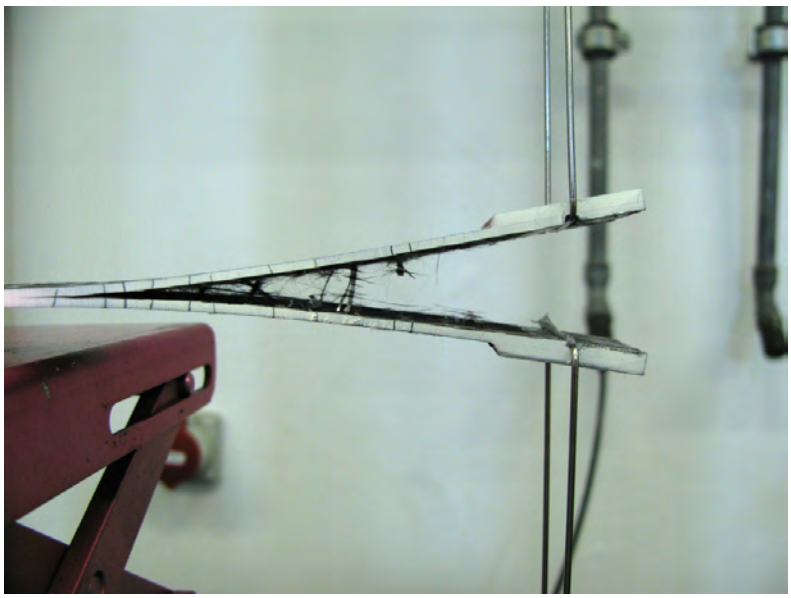

Figure 4.16 – G_I sample being tested

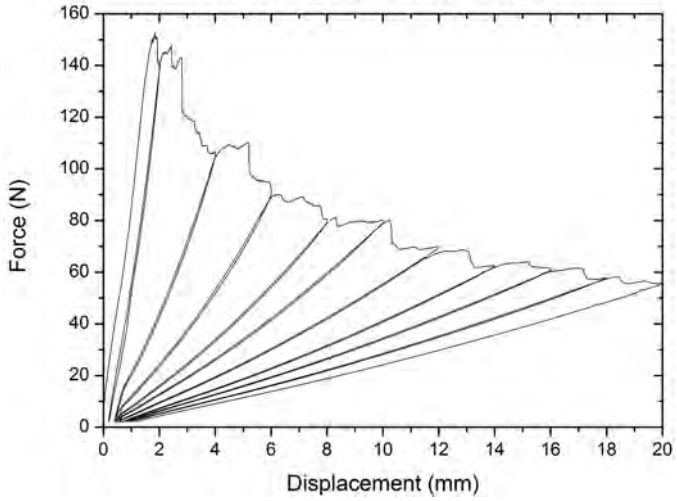

(a) Reference Infusion

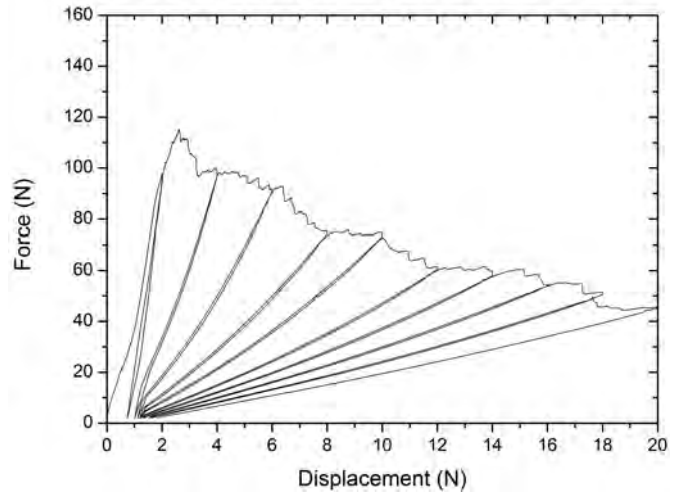

(b) Sprayed neat Epoxy

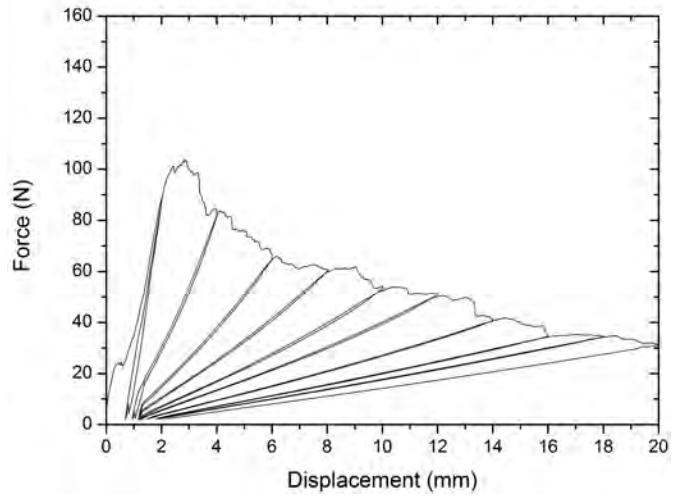

(c) Sprayed CNT-doped Epoxy

Figure 4.17 – Load / displacement curves for the three materials in mode I testing

Figure 4.17 shows that as the crack propagates inside the laminate, the load required to further fracture the sample decreases. The same decreasing trend can be observed for the three materials, but they exhibit different load values. Loads of respectively around 150, 110 and 100 N are required to initiate the crack propagation in the reference infusion, sprayed neat and CNT-doped spray samples. A higher load can be observed for the baseline material compared to the two other laminates, the influence of this values on the G_I will be examined later below. Sudden decreases in load can also be observed on these graphs. These are caused by the rupture of fiber bridges between the upper and lower parts of the samples. This phenomenon can also be observed on figure 4.16.

Compliance

The compliance is defined as the ratio between the displacement of the testing clamps and the applied load.

$$C = \frac{\delta}{F} \tag{4.4}$$

In this work, two models have been used in order to correlate the experimental results to those presented in the literature, the classical beam theory and Berry theory.

Classical Beam Theory

The classical beam theory is a simplification of the linear theory of elasticity which provides a means of calculating the load-carrying and deflection characteristics of beams. It covers the case for small deflections of a beam that is subjected to lateral loads only. In our case, the two half laminates separated by the crack are viewed as two cantilever beams that are built-in at one end and free at the other. In that case, the compliance can be written as in equation 4.5a [141]. With with a the crack length, and α, β and γ three parameters from the model, that can be determined through the plot of $C = f(a)$. In this case the energy release rate in mode I can be written as 4.5b, with w the samples width and F the applied load.

$$C = \alpha.a^3 + \beta.a + \gamma \tag{4.5a}$$

$$G_I = \frac{F^2}{2.w}\left(3.\alpha.a^2 + \beta\right) \tag{4.5b}$$

Berry Theory

Berry [142] presented the following relation between the compliance and the crack length (equation 4.6a), with n and k, two parameters of the model. For the Berry theory, the energy release rate in mode I can be written presented in equation 4.6b.

$$C = \frac{a^n}{k} \tag{4.6a}$$

$$G_I = \frac{n.F^2.a^{n-1}}{2.w.k} \tag{4.6b}$$

Furthermore as presented in section 2.3.6, the energy release rate in mode I can be directly calculated from the load / displacement diagram. The energy is directly proportional to the area under the curve, as represented in section 2.3.6, and can be written as following:

$$G_I = \frac{A}{a.w} \times 10^6 \tag{4.7}$$

Figure 4.18 presents the calculated compliance as a function of the crack length for one representative sample selected for the three materials manufactured (same as above). On this graph, the experimental data is also fitted with the beam and Berry model (equations 4.5a and 4.6a). This analysis was performed for each tested sample and the results are summarized in table 4.8.

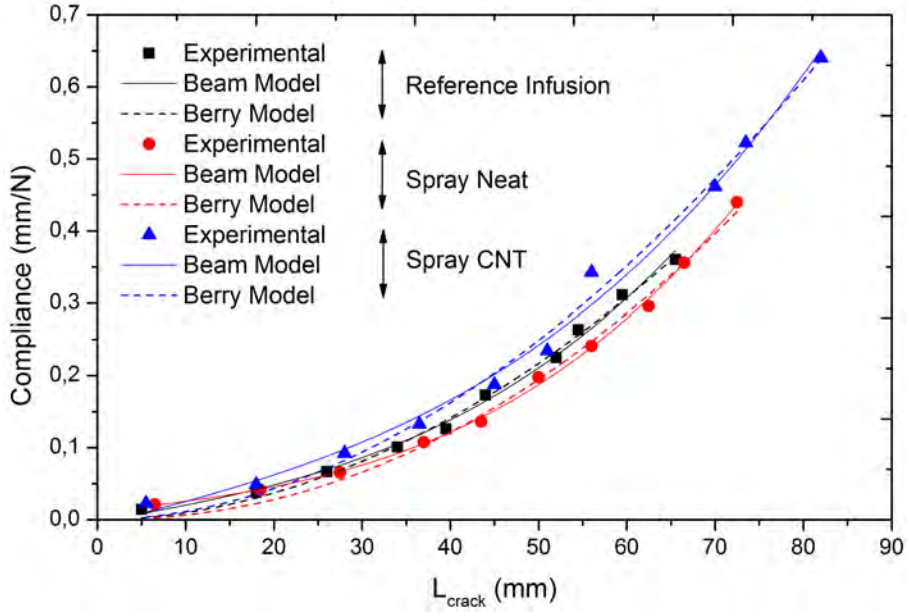

Figure 4.18 – Compliance as a function of crack length

Figure 4.18 shows a very good agreement between the experimental data and both beam and Berry models. This was confirmed by examining closely each sample tested. The parameters values obtained in table 4.8 were in agreement with those found in the relevant literature [143]. It is worth mentioning that the γ coefficient of the beam model give a good appreciation of the quality of the fit between model and experimental values. A low value of γ was obtained, accounting for a good agreement of the experimental data with the beam theory.

Sample	Beam model			Berry model	
	$\alpha \times 10^6$	$\beta \times 10^3$	$\gamma \times 10^{-3}$	n	k $\times 10^{-3}$
Reference infusion	1.16	2.20	3.52	1.89	7.68
Sprayed neat epoxy	0.92	2.51	6.01	1.92	5.55
Sprayed CNT-doped epoxy	0.75	3.08	7.72	1.84	5.64

Table 4.8 – Calculated parameters of the beam and Berry models

Energy release rates in mode I

The energy release rates in mode I were calculated using the surface method for each sample and each cycle performed. The results obtained for the three materials manufactured are presented as a function of the crack length in figure 4.19. A scatter plot is chosen, as to better evaluate the results dispersion. The examination of this data and especially figure 4.19a which presents the results of the infused baseline material, calls into question the results of this first series of test. First, a very high data dispersion can be observed, the results ranging from around 600 to 1300 J.m^{-2}. For the two other material a lower material dispersion is achieved, in the order of magnitude of what is typically achieved for fracture toughness testing. Furthermore, a critical assessment of the fracture toughness energies obtained for this baseline series compared to literature values shows that the G_I values obtained are far to high too be considered relevant.

Moreover, in frame of a previous testing campaign earlier in the doctoral work, an identical material was tested. This material was manufactured using the same base materials (matrix and carbon fibers) and through the same infusion process. The testing method, although only performing one opening / closing cycle, was nearly the same. Furthermore, additional mechanical testing on this laminate showed identical mechanical properties concerning interlaminar shear strength and dynamical mechanical analysis. The load / displacement curves of this previous characterization are presented in figure 4.20. Loads of around 100 N are required to initiate the crack propagation in this early testing laminate, which is in accordance with the sprayed neat and CNT-doped spay laminates. It has been decided to take this early laminate as a baseline value, which is calculated to be around 400 J.m^{-2} (see also table 4.9).

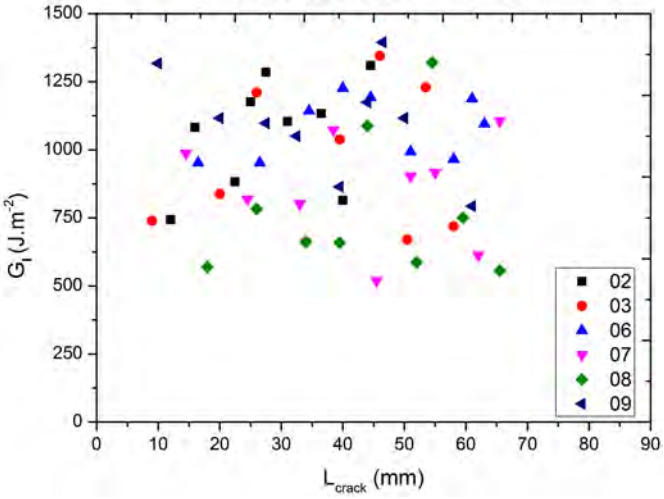

(a) Reference Infusion

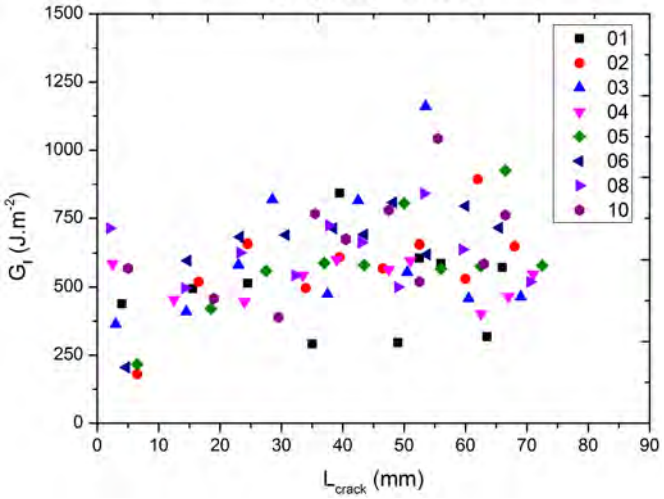

(b) Sprayed neat Epoxy

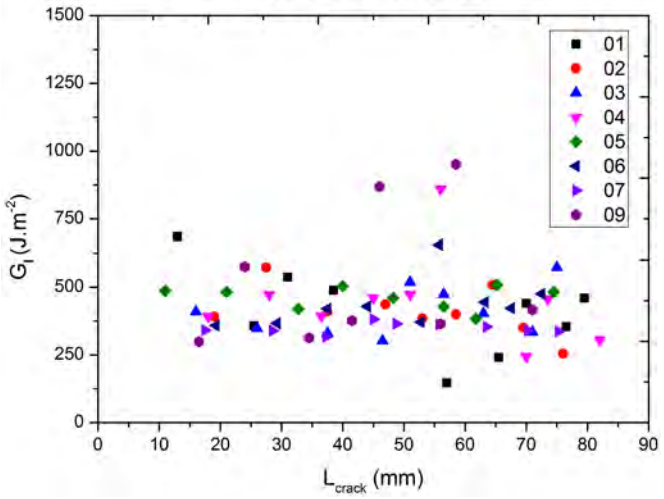

(c) Sprayed CNT-doped Epoxy

Figure 4.19 – G_I values as a function of the crack length

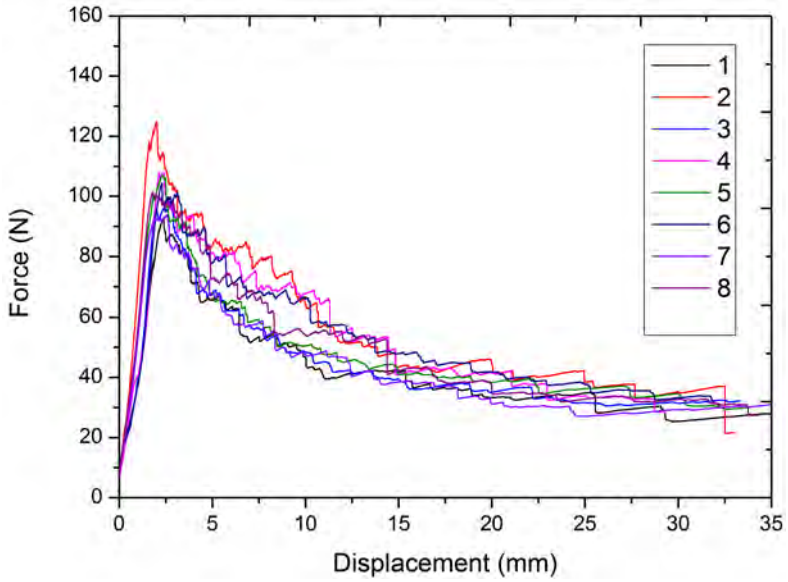

Figure 4.20 – Load / displacement curves for the early laminate testing (Reference Infusion)

Table 4.9 presents the energy release rates for the three materials. This mean value was determined as the center-line of the scatter plot for the sprayed laminates (doped and undoped) and as the mean value of the 8 samples tested in the early baseline material. A slight increase of the G_I value was observed for the neat epoxy sprayed material and a decrease to baseline levels for the 0.75 wt.% CNT doped sprayed material.

Sample	G_I (J.m^{-2})
Reference infusion	423 ± 47
Sprayed neat epoxy	557 ± 61
Sprayed CNT-doped epoxy	400 ± 32

Table 4.9 – G_I values for the three types of material manufactured

It can be assumed that the spray deposition process has a thickening effect on the matrix layer deposited at the mid-plane. A thicker matrix thickness at the fracture interface has been proved to increase G_I values [81]. Concerning the CNT doped material, we assume that the CNT may have in our case a weakening effect on the epoxy polymer, leading to lower G_I values. It was decided to perform SEM observations of the fractured surfaces in order to better understand these results.

SEM observation of the crack surfaces

Figures 4.21, 4.22 and 4.23 present scanning electron microscopy observations performed on the fracture surface of sprayed samples. Figure 4.21 was taken on the surface of a samples manufactured with pristine epoxy, while figures 4.22 and 4.23 were taken on a CNT-doped sample.

On the upper part of the photograph presented on figure 4.21a, the typical imprint left by torn-off carbon fibers can be observed, leaving an empty "bed" (semi-cylindrical pattern). This pattern can also be seen on the related enlargement on figure 4.21b. On these three photographs, it can also be observed the reinforcing threads made of glass-reinforced polypropylene (GFR-PP) appearing at a 60°. As mentioned previously and as observed on the pictures the fibers are hardly compressible. Therefore a certain amount of resin fills up the created cavities. This is a distinctive feature common to all three materials. At last, on these neat-epoxy sprayed samples, a thicker resin layer between carbon fiber plies can be observed (see in particular figure 4.21c. These thicker resin-rich interlayers were observed on both neat and CNT-doped sprayed samples and could be the cause of the higher G_I values obtained for the neat sprayed samples.

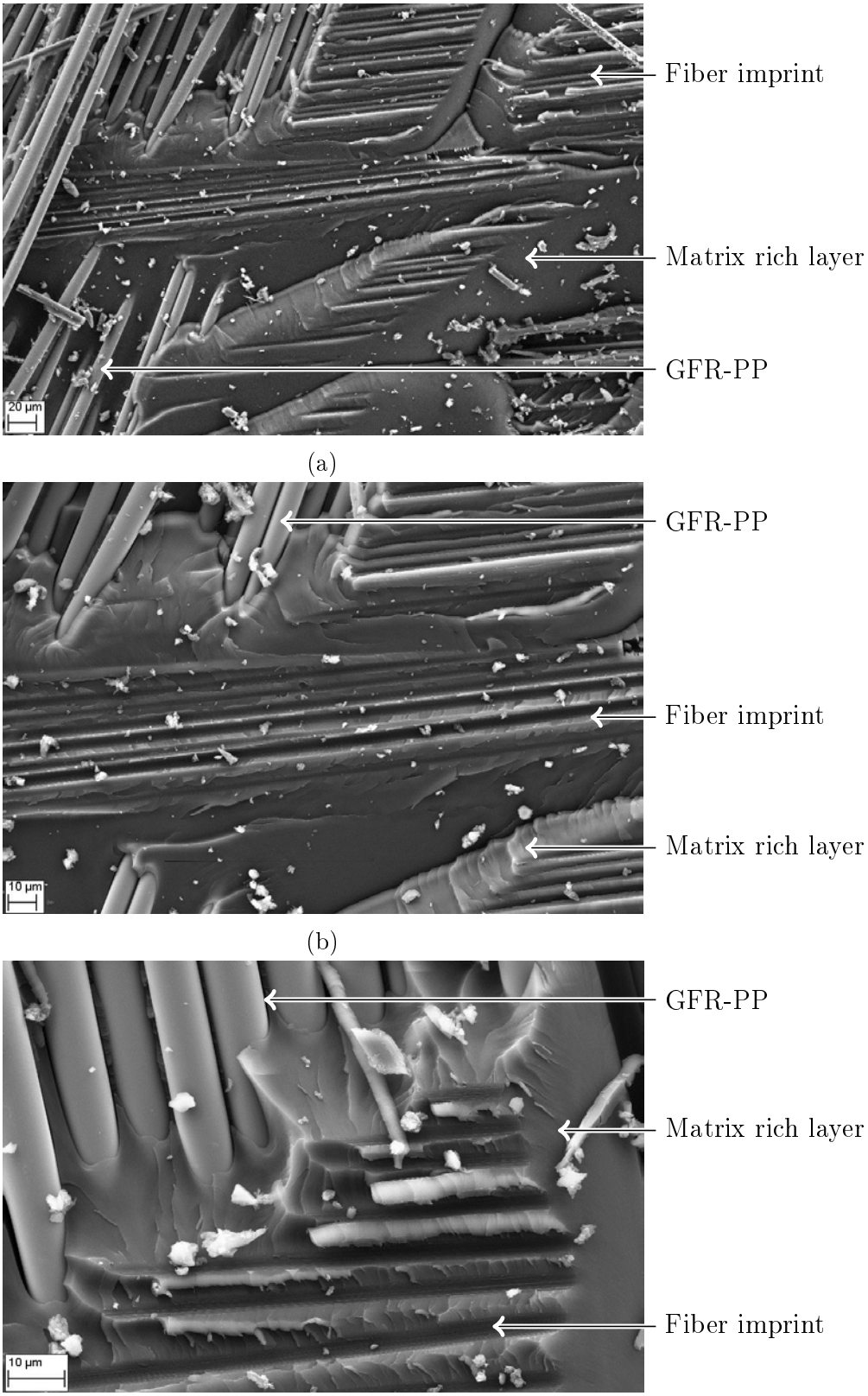

Figure 4.21 – Fracture surface observations of a neat epoxy sprayed sample

On figure 4.22a, the same carbon-fiber imprints can be observed on CNT-doped samples. Similar resin layers between carbon fiber plies can be observed. Figures 4.22b, 4.23a and 4.23b present the detailed observations of these areas. On these surfaces, CNT-rich regions were found at regular intervals. As we only have a two-dimensional overview of the sample, it is difficult to fully conclude on the homogeneous dispersion of the nanotubes throughout the sample. We can nevertheless observe that most of the surfaces where epoxy resin was found, a high density of CNTs could be observed.

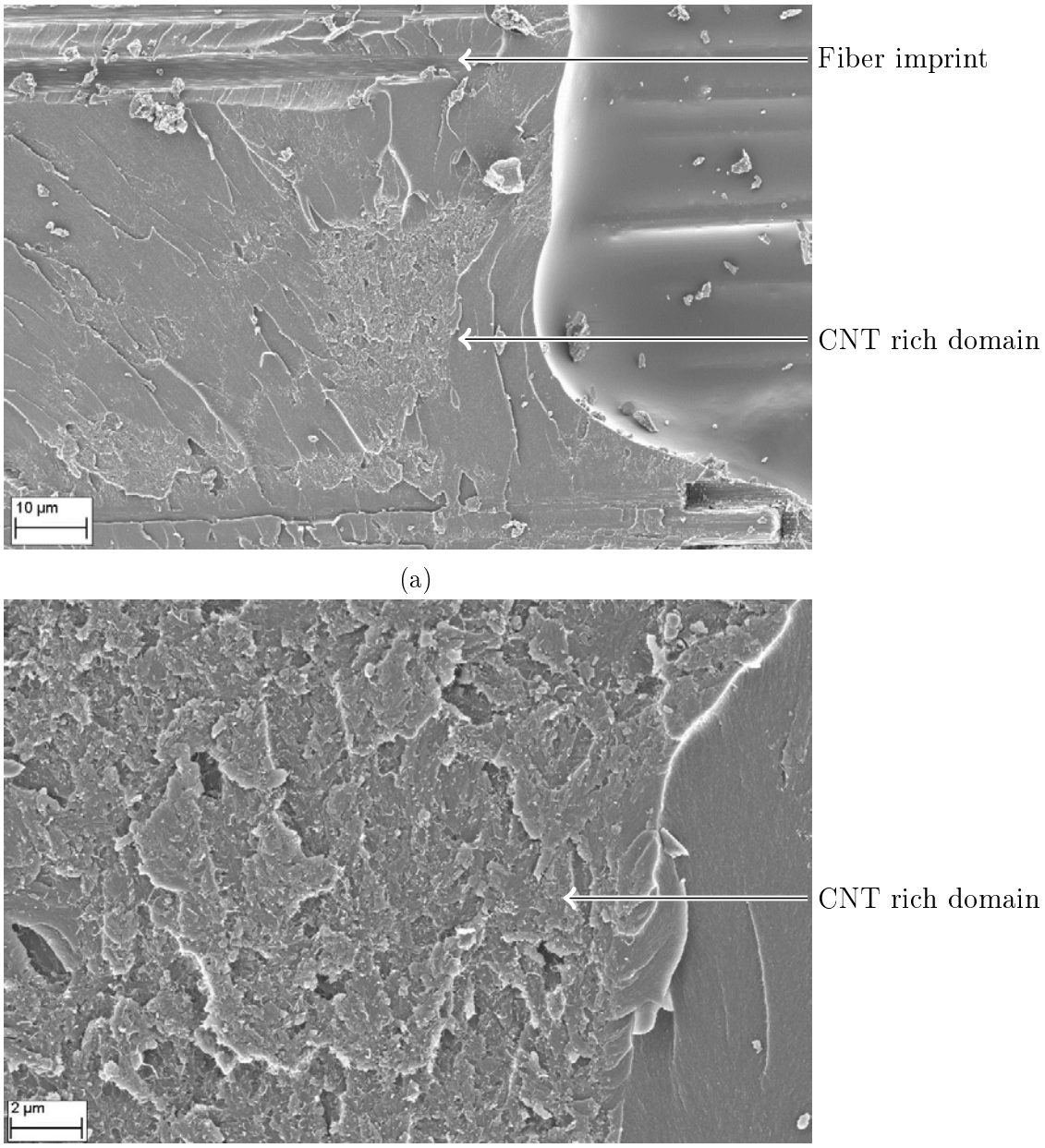

Figure 4.22 – Fracture surface observations of a CNT-doped sprayed sample

Figures 4.22b and 4.23a present two enlargements of these domains. A high density of CNTs can be found in these regions. The CNTs seem to be well dispersed, observing single CNTs was possible. The CNTs do not seem to adopt a preferential orientation, the nanotubes being randomly oriented. At last, further enlargements of these zones (figure 4.23b) made the measurement of the free standing length of the CNTs possible. We define the free standing length, as the length which can be observed standing out of the matrix. The free standing length was estimated to approximately 280 nm.

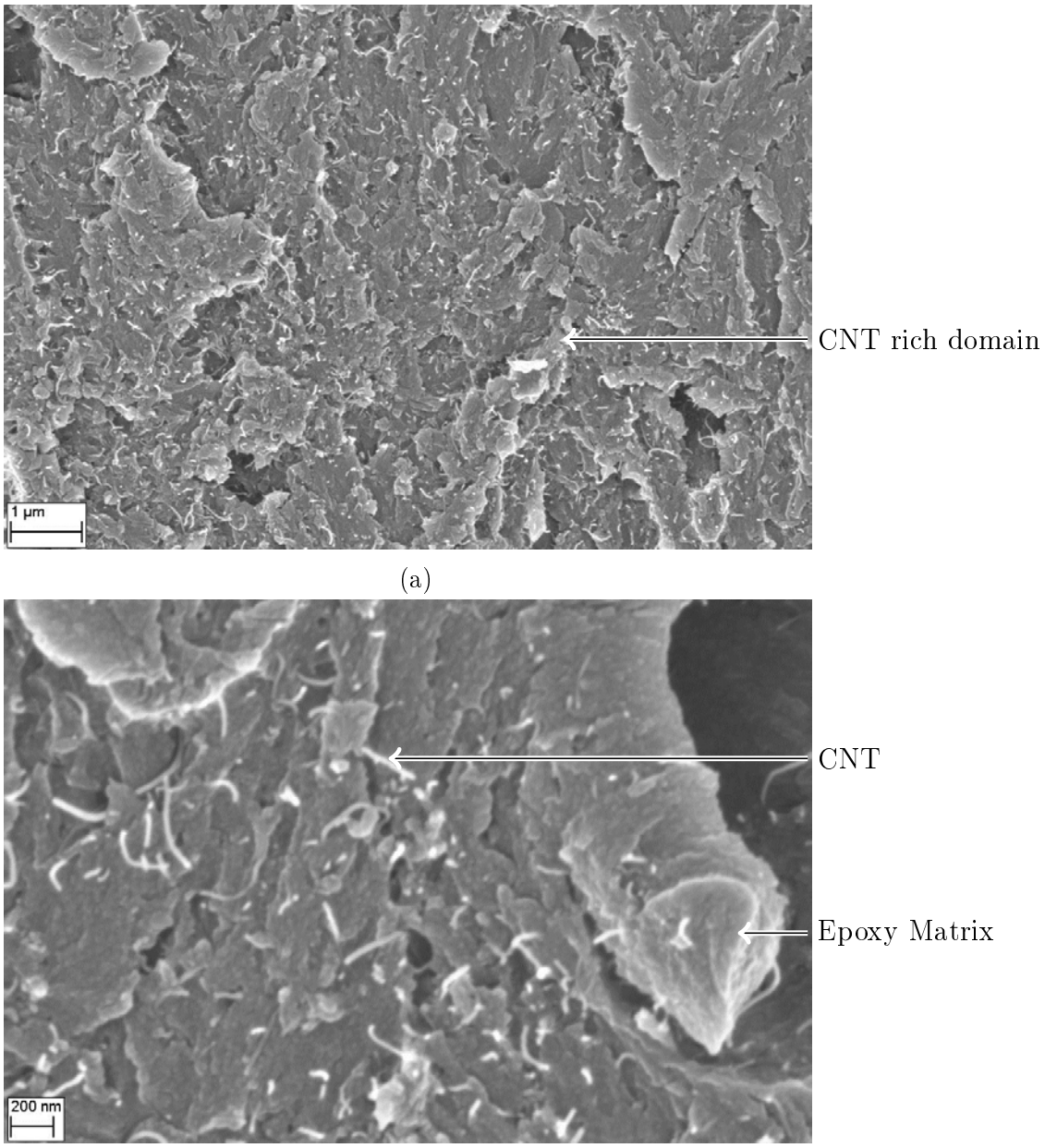

Figure 4.23 – Fracture surface observations of a CNT-doped sprayed sample

The G_I results obtained in this study, are in the same range of magnitude of those obtained by Maillot [21]. In this previous study, the three central interlayers were sprayed with neat and CNT-doped RTM6 resin. The neat-sprayed samples exhibited a G_I of 380 J.m^{-2} (same value as the infused baseline) and the 1 wt.% doped samples a G_I of 360 J.m^{-2}.

In the previous works, where an increase of the fracture toughness energy was observed (El-Sawi et al. [58], Garcia et al. [53], Wicks et al. [75]), overall longer CNTs were used: in the range of 10 μm for El-Sawi, and sometimes up to 20 μm for Wicks et al. This could lead to a higher energy involved when trying to pull out the CNTs during crack propagation.

By looking at the results from the SEM observations, it seems that the nanotubes used in our study are shorter (free standing length of around 280 nm). Pulling this shorter CNT length out of the laminate may require less energy than for higher CNT length, and we may thus suppose that the influence of the nanotubes on the energy release rate is negligible.

Conclusion and Outlook

In an introductory literature survey, it has been shown how the inhomogeneity of the electrical conductivity of laminated composite materials is one of the main obstacles this technology faces when applied to aircraft structures. Therefore, the first goal of this work was to improve and homogenize the through-thickness electrical conductivity of CFRPs. As a solution, multiscale composites manufacturing was proposed through addition of carbon nanotubes to a standard composite. Yet, the literature review reported several obstacles prohibiting the use of state-of-the-art composite manufacturing techniques to this purpose. In this work, it has been proposed to solve theses issues of CNT filtering, increase of resin viscosity and upscalability through the use of an innovative spraying process. Thanks to the combined use of a calendering and spraying process, MWCNTs were dispersed in the epoxy matrix then sprayed on the dry fiber plies and subsequently cured to produce CNT-doped CFRP.

At the same time, it was critical to assess the properties of the CNT / epoxy nanocomposite. The dispersion state of the nanotubes inside the epoxy matrix was assessed by the measurement of DC conductivity of the nanocomposites revealing a percolation threshold at around p_c=0.25 wt.% CNTs and that a maximum DC conductivity of 6.10^{-3} S.m^{-1} was achieved for a CNT concentration of 0.75 wt.% CNTs. This concentration was chosen for the spraying process as it is the best CNT loading / conductivity achieved ratio. From the rheological analysis it was observed that the viscosity at low shearing rates followed a different trend as a function of temperature, whether the MWCNT concentration was below or above the percolation threshold. Based on these observations, it was assumed that there might be a relation between the formation of the electrical percolation network and the mechanical behavior of the CNT / epoxy suspension. The analysis of the cure kinetics of the doped matrix provided relevant information and helped setting-up a suitable CFRP manufacturing process.

Little influence of the nanotubes or the spraying process on the mechanical properties (dynamical mechanical analysis, interlaminar shear strength and interlaminar fracture toughness) was noticed. The manufactured CNT-doped and / or sprayed material achieved similar mechanical properties compared to state-of-the-art CFRP materials. On the other hand, an influence of the carbon nanotubes on the transverse (Z direction) and orthogonal (Y direction) electrical conductivity could be obtained. A slight but noticeable increase of the conductivity was achieved (0.8 to 2.1 $S.m^{-1}$ for the Z-direction and 9.3 to 13.8 $S.m^{-1}$ for the Y-direction). More than the inherent values reached, the electrical conductivity was homogenized throughout the whole laminate. This achievement could be one step in order to solve the issue of "edge-glow" on aeronautical structures.

Outlook

This electrical conductivity improvement has to be put into perspective, especially considering the considerable challenges the aeronautical industry is facing concerning the electrical conductivity of CFRP. For instance, in order to be able to deal with the indirect effects of a lightning strike, CFRP materials should exhibit a transverse electrical conductivity around 10^2 $S.m^{-1}$.

In chapter 3, a local viscosity increase was noted when studying the thermorheological behavior of the CNT-doped matrix. This phenomenon, referred as "bump", should be further investigated to shed light on this particular behavior. Moreover, it would be relevant to look into the impact resistance of CNT-doped CFRP as it is a critical parameter in the case of laminated composite materials.

Thirdly, investigations are on-going to analyze the thermal conductivity of CNT / epoxy nanocomposites and CNT-doped CFRP. Current requirements in heat-dissipating structural components stimulate interest in the thermal conductivity of filled epoxy and epoxy composites.

At last, a suitable processing method to insert nanoparticles into the matrix of CFRPs was developed. This processing technology could be applied to nano- or micro-particles exhibiting a higher conductivity. For instance, Lonjon et al. [139] manufactured metallic nanowires nanocomposites, which reached a conductivity of 10^2 $S.m^{-1}$. A combination of both techniques appears promising, but should be limited to the outer ply of the laminate as the addition of nanowires generates additional weight to the material.

List of Tables

List of Figures

Bibliography

[1] B R. Swopes, "This day in aviation: 1 january 1914." http://www.thisdayinaviation.com/1-january-1914/, 2014.

[2] International Air Transport Association, "Passenger demand maintains historic growth rates in 2013."

[3] Airlines for America, "Cost of air travel compared to other goods and services."

[4] Ginger Gardiner, "Lightning strike protection for composite structures." http://www.compositesworld.com/articles/lightning-strike-protection-for-composite-structures, 2006.

[5] S. Iijima *et al.*, "Helical microtubules of graphitic carbon," *Nature*, vol. 354, no. 6348, pp. 56–58, 1991.

[6] D. D. Chung, *Conposite Materials : Science and Applications*. London: Springer, 2nd ed. ed., 2010.

[7] A. Loiseau, P. Launois, P. Petit, S. Roche, and J.-P. Salvetat, *Understanding Carbon Nanotubes: from Basics to Applications*, vol. 677. Berlin: Springer, 2006.

[8] M. Monthioux, E. Flahaut, C. Laurent, W. Escoffier, B. Raquet, W. Bacsa, P. Puech, B. Machado, and P. Serp, "Properties of carbon nanotubes," in *Handbook of Nanomaterials Properties*, pp. 1–49, Springer, 2014.

[9] M. Biron, *Thermoplastics and Thermoplastic Composites: Technical Information for Plastics Users*. Elsevier, 2007.

[10] G. Odian, *Principles of Polymerization*. Hoboken and New Jersey: John Wiley & Sons, Inc, fourth edition ed., 2004.

[11] C. Cassignol, *Mélanges conducteurs époxyde/polypyrrole: élaboration et caractérisation*. PhD thesis, Université Paul Sabatier, Toulouse, France, 1998.

[12] P. Bardonnet, *Matières thermodurcissables: monographies: Résines époxydes (EP) - Composants et propriétés*, vol. a3465. Paris, France: Éditions Techniques de l'ingénieur, 1992.

[13] N. Grossiord, J. Loos, O. Regev, and C. E. Koning, "Toolbox for dispersing carbon nanotubes into polymers to get conductive nanocomposites," *Chem. Mater.*, vol. 18, no. 5, pp. 1089–1099, 2006.

[14] K. L. Lu, R. M. Lago, Y. K. Chen, Green, M. L. H., Harris, P. J. F., and S. C. Tsang, "Mechanical damage of carbon nanotubes by ultrasound," *Carbon*, vol. 34, no. 6, pp. 814–816, 1996.

[15] J. Sandler, Shaffer, M. S. P, T. Prasse, W. Bauhofer, K. Schulte, and A. H. Windle, "Development of a dispersion process for carbon nanotubes in an epoxy matrix and the resulting electrical properties," *Polymer*, vol. 40, no. 21, pp. 5967–5971, 1999.

[16] O. Schwarz, F. W. Ebeling, and B. Furth, *Kunststoffverarbeitung*. Vogel-Fachbuch, Vogel Verlag Und Druck, 1997.

[17] F. H. Gojny, M. H. Wichmann, U. Köpke, B. Fiedler, and K. Schulte, "Carbon nanotube-reinforced epoxy-composites: enhanced stiffness and fracture toughness at low nanotube content," *Composites Science and Technology*, vol. 64, no. 15, pp. 2363–2371, 2004.

[18] F. H. Gojny, Wichmann, Malte H. G., B. Fiedler, W. Bauhofer, and K. Schulte, "Influence of nano-modification on the mechanical and electrical properties of conventional fibre-reinforced composites," *Composites Part A: Applied Science and Manufacturing*, vol. 36, no. 11, pp. 1525–1535, 2005.

[19] E. T. Thostenson and T.-W. Chou, "Processing-structure-multi-functional property relationship in carbon nanotube/epoxy composites," *Carbon*, vol. 44, no. 14, pp. 3022–3029, 2006.

[20] G. Olowojoba, S. Sathyanarayana, B. Caglar, B. Kiss-Pataki, I. Mikonsaari, C. Hübner, and P. Elsner, "Influence of process parameters on the morphology, rheological and dielectric properties of three-roll-milled multiwalled carbon nanotube/epoxy suspensions," *Polymer*, vol. 54, no. 1, pp. 188–198, 2013.

[21] A.-L. Tassel-Maillot, *On the potential of carbon nanotube as reinforcement for carbon-fiber reinforced epoxy for aeronautic applications*. PhD thesis, Technische Universität Hamburg-Harburg, Hamburg, Germany, To be published.

[22] S. Barrau, P. Demont, A. Peigney, C. Laurent, and C. Lacabanne, "Dc and ac conductivity of carbon nanotubes−polyepoxy composites," *Macromolecules*, vol. 36, no. 14, pp. 5187–5194, 2003.

[23] J. Cho, I. M. Daniel, and D. A. Dikin, "Effects of block copolymer dispersant and nanotube length on reinforcement of carbon/epoxy composites," *Composites Part A: Applied Science and Manufacturing*, vol. 39, no. 12, pp. 1844–1850, 2008.

[24] P. Liu, "Modifications of carbon nanotubes with polymers," *European Polymer Journal*, vol. 41, no. 11, pp. 2693–2703, 2005.

[25] S. Barrau, P. Demont, E. Perez, A. Peigney, C. Laurent, and C. Lacabanne, "Effect of palmitic acid on the electrical conductivity of carbon nanotubes−epoxy resin composites," *Macromolecules*, vol. 36, no. 26, pp. 9678–9680, 2003.

[26] A. Bassil, P. Puech, G. Landa, W. Bacsa, S. Barrau, P. Demont, C. Lacabanne, E. Perez, R. Bacsa, and E. Flahaut, "Spectroscopic detection of carbon nanotube interaction with amphiphilic molecules in epoxy resin composites," *Journal of applied physics*, vol. 97, no. 3, p. 034303, 2005.

[27] A.-C. Courbaron Gilbert, N.-E. El Bounia, E. Péré, L. Billon, and C. Derail, "Dispersion improvement of carbon nanotubes in epoxy resin using amphiphilic block copolymers," 2010.

[28] J. M. Brown, D. P. Anderson, R. S. Justice, K. Lafdi, M. Belfor, K. L. Strong, and D. W. Schaefer, "Hierarchical morphology of carbon single-walled nanotubes during sonication in an aliphatic diamine," *Polymer*, vol. 46, no. 24, pp. 10854–10865, 2005.

[29] P. Calvert, "Nanotube composites: a recipe for strength," *Nature*, vol. 399, no. 6733, pp. 210–211, 1999.

[30] S. J. Frankland, A. Caglar, D. W. Brenner, and M. Griebel, "Molecular simulation of the influence of chemical cross-links on the shear strength of carbon nanotube-polymer interfaces," *The Journal of Physical Chemistry B*, vol. 106, no. 12, pp. 3046–3048, 2002.

[31] M. Moniruzzaman and K. I. Winey, "Polymer nanocomposites containing carbon nanotubes," *Macromolecules*, vol. 39, no. 16, pp. 5194–5205, 2006.

[32] K. K. Wong, S. Q. Shi, and Lau, Alan Kin Tak, "Mechanical and thermal behavior of a polymer composite reinforced with functionalized carbon nanotubes," *Key Engineering Materials*, vol. 334, pp. 705–708, 2007.

[33] M. Moniruzzaman, F. Du, N. Romero, and K. I. Winey, "Increased flexural modulus and strength in swnt/epoxy composites by a new fabrication method," *Polymer*, vol. 47, no. 1, pp. 293–298, 2006.

[34] F. H. Gojny, J. Nastalczyk, Z. Roslaniec, and K. Schulte, "Surface modified multi-walled carbon nanotubes in cnt/epoxy-composites," *Chemical Physics Letters*, vol. 370, no. 5–6, pp. 820–824, 2003.

[35] M.-L. Sham and J.-K. Kim, "Surface functionalities of multi-wall carbon nanotubes after uv/ozone and teta treatments," *Carbon*, vol. 44, no. 4, pp. 768–777, 2006.

[36] J. A. Kim, D. G. Seong, T. J. Kang, and J. R. Youn, "Effects of surface modification on rheological and mechanical properties of cnt/epoxy composites," *Carbon*, vol. 44, no. 10, pp. 1898–1905, 2006.

[37] E. T. Mickelson, C. B. Huffman, A. G. Rinzler, R. E. Smalley, R. H. Hauge, and J. L. Margrave, "Fluorination of single-wall carbon nanotubes," *Chemical Physics Letters*, vol. 296, no. 1–2, pp. 188–194, 1998.

[38] V. N. Khabashesku, J. L. Margrave, and E. V. Barrera, "Functionalized carbon nanotubes and nanodiamonds for engineering and biomedical applications," *Proceedings of Diamond 2004, the 15th European Conference on Diamond, Diamond-Like Materials, Carbon Nanotubes, Nitrides and Silicon Carbide*, vol. 14, no. 3–7, pp. 859–866, 2005.

[39] H. Xie, B. Liu, Z. Yuan, J. Shen, and R. Cheng, "Cure kinetics of carbon nanotube/tetrafunctional epoxy nanocomposites by isothermal differential scanning calorimetry," *Journal of Polymer Science Part B: Polymer Physics*, vol. 42, no. 20, pp. 3701–3712, 2004.

[40] K. Tao, S. Yang, J. C. Grunlan, Y.-S. Kim, B. Dang, Y. Deng, R. L. Thomas, B. L. Wilson, and X. Wei, "Effects of carbon nanotube fillers on the curing processes of epoxy resin–based composites," *Journal of applied polymer science*, vol. 102, no. 6, pp. 5248–5254, 2006.

[41] D. Puglia, L. Valentini, I. Armentano, and J. M. Kenny, "Effects of single-walled carbon nanotube incorporation on the cure reaction of epoxy resin and its detection by raman spectroscopy," *Diamond and related materials*, vol. 12, no. 3, pp. 827–832, 2003.

[42] A.-C. Courbaron Gilbert, L. Billon, N. El Bounia, and C. Derail, "Multi-walled carbon nanotubes as unexpected accelerators of chemical reactions," *Polymer International*, vol. 62, no. 4, pp. 616–620, 2013.

[43] M. Abdalla, D. Dean, P. Robinson, and E. Nyairo, "Cure behavior of epoxy/mwcnt nanocomposites: The effect of nanotube surface modification," *Polymer*, vol. 49, no. 15, pp. 3310–3317, 2008.

[44] J. Bae, J. Jang, and S.-H. Yoon, "Cure behavior of the liquid–crystalline epoxy/carbon nanotube system and the effect of surface treatment of carbon fillers on cure reaction," *Macromolecular Chemistry and Physics*, vol. 203, no. 15, pp. 2196–2204, 2002.

[45] K. Yang, M. Gu, Y. Jin, G. Mu, and X. Pan, "Influence of surface treated multi-walled carbon nanotubes on cure behavior of epoxy nanocomposites," *Composites Part A: Applied Science and Manufacturing*, vol. 39, no. 10, pp. 1670–1678, 2008.

[46] H. Miyagawa and L. T. Drzal, "Thermo-physical and impact properties of epoxy nanocomposites reinforced by single-wall carbon nanotubes," *Polymer*, vol. 45, no. 15, pp. 5163–5170, 2004.

[47] E. S. Choi, J. S. Brooks, D. L. Eaton, M. S. Al-Haik, M. Y. Hussaini, H. Garmestani, D. Li, and K. Dahmen, "Enhancement of thermal and electrical properties of carbon nanotube polymer composites by magnetic field processing," *Journal of applied physics*, vol. 94, no. 9, pp. 6034–6039, 2003.

[48] E. Camponeschi, R. Vance, M. Al-Haik, H. Garmestani, and R. Tannenbaum, "Properties of carbon nanotube–polymer composites aligned in a magnetic field," *Carbon*, vol. 45, no. 10, pp. 2037–2046, 2007.

[49] C. A. Martin, Sandler, J. K. W., A. H. Windle, M.-K. Schwarz, W. Bauhofer, K. Schulte, and Shaffer, M. S. P., "Electric field-induced aligned multi-wall carbon nanotube networks in epoxy composites," *Polymer*, vol. 46, no. 3, pp. 877–886, 2005.

[50] Q. Wang, J. Dai, W. Li, Z. Wei, and J. Jiang, "The effects of cnt alignment on electrical conductivity and mechanical properties of swnt/epoxy nanocomposites," *Composites Science and Technology*, vol. 68, no. 7–8, pp. 1644–1648, 2008.

[51] R. A. Pearson and A. F. Yee, "Toughening mechanisms in thermoplastic-modified epoxies: 1. modification using poly(phenylene oxide)," *Polymer*, vol. 34, no. 17, pp. 3658–3670, 1993.

[52] F. H. Gojny, Wichmann, Malte H. G., B. Fiedler, W. Bauhofer, and K. Schulte, "Influence of nano-modification on the mechanical and electrical properties of conventional fibre-reinforced composites," *Composites Part A: Applied Science and Manufacturing*, vol. 36, no. 11, pp. 1525–1535, 2005.

[53] E. J. Garcia, B. L. Wardle, and A. John Hart, "Joining prepreg composite interfaces with aligned carbon nanotubes," *Composites Part A: Applied Science and Manufacturing*, vol. 39, no. 6, pp. 1065–1070, 2008.

[54] B. Kim, J. Lee, and I. Yu, "Electrical properties of single-wall carbon nanotube and epoxy composites," *Journal of applied physics*, vol. 94, no. 10, pp. 6724–6728, 2003.

[55] J. K. Sandler, J. E. Kirk, I. A. Kinloch, M. S. Shaffer, and A. H. Windle, "Ultra-low electrical percolation threshold in carbon-nanotube-epoxy composites," *Polymer*, vol. 44, no. 19, pp. 5893–5899, 2003.

[56] A. Allaoui, S. Bai, H.-M. Cheng, and J. B. Bai, "Mechanical and electrical properties of a mwnt/epoxy composite," *Composites Science and Technology*, vol. 62, no. 15, pp. 1993–1998, 2002.

[57] S. Cui, R. Canet, A. Derre, M. Couzi, and P. Delhaes, "Characterization of multiwall carbon nanotubes and influence of surfactant in the nanocomposite processing," *Carbon*, vol. 41, no. 4, pp. 797–809, 2003.

[58] I. El Sawi, *Dispersion de nanotubes de carbone et intégration de la fonction de conductivité électrique dans les matériaux composites structuraux*. PhD thesis, Université de Toulouse, Toulouse, France, 2010.

[59] F. H. Gojny, Wichmann, Malte H. G., B. Fiedler, I. A. Kinloch, W. Bauhofer, A. H. Windle, and K. Schulte, "Evaluation and identification of electrical and thermal conduction mechanisms in carbon nanotube/epoxy composites," *Polymer*, vol. 47, no. 6, pp. 2036–2045, 2006.

[60] W. K. Hsu, V. Kotzeva, Watts, P. C. P, and G. Z. Chen, "Circuit elements in carbon nanotube-polymer composites," *Carbon*, vol. 42, no. 8–9, pp. 1707–1712, 2004.

[61] J. Li, P. C. Ma, W. S. Chow, C. K. To, B. Z. Tang, and J.-K. Kim, "Correlations between percolation threshold, dispersion state, and aspect ratio of carbon nanotubes," *Advanced Functional Materials*, vol. 17, no. 16, pp. 3207–3215, 2007.

[62] M. B. Bryning, D. E. Milkie, M. F. Islam, J. M. Kikkawa, and A. G. Yodh, "Thermal conductivity and interfacial resistance in single-wall carbon nanotube epoxy composites," *Applied Physics Letters*, vol. 87, no. 16, p. 161909, 2005.

[63] M. J. Biercuk, M. C. Llaguno, M. Radosavljevic, J. K. Hyun, A. T. Johnson, and J. E. Fischer, "Carbon nanotube composites for thermal management," *Applied Physics Letters*, vol. 80, no. 15, pp. 2767–2769, 2002.

[64] A. Yu, M. E. Itkis, E. Bekyarova, and R. C. Haddon, "Effect of single-walled carbon nanotube purity on the thermal conductivity of carbon nanotube-based composites," *Applied Physics Letters*, vol. 89, no. 13, p. 133102, 2006.

[65] H. Qian, E. S. Greenhalgh, Shaffer, Milo S. P., and A. Bismarck, "Carbon nanotube-based hierarchical composites: a review," *J. Mater. Chem.*, vol. 20, no. 23, pp. 4751–4762, 2010.

[66] A. B. Strong, *Fundamentals of composites manufacturing: materials, methods and applications*. Society of Manufacturing Engineers, 2008.

[67] A. Godara, L. Mezzo, F. Luizi, A. Warrier, S. V. Lomov, A. W. van Vuure, L. Gorbatikh, P. Moldenaers, and I. Verpoest, "Influence of carbon nanotube reinforcement on the processing and the mechanical behaviour of carbon fiber/epoxy composites," *Carbon*, vol. 47, no. 12, pp. 2914–2923, 2009.

[68] M. Kim, Y.-B. Park, O. I. Okoli, and C. Zhang, "Processing, characterization, and modeling of carbon nanotube-reinforced multiscale composites," *Composites Science and Technology*, vol. 69, no. 3, pp. 335–342, 2009.

[69] J. Zhao, L. Liu, Q. Guo, J. Shi, G. Zhai, J. Song, and Z. Liu, "Growth of carbon nanotubes on the surface of carbon fibers," *Carbon*, vol. 46, no. 2, pp. 380–383, 2008.

[70] E. Bekyarova, Thostenson, E. T., A. Yu, H. Kim, J. Gao, J. Tang, Hahn, H. T., T.-W. Chou, Itkis, M. E., and Haddon, R. C., "Multiscale carbon nanotube−carbon fiber reinforcement for advanced epoxy composites," *Langmuir*, vol. 23, no. 7, pp. 3970–3974, 2007.

[71] S.-L. Gao, E. Mäder, and R. Plonka, "Nanocomposite coatings for healing surface defects of glass fibers and improving interfacial adhesion," *Composites Science and Technology*, vol. 68, no. 14, pp. 2892–2901, 2008.

[72] P. Karapapas, S. Tsantzalis, E. Fiamegou, A. Vavouliotis, K. Dassios, and V. Kostopoulos, "Multi-wall carbon nanotubes chemically grafted and physically adsorpted on reinforced carbon fibres," *Adv Compos Lett*, vol. 17, pp. 103–107, 2008.

[73] I. El Sawi, P. A. Olivier, P. Demont, and H. Bougherara, "Investigation of the effect of double-walled carbon nanotubes on the curing reaction kinetics and shear flow of an epoxy resin," *Journal of Applied Polymer Science*, vol. 126, no. 1, pp. 358–366, 2012.

[74] S. S. Wicks, R. G. de Villoria, and B. L. Wardle, "Interlaminar and intralaminar reinforcement of composite laminates with aligned carbon nanotubes," *Composites Science and Technology*, vol. 70, no. 1, pp. 20–28, 2010.

[75] S. S. Wicks, W. Wang, M. R. Williams, and B. L. Wardle, "Multi-scale interlaminar fracture mechanisms in woven composite laminates reinforced with aligned carbon nanotubes," *Composites Science and Technology*, vol. 100, no. 0, pp. 128–135, 2014.

[76] K.-T. Hsiao, J. Alms, and S. G. Advani, "Use of epoxy/multiwalled carbon nanotubes as adhesives to join graphite fibre reinforced polymer composites," *Nanotechnology*, vol. 14, no. 7, p. 791, 2003.

[77] M. Arai, Y. Noro, K.-i. Sugimoto, and M. Endo, "Mode i and mode ii interlaminar fracture toughness of cfrp laminates toughened by carbon nanofiber interlayer," *Composites Science and Technology*, vol. 68, no. 2, pp. 516–525, 2008.

[78] D. C. Davis and B. D. Whelan, "An experimental study of interlaminar shear fracture toughness of a nanotube reinforced composite," *Composites Part B: Engineering*, vol. 42, no. 1, pp. 105–116, 2011.

[79] F. L. Shan, Y. Z. Gu, M. Li, Y. N. Liu, and Z. G. Zhang, "Effect of deposited carbon nanotubes on interlaminar properties of carbon fiber-reinforced epoxy composites using a developed spraying processing," *Polymer Composites*, vol. 34, no. 1, pp. 41–50, 2013.

[80] Y. Li, N. Hori, M. Arai, N. Hu, Y. Liu, and H. Fukunaga, "Improvement of interlaminar mechanical properties of cfrp laminates using vgcf," *Special Issue: CompTest 2008*, vol. 40, no. 12, pp. 2004–2012, 2009.

[81] S. Singh and I. K. Partridge, "Mixed-mode fracture in an interleaved carbon-fibre/epoxy composite," *Composites Science and Technology*, vol. 55, no. 4, pp. 319–327, 1995.

[82] D. R. Bortz, C. Merino, and I. Martin-Gullon, "Mechanical characterization of hierarchical carbon fiber/nanofiber composite laminates," *Composites Part A: Applied Science and Manufacturing*, vol. 42, no. 11, pp. 1584–1591, 2011.

[83] P. R. Thakre, D. C. Lagoudas, J. Zhu, E. V. Barrera, and T. S. Gates, eds., *Processing and characterization of epoxy-SWCNT-woven fabric composites*, 2006.

[84] A. Kousourakis, A. P. Mouritz, and M. K. Bannister, "Interlaminar properties of polymer laminates containing internal sensor cavities," *Thirteenth International Conference on Composite Structures*, vol. 75, no. 1–4, pp. 610–618, 2006.

[85] Y. Lin, M. Gigliotti, M. C. Lafarie-Frenot, and J. Bai, "Effect of carbon nanotubes on the thermoelectric properties of cfrp laminate for aircraft applications," *Journal of Reinforced Plastics and Composites*, vol. 34, no. 2, pp. 173–184, 2015.

[86] Cytec, "Mvr444 technical datasheet." http://www.cytec.com.

[87] P. Navabpour, A. Nesbitt, B. Degamber, G. Fernando, T. Mann, and R. Day, "Comparison of the curing kinetics of the rtm6 epoxy resin system using differential scanning calorimetry and a microwave–heated calorimeter," *Journal of applied polymer science*, vol. 99, no. 6, pp. 3658–3668, 2006.

[88] N. Causse, S. Benchimol, L. Martineau, D. Carponcin, A. Lonjon, M. Fogel, J. Dandurand, E. Dantras, and C. Lacabanne, "Polymerization study and rheological behavior of a rtm6 epoxy resin system during preprocessing step," *Journal of Thermal Analysis and Calorimetry*, pp. 1–8, 2015.

[89] S. Bordere, J. Corpart, N. El Bounia, P. Gaillard, N. Passade-Boupat, P. M. Piccione, and D. Plée, "Industrial production and applications of carbon nanotubes," *Materials Design*, vol. 28, pp. 1477–1489, 2011.

[90] J. Grenet and B. Legendre, *Méthodes thermiques d'analyse: Analyse calorimétrique différentielle à balayage (DSC).* Paris and France: Éditions Techniques de l'ingénieur, 2010.

[91] AITM2-0064, "Electrical resistance for a composite laminate with carbon fibre: measurement along x or y direction," 2010.

[92] AITM2-0065, "Electrical resistance for a composite laminate with carbon fibre: measurement along z direction," 2010.

[93] P. J. W. Debye, *The collected papers of Peter JW Debye.* Interscience Publishers, 1954.

[94] S. Havriliak and S. Negami, "A complex plane representation of dielectric and mechanical relaxation processes in some polymers," *Polymer*, vol. 8, pp. 161–210, 1967.

[95] M. Chevalier, *Vieillisement hygrothermique d'assemblages structuraux polyepoxy: analyse de la mobilité moléculaire par spectroscopie diélectrique dynamique.* PhD thesis, Université Paul Sabatier, Toulouse, France, 2008.

[96] S. Barrau, *Élaboration de étude du comportement électrique et mécanique de composite nanotubes de carbone - polyépoxy.* PhD thesis, Université Paul Sabatier, Toulouse, France, 2004.

[97] N. Caussé, *Analyse des relaxations enthalpiques, mécaniques et diélectriques pour l'étude du vieillissement d'assemblages collés structuraux.* PhD thesis, Université Paul Sabatier, Toulouse, France, 2012.

[98] A. K. Jonscher, "The 'universal' dielectric response," *Nature*, vol. 267, no. 5613, pp. 673–679, 1977.

[99] J. C. Dyre and T. B. Schrøder, "Universality of ac conduction in disordered solids," *Reviews of Modern Physics*, vol. 72, no. 3, p. 873, 2000.

[100] L. Heux, J. L. Halary, F. Lauprêtre, and L. Monnerie, "Dynamic mechanical and 13c nmr investigations of molecular motions involved in the beta relaxation of epoxy networks based on dgeba and aliphatic amines," *Polymer*, vol. 38, no. 8, pp. 1767–1778, 1997.

[101] A. Apicella and L. Nicolais, "Role of processing on the durability of epoxy composites in humid environments," *Industrial & engineering chemistry product research and development*, vol. 23, no. 2, pp. 288–297, 1984.

[102] J. D. Keenan, J. C. Seferis, and J. T. Quinlivan, "Effects of moisture and stoichiometry on the dynamic mechanical properties of a high–performance structural epoxy," *Journal of applied polymer science*, vol. 24, no. 12, pp. 2375–2387, 1979.

[103] C. E. Browning, "The mechanisms of elevated temperature property losses in high performance structural epoxy resin matrix materials after exposures to high humidity environments," *Polymer Engineering & Science*, vol. 18, no. 1, pp. 16–24, 1978.

[104] V. B. Gupta, C. Ramesh, and A. K. Gupta, "Structure–property relationship in heat–set poly (ethylene terephthalate) fibers. i. structure and morphology," *Journal of applied polymer science*, vol. 29, no. 10, pp. 3115–3129, 1984.

[105] P. Robinson and J. M. Hodgkinson, "Interlaminar fracture toughness," *Mechanical testing of advanced fibre composites*, pp. 170–210, 2000.

[106] AITM1-0005, "Carbon fiber reinforced plastics - determination of interlaminar toughness energy - mode i," June 1994.

[107] AITM1-0006, "Carbon fiber reinforced plastics - determination of the interlaminar fracture toughness energy - mode ii," June 1994.

[108] EN 2563, "Carbon fibre reinforced plastics - unidirectional laminates - determination of the apparent interlaminar shear strength," January 1997.

[109] A.-L. Maillot, H. Luinge, and K. Schulte, "Cnt-modified carbon-fiber-reinforced composites for aerospace applications," in *Proceedings of the 16th International Conference on Composite Structures*, 2011.

[110] A. T. DiBenedetto, "Prediction of the glass transition temperature of polymers: A model based on the principle of corresponding states," *Journal of Polymer Science Part B: Polymer Physics*, vol. 25, no. 9, pp. 1949–1969, 1987.

[111] J. P. Pascault and Williams, R. J. J., "Glass transition temperature versus conversion relationships for thermosetting polymers," *Journal of Polymer Science Part B: Polymer Physics*, vol. 28, no. 1, pp. 85–95, 1990.

[112] N. Rabearison, C. Jochum, and J. C. Grandidier, "A cure kinetics, diffusion controlled and temperature dependent, identification of the araldite ly556 epoxy," *Journal of Materials Science*, vol. 46, no. 3, pp. 787–796, 2011.

[113] A. Dimopoulos, A. A. Skordos, and I. K. Partridge, "Cure kinetics, glass transition temperature development, and dielectric spectroscopy of a low temperature cure epoxy/amine system," *Journal of applied polymer science*, vol. 124, no. 3, pp. 1899–1905, 2012.

[114] A. M. Marconnet, N. Yamamoto, M. A. Panzer, B. L. Wardle, and K. E. Goodson, "Thermal conduction in aligned carbon nanotube–polymer nanocomposites with high packing density," *ACS Nano*, vol. 5, no. 6, pp. 4818–4825, 2011.

[115] I. El Sawi, P. A. Olivier, P. Demont, and H. Bougherara, "Processing and electrical characterization of a unidirectional cfrp composite filled with double walled carbon nanotubes," *Composites Science and Technology*, vol. 73, no. 0, pp. 19–26, 2012.

[116] T. Zhou, X. Wang, and T. Wang, "Cure reaction of multi-walled carbon nanotubes/diglycidyl ether of bisphenol a/2-ethyl-4-methylimidazole (mwcnts/dgeba/emi-2,4) nanocomposites: effect of carboxylic functionalization of mwcnts," *Polymer International*, vol. 58, no. 4, pp. 445–452, 2009.

[117] M. R. Kamal and S. Sourour, "Kinetics and thermal characterization of thermoset cure," *Polymer Engineering and Science*, vol. 13, no. 1, pp. 59–64, 1973.

[118] S. Sourour and M. R. Kamal, "Differential scanning calorimetry of epoxy cure: isothermal cure kinetics," *Thermochimica Acta*, vol. 14, no. 1-2, pp. 41–59, 1976.

[119] C. Paris, *Étude et modélisation de la polymérisation dynamique de composites à matrice thermodurcissable*. PhD thesis, Université de Toulouse, Toulouse, France, 2011.

[120] P. J. Carreau, "Rheological equations from molecular network theories," *Journal of Rheology*, vol. 16, no. 1, p. 99, 1972.

[121] K. Yasuda, R. C. Armstrong, and R. E. Cohen, "Shear flow properties of concentrated solutions of linear and star branched polystyrenes," *Rheologica Acta*, vol. 20, no. 2, pp. 163–178, 1981.

[122] P. Pötschke, T. D. Fornes, and Paul, "Rheological behavior of multiwalled carbon nanotube/polycarbonate composites," *Polymer*, vol. 43, no. 11, pp. 3247–3255, 2002.

[123] R. Kotsilkova, *Thermoset nanocomposites for engineering applications*. Smithers Rapra Publishing, 2007.

[124] C. McClory, T. McNally, M. Baxendale, P. Pötschke, W. Blau, and M. Ruether, "Electrical and rheological percolation of pmma/mwcnt nanocomposites as a function of cnt geometry and functionality," *European Polymer Journal*, vol. 46, no. 5, pp. 854–868, 2010.

[125] J. Sumfleth, S. T. Buschhorn, and K. Schulte, "Comparison of rheological and electrical percolation phenomena in carbon black and carbon nanotube filled epoxy polymers," *Journal of Materials Science*, vol. 46, no. 3, pp. 659–669, 2011.

[126] Y. Liu and A. Wilkinson, "Processing behaviour of a nanocomposite matrix for multiscale composites," in *Proceedings of the 16th European Conference on Composite Materials*, 2014.

[127] T. Mezger, *Das Rheologie Handbuch: Für Anwender von Rotations-und Oszillations-Rheometern*. Vincentz Network GmbH & Co KG, 2007.

[128] H. A. Barnes, J. F. Hutton, and K. Walters, *An introduction to rheology*, vol. 3. Elsevier, 1989.

[129] D. Stauffer and A. Aharony, *Introduction to percolation theory*. Taylor and Francis, 1994.

[130] N. F. Mott and E. A. Davis, "Electronic processes in non-crystalline solids," *Clarendon, Oxford*, p. 465, 1979.

[131] G. P. Triberis and L. R. Friedman, "The effect of correlations on the conductivity of the small-polaron regime in disordered systems," *Journal of Physics C: Solid State Physics*, vol. 18, no. 11, p. 2281, 1985.

[132] J. M. Benoit, B. Corraze, and O. Chauvet, "Localization, coulomb interactions and electrical heating in single-wall carbon nanotubes/polymer composites," *arXiv preprint cond-mat/0204520*, 2002.

[133] J. Filsinger, T. Lippert, F. Stadler, and S. Utecht, "Method and apparatus for producing fiber-reinforced components by means of an injection process." German Patent, 2003.

[134] SAERTEX GmbH, "Vap technology." http://www.saertex.com.

[135] Nanosafe, "Safe production and use of nanomaterials: Are conventional protective devices such as fibrous filter media, cartridge for respirators, protective clothing and gloves also effcient for nanoaerosols ?." http://www.nanosafe.org/home/liblocal/docs/Dissemination2008.

[136] E. 2564, "Carbon fibre laminates - determination of the fibre-, resin- and void contents," August 1998.

[137] A. 3-0008, "Determination of the extent of cure by differential scanning calorimetry," June 1995.

[138] A. Lonjon, P. Demont, E. Dantras, and C. Lacabanne, "Electrical conductivity improvement of aeronautical carbon fiber reinforced polyepoxy composites by insertion of carbon nanotubes," *Journal of Non-Crystalline Solids*, vol. 358, no. 15, pp. 1859–1862, 2012.

[139] A. Lonjon, *Nanocomposite conducteur polymère/nanofils métalliques: élaboration et analyse des propriétés mécaniques*. PhD thesis, Université Paul Sabatier, Toulouse, France, 2010.

[140] G. Zhou, E. R. Green, and C. Morrison, "In-plane and interlaminar shear properties of carbon/epoxy laminates," *Composites Science and Technology*, vol. 55, no. 2, pp. 187–193, 1995.

[141] J.-P. Favre, "Residual thermal stresses in fibre reinforced composite materials- a review," *Journal of the Mechanical Behavior of Materials*, vol. 1, no. 1, pp. 37–53, 1988.

[142] J. P. Berry, "Determination of fracture surface energies by the cleavage technique," *Journal of applied physics*, vol. 34, no. 1, pp. 62–68, 1963.

[143] K. E. Tarsha Kurdi, *Contraintes résiduelles de cuisson dans les stratifiés composites à finalité aéronautique: intégration du procédé de mise en oeuvre et étude de leur influence sur les caractéristiques mécaniques*. PhD thesis, Université Paul Sabatier, Toulouse, France, 2003.

Appendix A - List of Samples

Laminate Name	Layup	Sprayed Interlayer		FVF	Thickness
		Type	Amount ($g.m^{-2}$)	vol.%	mm
Reference Infusion Elec.	$[0]_8$	-	-	58.7	2.28
Reference Infusion Meca.	$[0]_{12}$	-	-	59.6	3.37
Sprayed Neat Elec.	$[0]_8$	MVR444	143	58.4	2.29
Sprayed Neat Meca.	$[0]_{12}$	MVR444	140	60.4	3.33
Sprayed CNT Elec.	$[0]_8$	MVR444 + 0.75wt.% CNT	138	59.8	2.24
Sprayed CNT Meca.	$[0]_{12}$	MVR444 + 0.75wt.% CNT	137	59.8	3.36
Reference Infusion GIc	$[0]_{12}$	-	-	61.7	3.26
Sprayed Neat GIc	$[0]_{12}$	MVR444	148	62.0	3.24
Sprayed CNT GIc	$[0]_{12}$	MVR444 + 0.75wt.% CNT	140	62.2	3.23

List of manufactured laminates

Appendix B - Electrical conductivity measurement procedure

This appendix presents the procedure used in order to perform the measurement of the volume electrical conductivity on CFRP samples. The principle of the method is to inject an electrical direct current through the upper and lower faces of the specimen while the voltage drop between the faces is measured.

Number and cutting of the specimens

The measurements were achieved on a minimum of five samples coming from a defect-free panel. These samples were cut using water-jet cutting. This proved to be a reliable method to achieve the desired tolerance and to minimize the local delamination and thermal damage created on the edges of the sample when using a standard cutting saw (not cooled with water).

Preparation of the specimens surface

The two faces of each specimen were first cleaned with isopropanol and then covered with silver paint. Adequate care shall be taken to ensure a uniform and sufficient coating and to avoid that silver paint be applied on the panel edges.

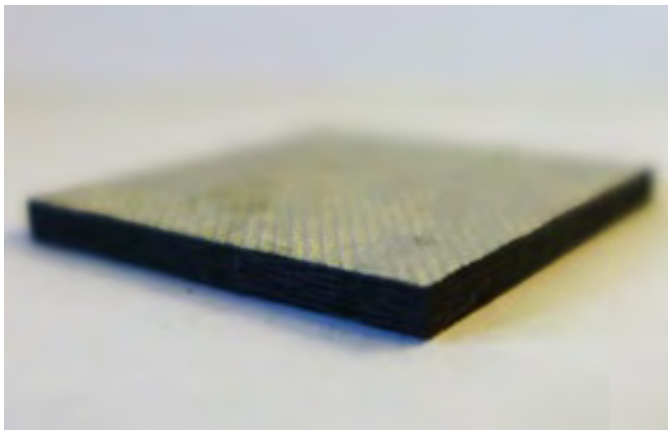

Silver paint deposit on a CFRP sample

Test Procedure

Calibration

The measurement shall be performed with a four probes ohmmeter. Two electrodes connected to the ohmmeter through crocodile clips are required. Electrodes shall be held by clips and cleaned with a solvent such as isopropanol. An insulating piece shall be used to support the assembly. The calibration of the entire electrical setup was performed before achieving a set of measurements. This was also done at the end of the set, to verify that the setup is still working correctly. This calibration consists of the measurement of a resistance of known value connected to the ohmmeter by two crocodile clips.

Measurement of the specimen resistance

The sample shall be placed between the two electrodes as presented on the figure below. In order to hold the two electrodes upon each other, two clips are used. Given that the clips have to hold strongly the two electrodes, it is not recommended to use polymer clips that can be plastically deformed. Indeed, an adequate force shall be applied on the electrodes in order to insure a good contact between them. The clips also have to be non-conductive or insulated.

Adequate care shall be taken to insure that the entire panel surface is covered by the two electrodes as shown on the figure below.

(a) Side view

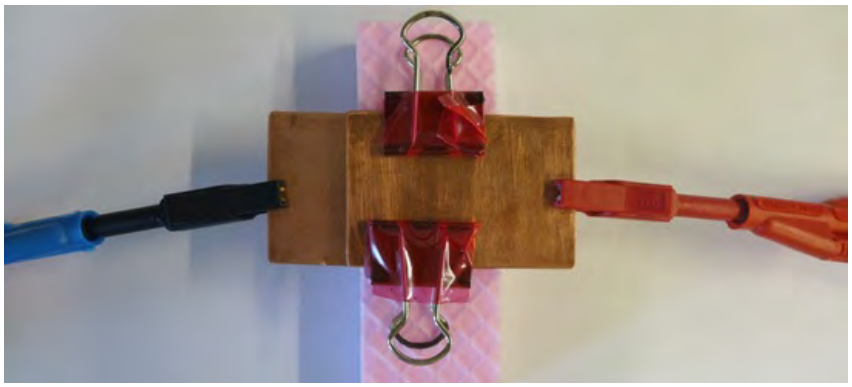

(b) Top view

Final assembly required for the measurement

For each specimen, a minimum of four measurements shall be repeated in order to determine the uncertainty on the measurement and an average resistance value. Between each measurement, the panel should be removed from the assembly and re-installed as shown above. This procedure shall be repeated for each specimen of the test set. The electrodes shall be cleaned with isopropanol between each measurement.

Appendix C - Dynamic Dielectric Spectroscopy Results

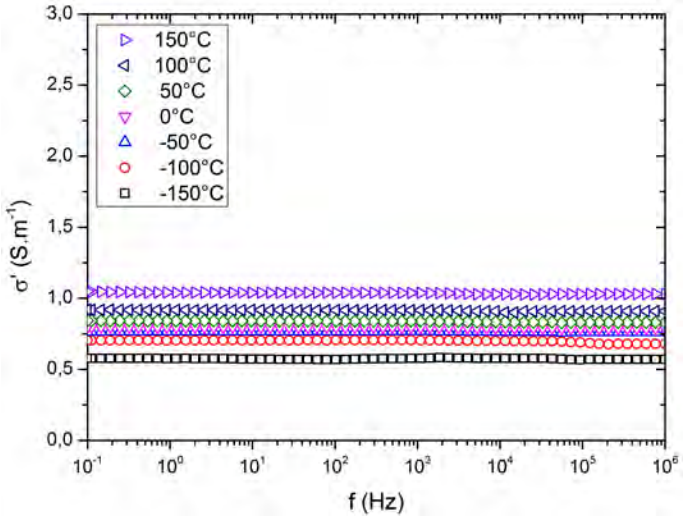

Reference Infusion

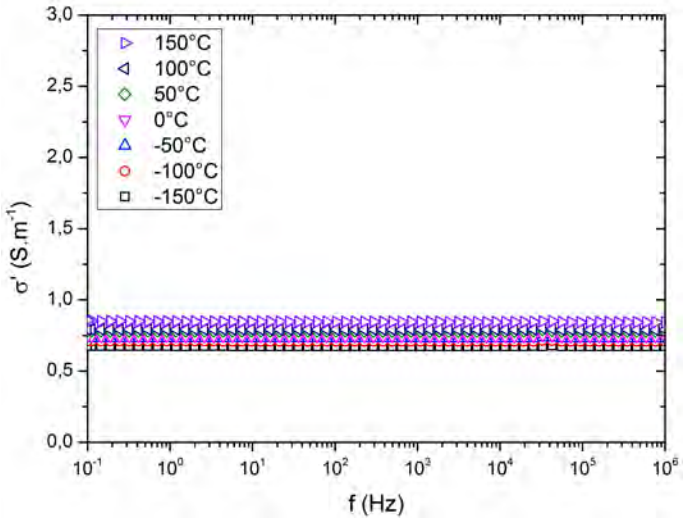

Sprayed Reference

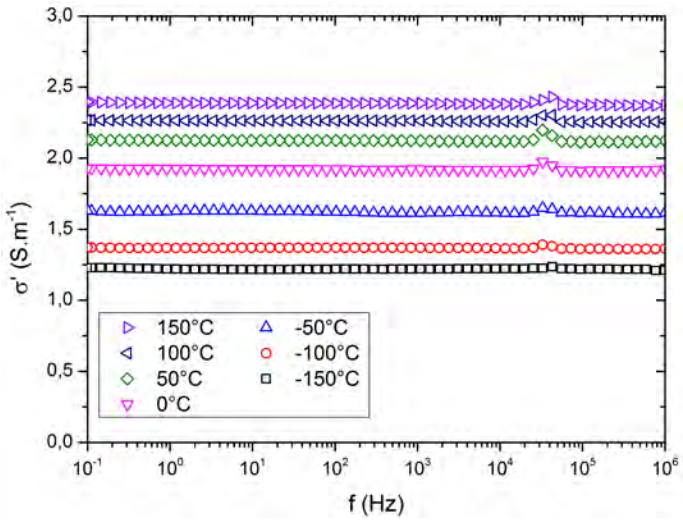

Sprayed CNT

Real part of the complex conductivity for the three types of materials produced

Résumé

Introduction

Au cours des dernières décennies, l'utilisation des composites à renforts fibres de carbone s'est accrue, portée par l'excellent ratio entre propriétés mécaniques et masse de ces matériaux. Dans l'industrie aéronautique, ces matériaux remplacent les structures métalliques, permettant aux avionneurs de réduire la masse des aéronefs de dernière génération.

A la différence des matériaux métalliques, les polymères à renforts fibres de carbone présentent des niveaux de conductivité électriques faibles, en particulier dans le sens transverse (épaisseur du matériau). En effet, la structure stratifiée du matériau, c'est à dire l'alternance de plis de fibres de carbone conducteurs et d'interplis de matrice isolante, crée une inhomogénéité de la conductivité électrique.

Une application pratique de ce phénomène concerne les réservoirs de carburant des avions. Les arêtes des stratifiés constituant les parois de ces derniers doivent êtres recouvertes d'un enduit pour les isoler du carburant. La formation de structures similaires à des condensateurs (successions de couches conductrices et isolantes de par la structure du stratifié) peut donner lieu à un phénomène d'étincelage en présence d'une différence de potentiel suffisante.

En réponse à cette problématique, le concept de matériaux multifonctionnels émerge. Il est souhaité qu'à l'avenir, les matériaux composites ne contribuent pas uniquement en tant que matériaux de structure, mais apportent également d'autres fonctions telles que : résistance au feu, isolation thermique et acoustique et, dans notre application, conductivité électrique.

L'objectif premier de ce travail de thèse est l'intégration et l'homogénéisation de la

conductivité électrique au sein d'un matériau composite multifonctionnel. La réalisation de cet objectif se fera grâce à la conception d'un matériau multi-échelles, où l'insertion de nanotubes de carbone (NTC) en tant que charge conductrice conférera au composite à renforts macroscopiques (fibre de carbone) une nouvelle dimension nanoscopique (nanotubes de carbone).

L'étude bibliographique présentée en première partie montre le potentiel des NTC en tant que vecteurs de conductivité électrique. Cette revue montre également les obstacles et défis à relever pour procéder à la mise en œuvre des composites chargés en NTC. Une seconde partie présente les matériaux et méthodes utilisés dans ces travaux. Une troisième partie décrit une étape cruciale avant le passage à la mise en œuvre des composites. En effet, cette troisième partie présente la dispersion des NTC dans la matrice époxy ainsi que l'analyse des propriétés thermocinétiques, rhéologiques et électriques des dispersions NTC / époxy. Enfin, une quatrième expose la mise en œuvre, puis l'analyse de la qualité des stratifiés produits ainsi que des propriétés électriques et mécaniques des composites à renforts fibres de carbone chargés en nanotubes de carbone.

Étude bibliographique

Nanocomposites nanotubes de carbone / époxy

Le facteur de forme élevé ainsi que la conductivité électrique importante des NTC, font de ce matériau un candidat idéal pour la création de composites multi-échelles intégrant la fonction conductivité électrique. Différentes méthodes cœxistent afin de disperser les nanotubes dans les matrices thermodurcissables. Une de ces méthodes consiste en l'application d'importantes forces de cisaillement afin de procéder à la rupture des agglomérats et à la dispersion des nanocharges dans le polymère. Une des applications de cette méthode de dispersion consiste en l'utilisation d'une calandreuse, comme présentée en figure 1. En plus de l'excellente dispersion obtenue, cette technique permet le mélange de grandes quantités de matrice afin de procéder à la mise en œuvre du matériau composite fibres de carbone / époxy.

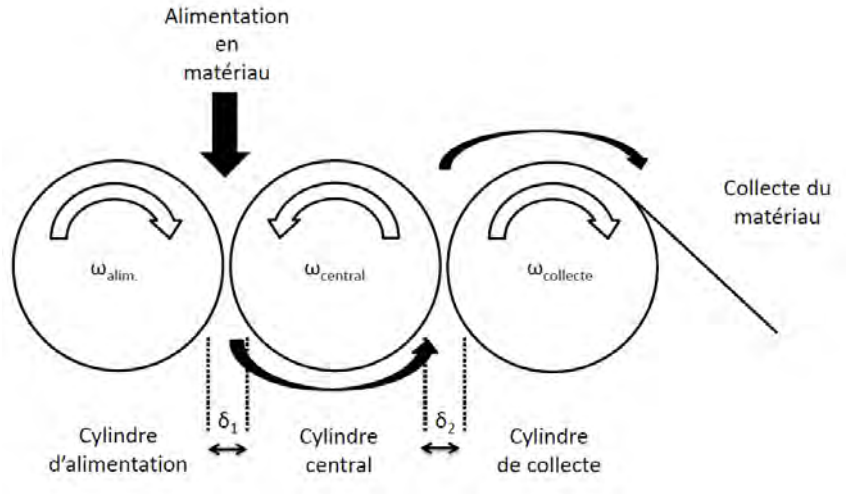

Figure 1 – Principe de fonctionnement de la calandreuse

De nombreux auteurs se sont penchés sur les propriétés thermocinétiques, mécaniques et électriques des dispersions NTC / époxy. El Sawi et al. [58] ont montré que les NTC double-feuillets ont un effet accélérateur sur la cinétique de polymérisation du polyépoxy, mais aucun effet n'a été noté sur la température de transition vitreuse. Ces travaux ont également montré un effet rhéofluidifiant des NTC sur le comportement rhéologique du polymère en particulier à haute température. Barrau et al. [22] ont étudié les propriétés électriques des nanocomposites époxy / NTC dispersés grâce aux ultrasons. Ces travaux

ont permis de déterminer la présence d'un seuil de percolation p_c = 0,3 %m et d'une conductivité maximale σ_{max}= 10^{-3} S.m^{-1}. Il est à noter également que les travaux de Gojny et al. [17, 18] ont permis d'atteindre des seuils de percolation inférieurs ou égaux à p_c = 0,1 %m mais en obtenant des conductivités maximales moins élevées.

Composites à renforts fibres de carbone chargés en NTC

L'utilisation des techniques classiques de mise en œuvre des matériaux composites par infusion semble au vu des difficultés rencontrées lors de l'ajout de NTC (augmentation de la viscosité, filtration des nanotubes) difficilement envisageable. C'est pourquoi des alternatives à ces méthodes doivent être développées.

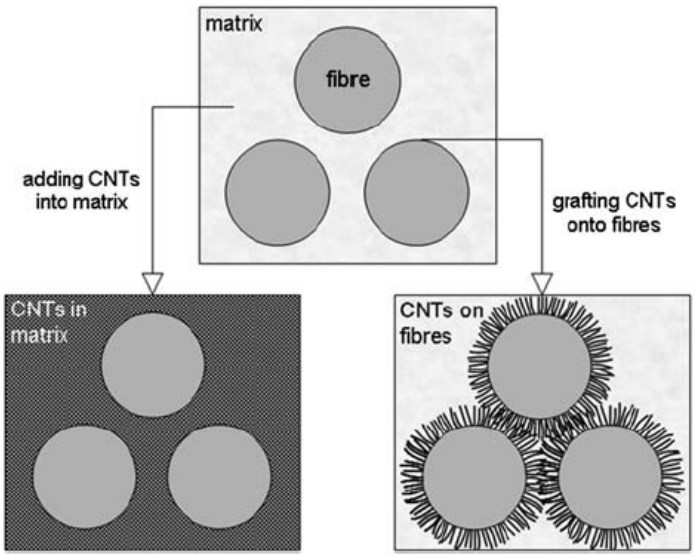

Figure 2 – Représentation schématique des deux routes de mise en œuvre des composites multi-échelles [65]

La figure 2 présente les deux grandes voies possibles. La modification des composites par les nanotubes peut être faite soit à la surface des fibres de carbone, soit au sein de la matrice. Ce travail doctoral fait le choix de la modification de la matrice du composite. Une revue de la littérature montre que des amélioration des propriétés mécaniques grâce aux NTC ont pu être relevées par certains auteurs. Néanmoins très peu d'auteurs ont été en mesure de démontrer une augmentation sensible de la conductivité électrique grâce à l'ajout de NTC.

Matériaux et Méthodes

Cette seconde partie présente les matériaux et méthodes expérimentales mis en œuvre dans ce travail de thése.

Matériaux

Matrice époxy

La matrice polyépoxy utilisée pour la mise en œuvre des composites est la MVR 444 produite par Cytec Industries Inc. Cette matrice est une résine monocomposant composée d'un prépolymère époxyde et d'un durcisseur amine. Cette résine est destinée à la fabrication de composants aéronautiques grâce au procédé d'injection sous vide (*VARTM : Vacuum Assisted Resin Transfer Molding*) et est généralement polymérisée à 180°C.

À ce jour, de nombreuses études se sont penchées principalement sur les propriétés de la résine RTM6 produite par Hexcel [87, 88]. C'est pourquoi, il a été décidé d'étudier avec attention les propriétés thermocinétiques, rhéologiques et électriques des dispersions NTC / époxy.

Renforts fibres de carbone

Les fibres de carbone TENAX J IMS60 E13 24K constituant le renfort employé sont commercialisées ici sous forme de non-tissé unidirectionnel reliées entre elles par des fils de maintien en polypropylène à renfort fibres de verre (directions 90° et ± 60°) et des fils de coutures en polyester dans la direction 0°. Les fibres TENAX J IMS60 E13 24K sont des fibres à module intermédiaire produites à partir des précurseurs polyacrylonitrile (PAN) et recouvertes d'un traitement de surface

Nanotubes de carbone

Les nanotubes de carbone (NTC) sélectionnés pour ces travaux sont les nanotubes multiparois (*MWCNT : Multi-Walled Carbon Nanotube*) produits par Arkema. Un mélange-maître (*Masterbatch*) a été réalisé en diluant des nanotubes Graphistrength CS1-25 dans une matrice époxy MVR 444 fournie par Cytec (concentration de 25 % en masse).

Grâce à cette méthode, il est possible d'obtenir une parfaite compatibilité entre le polymère encapsulant le mélange-maître et celui utilisé pour la mise en œuvre du composite à renforts fibres de carbone : ceux-ci étant identiques.

Méthodes

Les principales méthodes expérimentales employées dans ce travail de thèse peuvent être regroupées en trois catégories : analyse calorimétrique, propriétés électriques et propriétés mécaniques.

Analyse calorimétrique

L'analyse des propriétés thermiques est effectuée par analyse thermique différentielle (ATD). Cette mesure se base sur la mesure de la différence de température entre un échantillon et une référence soumis tout deux à un flux de chaleur. Le calorimètre utilisé est un calorimètre Q2000 produit par TA Instruments.

Conductivité électrique

L'analyse des propriétés électriques des matériaux est réalisée à l'aide de deux méthodes d'analyse : mesures de conductivité électrique en courant continu et spectroscopie diélectrique dynamique.

Des mesures de conductivité électrique en courant continu ont été réalisées grâce à un multimètre numérique Keithley 2400. Cette méthode se base sur l'injection d'un courant électrique continu dans l'échantillon, tout en mesurant la différence de potentiel entre les deux faces métallisées de l'échantillon. Cette méthode de mesure à 4 points, utilise deux circuits de mesure différents pour l'injection du courant et la mesure de la différence de potentiel, afin de s'affranchir de la résistance de l'appareillage de mesure (voir figure 3). Le multimètre numérique ne pouvant mesurer des résistances supérieures à 200 MΩ, cette méthode est uniquement applicable aux composites à renforts fibres de carbone présentant une résistance plus faible que les nanocomposites NTC / époxy pour lesquels seule la spectroscopie diélectrique dynamique est adaptée.

La spectroscopie diélectrique dynamique (SDD) permet une analyse diélectrique d'un

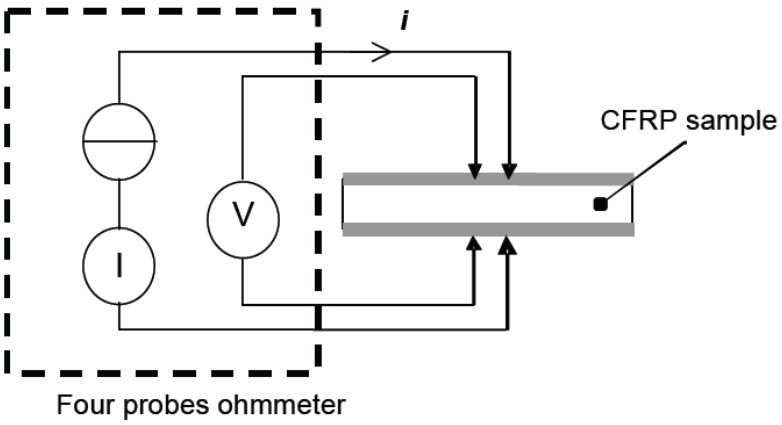

Figure 3 – Montage de mesure de conductivité électrique en courant continu [92]

échantillon placé entre deux électrodes aux bornes desquelles une tension sinusoïdale de pulsation ω est appliquée. Les courants induits permettent de déduire l'impédance complexe $Z^*(\omega)$ ainsi que la permittivité diélectrique complexe $\epsilon^*(\omega)$. Celles-ci sont déterminées à l'aide d'un analyseur d'impédance Solartron 1260 couplé à un spectromètre Novocontrol BDS 4000. Le domaine de fréquences de mesure est compris entre 10^{-1} et 10^6 Hz et les mesures sont effectuées pour des isothermes de -150 à +150°C avec un pas de 10°C. Des nanocomposites époxy / NTC ainsi que des composites à renforts fibres de carbone dopés en NTC ont pu êtres testés grâce à cette technique d'analyse.

Propriétés mécaniques

Les propriétés mécaniques des composites fibres de carbone / époxy ont été étudiées grâce à trois méthodes : analyse mécanique dynamique, résistance au cisaillement interlaminaire et résistance à la propagation de fissure.

Le module mécanique complexe d'un matériau polymère peut être déterminé par l'analyse mécanique dynamique. L'échantillon est soumis à un déplacement angulaire qui produit une déformation sinusoïdale. En torsion, le module de cisaillement complexe, noté $G^*(\omega)$ peut s'écrire :

$$G^*(\omega) = \frac{\sigma^*(\omega)}{\gamma^*(\omega)} = G^{'}(\omega) + iG^{''}(\omega) \quad (1)$$

où γ est la déformation de pulsation ω, σ la contrainte induite, $G^{'}(\omega)$ la partie réelle (avec $G^{'}$ le module conservatif) et $G^{''}(\omega)$ la partie imaginaire (avec $G^{''}$ le module dissipa-

tif) du module mécanique complexe. L'appareillage utilisé est un rhéomètre ARES de TA Instruments utilisé en torsion rectangulaire pour des échantillons solides et avec un montage de Couette pour l'analyse des propriétés mécaniques des suspensions époxy / NTC.

Des essais de détermination de la résistance au cisaillement interlaminaire par essai de flexion 3 points sur appuis rapprochés ont été réalisés sur des composites à renforts fibres de carbone. À cet effet un échantillon de section rectangulaire est placé sur deux supports et une charge est appliquée par la flèche de la machine d'essai au centre de l'échantillon. La géométrie de l'échantillon est choisie pour solliciter celui-ci principalement en cisaillement. La résistance au cisaillement est calculée suivant la formule suivante où P_R est la force atteinte à la première rupture interlaminaire, b la largeur et h l'épaisseur de l'échantillon.

$$\tau = \frac{3P_R}{4bh} \tag{2}$$

Enfin, des essais de détermination de la résistance des matériaux à l'initiation et à la propagation de fissures interlaminaires ont été réalisés sur des stratifiés époxy / fibres de carbone. Des cycles de chargements en mode I (10 cycles par échantillon) ont été réalisés sur des éprouvettes de section rectangulaire comportant une pré-fissure. Le diagramme charge / déplacement est enregistré, ainsi que la longueur de délamination, permettant le calcul du taux de restitution d'énergie.

Comportements thermocinétiques, rhéologiques et électriques des dispersions NTC / époxy

Le premier objectif de ces travaux de thèse est d' élaborer des nanocomposites NTC / époxy et d'en caractériser les propriétés thermocinétiques, rhéologiques et électriques.

Mise en œuvre des nanocomposites NTC - époxy

La dispersion des NTC s'effectue grâce à une calandreuse Exakt 80E. Le mélange-maître contenant 25 % en masse de nanotubes est tout d'abord dilué à la concentration souhaitée avant d'être calandré. Un cycle de calandrage développé dans le cadre des travaux de thèse de Maillot [21] est utilisé (tableau 1). Ce cycle est optimisé pour obtenir la meilleure dispersion possible et limiter le degré de polymérisation de la résine pendant le procédé. Des mélanges contenant 0,10 ; 0,25 ; 0,50 ; 0,75 et 1,00 %m de NTC sont produits. En complément, la qualité de la dispersion des nanotubes est évaluée grâce à l'analyse du réseau percolant et présentée ci-après.

Passage	δ_1	δ_2	$\omega_{collecte}$
	μm	μm	(rpm)
1	120	40	100
2	120	40	300
3	45	15	300
4	15	5	300
5	15	5	500
6	15	5	500
7	5	5	500
8	5	5	500
9	5	5	500

Tableau 1 – Procédure de calandrage utilisée [109]

Comportement thermocinétique

Le suivi de la cinétique de polymérisation est effectué par détermination, grâce à l'analyse calorimétrique, de l'enthalpie résiduelle et de la température de transition vitreuse sur des échantillons de résine MVR 444 seule et dopée à 1 %m, en conditions isothermes à 60, 80 et 100°C. Le degré de polymérisation α est déterminé grâce aux équations 3 et 4.

$$\frac{T_g - T_{g0}}{T_{g\infty} - T_{g0}} = \frac{\lambda\alpha}{1-(1-\lambda)\alpha} \tag{3}$$

$$\alpha_t = \frac{\Delta H_{total} - \Delta H_{residuelle}(t)}{\Delta H_{total}} \tag{4}$$

La figure 4 présente le degré d'avancement α en fonction du temps passé en conditions isothermes (ne sont représentées que les isothermes 60 et 100°C). Aucune influence notable des NTC sur la cinétique de polymérisation à 60, 80 et 100°C n'a pu être constatée. Les cinétiques de polymérisation à ces températures sont en accord avec le modèle décrit par Kamal et Sorour [117, 118]. De plus, grâce à ces informations il nous est possible de déterminer le temps disponible pour procéder au dépôt par pulvérisation du polymère avant que celui-ci ne gélifie.

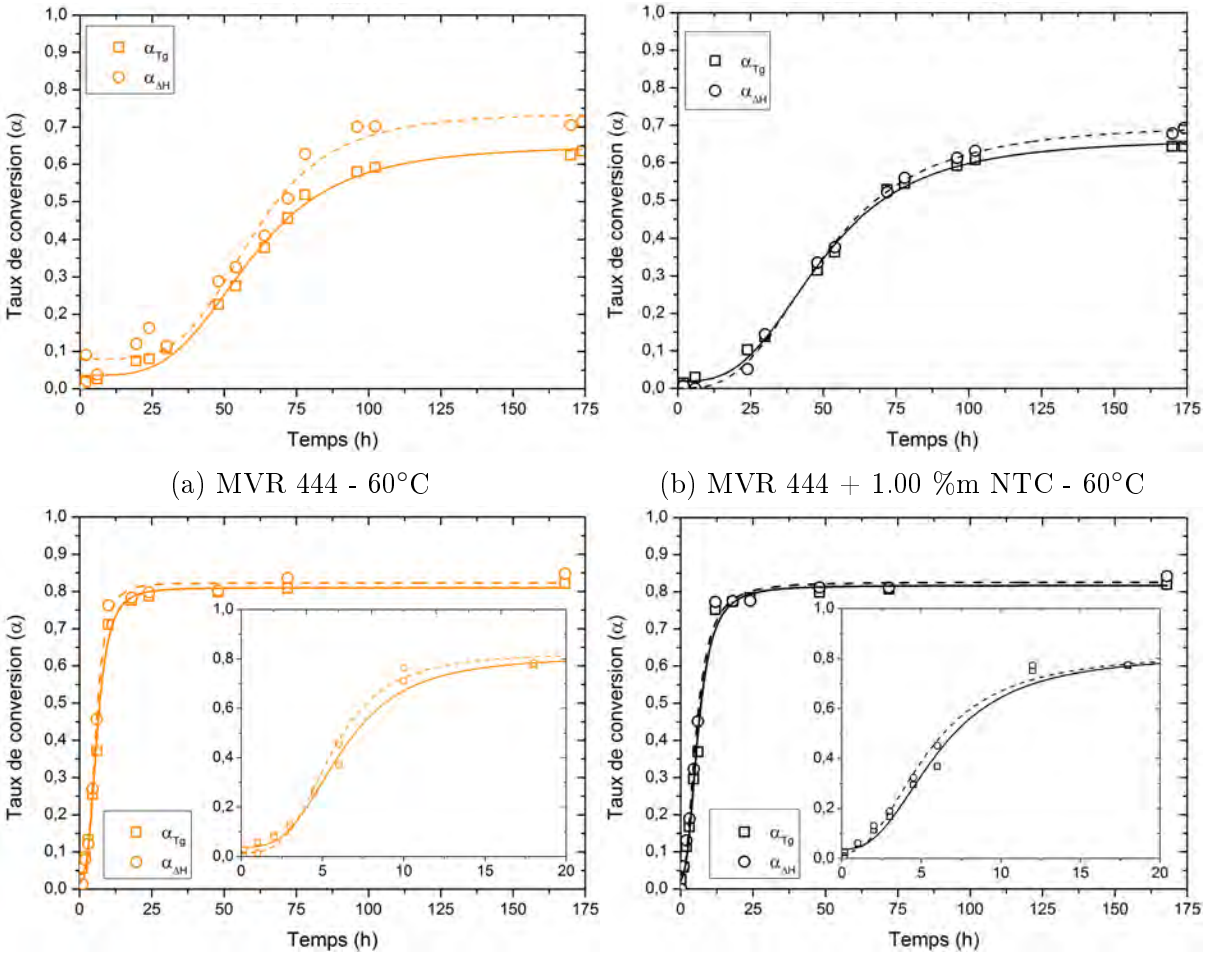

(a) MVR 444 - 60°C

(b) MVR 444 + 1.00 %m NTC - 60°C

(c) MVR 444 - 100°C

(d) MVR 444 + 1.00 %m NTC - 100°C

Figure 4 – Taux de conversion en fonction du temps pour les échantillons MVR444 seule et dopés à 1 %m aux isothermes 60°C et 100°C

Comportement rhéologique

Il a été choisi de déterminer le domaine de réponse linéaire du matériau. Cette démarche permet de s'assurer que pour les époxydes seules et chargées en NTC la réponse mécanique du matériau est linéairement proportionnelle à la contrainte appliquée dans la plage de fréquence choisie. Une partie de ces résultats est présentée sur la figure 5a.

Une fois ces paramètres déterminés, il est possible d'effectuer des balayages en fréquences tels que ceux présentés en exemple en figure 5b pour une température de 100°C. Pour des températures supérieures ou égales à 80°C, et pour des concentrations en NTC supérieures ou égales à 0,50 %m, un effet rhéofluidifiant peut être observé. Les dispersions dont le taux de charge est inférieur ou égal à 0,25 %m présentent un comportement

newtonien, ainsi que tous les mélanges $\leq$ 0,75 %m lorsqu'ils sont testés à 60°C. De plus il a pu être constaté que le comportement rhéologique en fréquences est en accord avec le modèle proposé par Carreau et Yasuda [120, 121].

Enfin, l'étude de la viscosité à basse fréquence (η_0, présenté en figure 5c) montre que le comportement de cette dernière en fonction de la température semble suivre deux tendances différentes en fonction du taux de charge en NTC. Pour un taux inférieur au seuil de percolation, η_0 décroit avec l'augmentation de la température, à l'inverse si le taux de charge est supérieur au taux de percolation, η_0 croît avec l'augmentation de la température. Ce comportement pourrait être associé à une manifestation mécanique du phénomène de formation de l'amas percolant. Ce phénomène est mis en évidence par la figure 5d qui présente la pente de la régression linéaire des données η_0 = f(T). Sur ce graphe, un saut peut être observé entre les valeurs situées avant et après le seuil de percolation (présenté en pointillés).

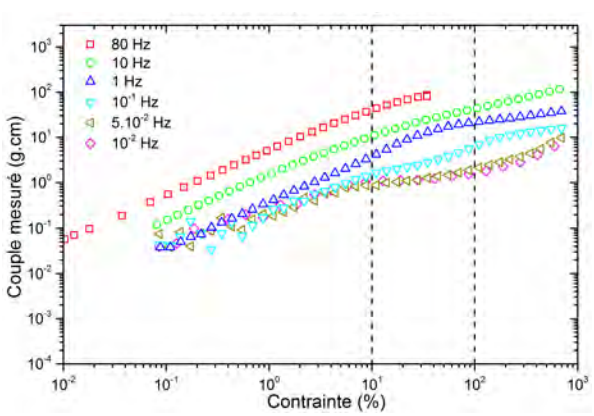

(a) Détermination du domaine de linéarité - MVR 444 + 1.00 %m NTC - 100°C

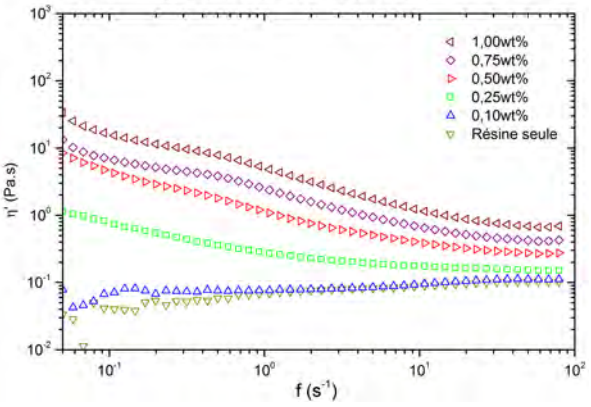

(b) Balayages en fréquence - 100°C

Contrainte 10 %

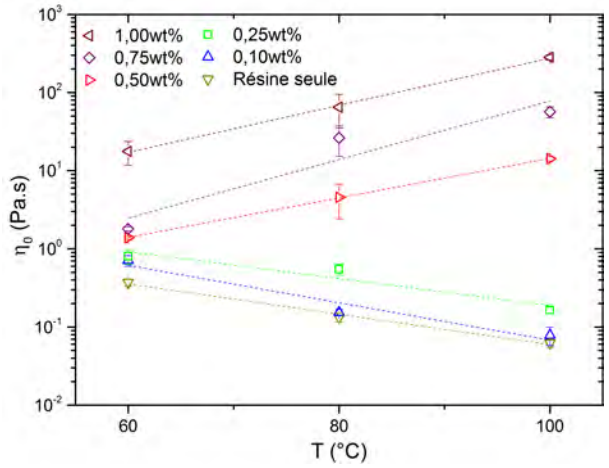

(c) Influence de la température sur la viscosité $\eta_0 = f(T)$

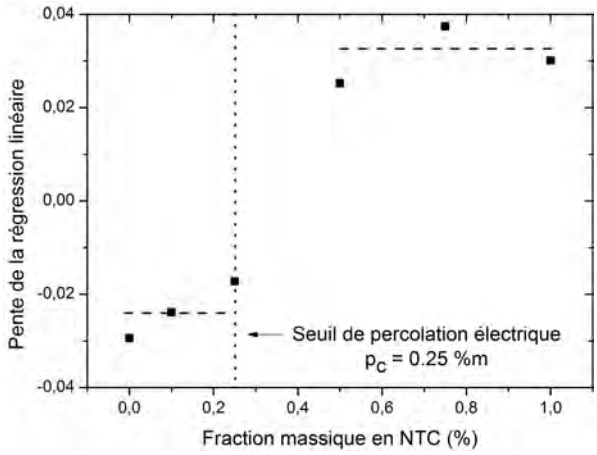

(d) Pente de la régression linéaire des données à basse fréquence des dispersions époxy / NTC

Figure 5 – Étude du comportement rhéologique des dispersions époxy / NTC

Comportement électrique

Enfin, l'état de dispersion des NTC et la formation du réseau percolant ont été étudiés grâce à la mesure de la conductivité électrique en courant continue σ_{DC} en fonction du taux de charge en NTC. Sur la figure 6, un seuil de percolation $p_c = 0{,}25$ %m et une conductivité maximale $\sigma_{max} = 10^{-2}$ S.m^{-1} (pour un taux de charge de 0,75 %m) ont pu être relevés. Cette concentration sera retenue pour la suite de nos travaux, car il s'agit du meilleur compromis entre conductivité électrique et facilité de mise en œuvre. Enfin la qualité de dispersion des nanotubes évaluée grâce au seuil de percolation est conforme aux résultats reportés dans la littérature pour les mêmes matériaux et méthodes de dispersion.

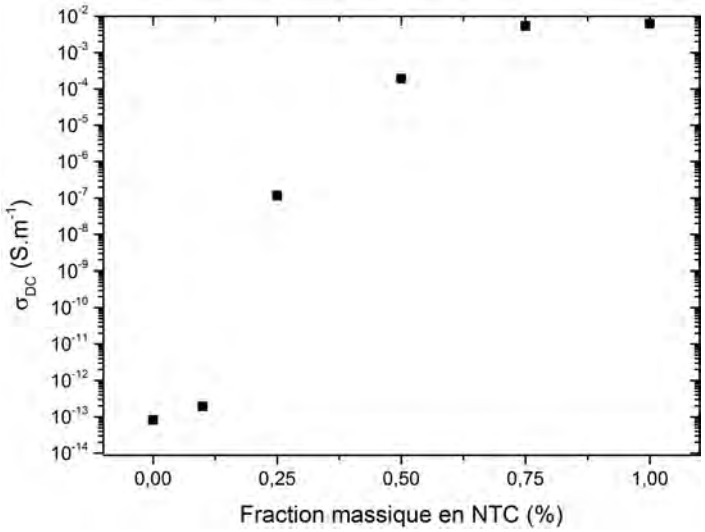

Figure 6 – Influence du taux de charge en NTC sur la conductivité électrique

Grâce à cette étude thermocinétique, rhéologique et électrique, de nombreuses informations et paramètres utiles à la mise en œuvre ont pu être recueillis et permettent d'envisager le dépôt par pulvérisation comme méthode d'insertion des nanoparticules au cœur des stratifiés.

Mise en œuvre et propriétés des composites à renfort fibres de carbone chargés en NTC

Dans cette section, la mise en œuvre des composites à renforts fibres de carbone chargés en NTC est présentée. Nous présentons également une démarche visant à s'assurer de la fiabilité du procédé et de la qualité des matériaux produits, ainsi que l'analyse des propriétés électriques et mécaniques des composites fibres de carbone / époxy chargés en NTC.

Mise en œuvre des composites chargés en NTC

Échantillons de référence

Afin de pouvoir mettre en évidence une potentielle influence du procédé de dépôt par pulvérisation et / ou des nanotubes de carbone, il est nécessaire de disposer d'échantillons de référence. Il a été décidé de réaliser ces échantillons grâce au procédé *VAP : Vacuum Assisted Process*. Ce procédé développé par Airbus Group Innovations [133] utilise, contrairement aux procédés standards d'infusion sous vide (*VARI : Vacuum Assisted Resin Infusion*), une membrane semi-perméable retenant la matrice infiltrée dans la préforme mais permettant un dégazage continu pendant la polymérisation

Procédé de dépôt par pulvérisation

Comme mentionné précédemment, l'utilisation des méthodes connues de mise en œuvre des composites se montre inadaptée pour des matrices chargées en nanotubes. C'est pourquoi, basé sur les travaux de Maillot [21], un procédé de dépôt par pulvérisation a été développé. A l'aide d'un pistolet pressurisé et chauffé (voir figure 7a), il est possible de pulvériser la dispersion époxy / NTC en fine gouttelettes projetées sur les plis de fibres de carbone secs (figure 7b). Une unité de contrôle (non représentée sur la figure) permet de réguler pression et température. La quantité déposée correspond à celle nécessaire pour atteindre une fraction volumique en fibre de 60 %vol. (soit environ 140 g.m^{-2} par pli). Cette quantité est contrôlée en temps réel par pesée. Ce procédé s'est avéré être une méthode de mise en œuvre fiable, reproductible et adaptée à la dépose de

nanoparticules en suspension.

(a) Pistolet utilisé (b) Pulvérisation sur fibres carbone séches

Figure 7 – Procédé de dépôt par pulvérisation

Polymérisation des préformes pulvérisées

Après avoir déposé la matrice chargée en nanotubes, il est important de se pencher sur le procédé de polymérisation des préformes. Deux objectifs doivent être atteints. Le premier se concentre sur l'évacuation de la préforme afin de limiter la présence de porosités dues à l'air inclus lors de la dépose par pulvérisation, le second a pour but la polymérisation complète et homogène de la matrice.

Pour la phase de mise sous vide de la préforme, un montage similaire à celui du VAP est utilisé tirant parti de la semi-perméabilité de la membrane retenant la matrice au sein de la préforme. Cette étape est rendue délicate par la faible viscosité de la MVR 444 à haute température (cette résine étant destinée aux procédés d'infusion), qui en l'absence d'un contrôle précis du procédé s'écoule hors de la préforme. En conséquence, un cycle d'évacuation sous vide (10^{-2} mbar), à une température de 80°C et pendant 30 min s'est montré indispensable. Il est ensuite nécessaire de sceller la conduite de vide pour empêcher

un écoulement de la résine lors de la montée en température lors de la polymérisation.

Dans une seconde phase de réticulation, un cycle thermique de 1 h à 120°C (Cette étape est également utilisée lors du procédé VAP pour favoriser la pénétration de la matrice au cœur des fibres et conservé par souci de comparabilité des échantillons), puis de 2 h à 180°C est appliqué aux échantillons.

Influence des NTC sur les propriétés électriques et mécaniques des composites fibres de carbone / époxy

Étude de la qualité des composites produits

Afin de garantir la pertinence, la reproductibilité ainsi que la comparabilité des analyses électriques et mécaniques des matériaux obtenus, il est important d'évaluer la qualité de ceux-ci.

Microscopie

Des observations en microscopie optique n'ont pas permis de déceler la présence de porosités. La figure 8 présente une de ces observations pour un échantillon chargé à 0,75 %m. Mis à part la présence d'inclusions de résine (zones sombres sur la photographie) dues aux interstices laissés libres par les fibres de maintien (non compressibles), les matériaux montrent une bonne qualité apparente et ne témoignent pas d'une influence des NTC ou du procédé de pulvérisation.

Figure 8 – Observation microscopique d'un échantillon chargé à 0,75 %m en NTC

Cartographie aux ultrasons

Une cartographie bidimensionnelle des matériaux produits est réalisée grâce au contrôle par ultrasons (type C). Un exemple de ces cartographies est présenté en figure 9 pour un échantillon chargé à 0,75 %m en NTC.

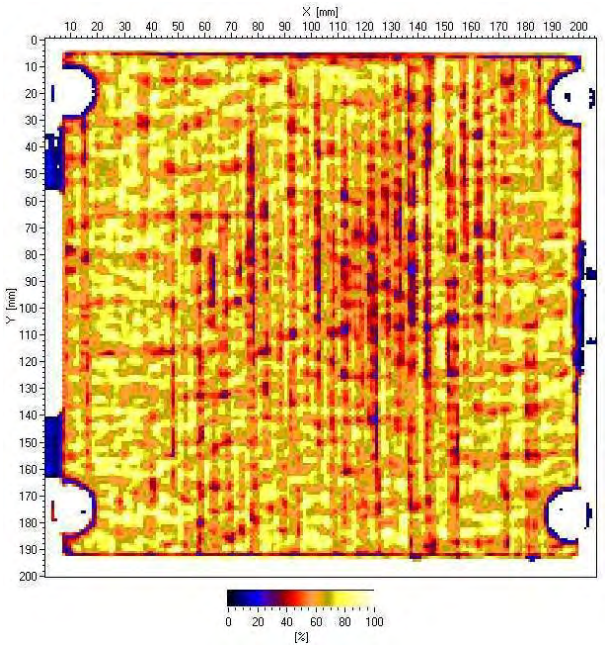

Figure 9 – Cartographie ultrasons d'un échantillon chargé à 0,75 %m en NTC

Ce contrôle non-destructif permet de localiser la présence de défauts (zones sombres) à l'intérieur des stratifiés. Hormis quelques défauts sporadiques, les matériaux mis en œuvre par pulvérisation et / ou avec NTC présentent des densités de défauts similaires aux matériaux mis en œuvre par infusion, indiquant la maturité du procédé de pulvérisation.

Fraction volumique en fibre, porosité et degré de réticulation

Fraction volumique en fibre, taux de porosité ainsi que degré de réticulation des stratifiés sont trois paramètres témoignant de la qualité d'un matériau composite. De plus, la fraction volumique en fibre influence grandement les propriétés électriques et mécaniques d'un stratifié. Le tableau 2 présente un résumé de ces trois paramètres pour les trois types de matériaux produits.

Échantillon	Fraction vol. en fibres (%vol.)	Porosité (%vol.)	Taux de réticulation (%)
Référence (VAP)	61.1	1.0	98,5
Spray MVR 444 seule	62.2	0.8	98,5
Spray 0,75 %. NTC	61.9	0.4	98,8

Tableau 2 – Fraction volumique en fibre, porosité et degré de réticulation des matériaux mis en œuvre

Les fractions volumiques en fibres et taux de porosité, déterminées ici par attaque acide, se trouvent à des niveaux similaires pour les trois matériaux et, de plus, au niveau requis pour un composite structural concernant la fraction volumique en fibre. Le taux de réticulation, déterminé par analyse calorimétrique, témoigne d'une réticulation complète des trois matériaux, atteignant des taux supérieurs à 90 %.

Propriétés électriques

Conductivité électrique en courant continu

Des mesures de conductivité électrique en courant continu sont réalisées sur les échantillons en mesurant la résistance aux bornes d'une éprouvette composite préalablement recouverte d'une peinture conductrice pour favoriser le contact entre les surfaces de l'échantillon et les électrodes de test. Des analyses en sens transverse (axe Z, voir figure 10a) et en sens Y (voir figure 10c) sont réalisées sur des échantillons $[0]_8$.

La figure 10b présente les résultats de ces analyses en sens transverse. Le matériau de référence montre une conductivité atteignant 0,9 ± 0,1 $S.m^{-1}$, une valeur légèrement plus faible est obtenue pour les matériaux mis en œuvre par pulvérisation avec une résine non-chargée : 0,6 ± 0,1 $S.m^{-1}$. Les matériaux pulvérisés avec une résine chargée en NTC présentent une augmentation de la conductivité en sens transverse atteignant 1,6 ± 0,2 $S.m^{-1}$. Ces résultats montrent une influence modérée mais notable de la conductivité en sens transverse grâce aux nanotubes. La figure 10d présente la conductivité électrique en sens Y. Les matériaux de référence montrent pour cette direction une conductivité atteignant 9,3 ± 0,3 $S.m^{-1}$, la conductivité des échantillons mis en œuvre

par pulvérisation avec une résine non chargée atteint une valeur légèrement inférieure : 8,0 ± 0,4 S.m^{-1}, enfin les matériaux produits par pulvérisation avec une résine chargée en NTC atteignent 13,8 ± 0,8 S.m^{-1}, témoignant d'une influence notable des NTC en sens Y.

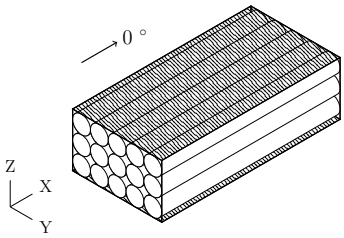

(a) Essai sens Z

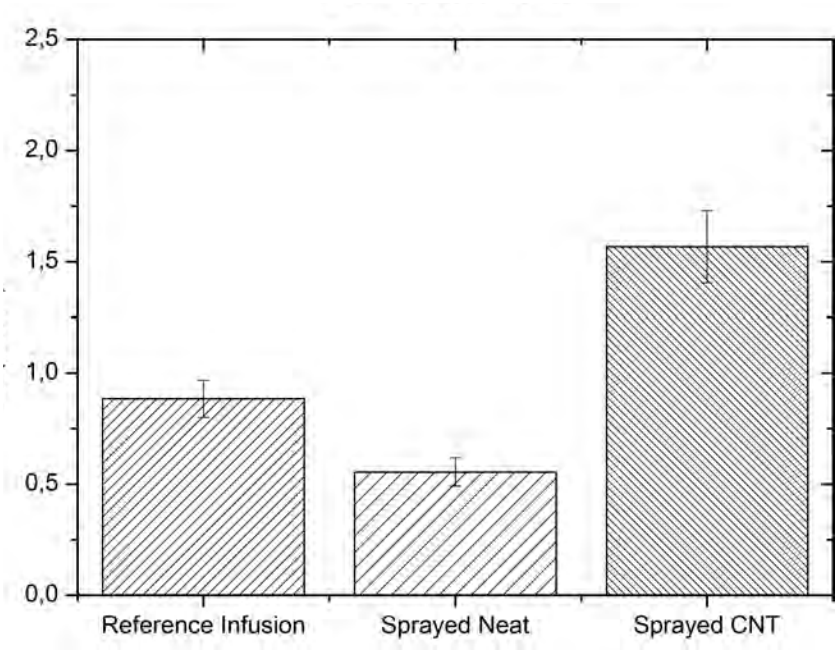

(b) Conductivité électrique sens Z

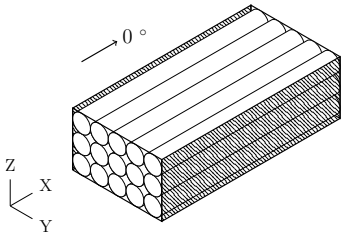

(c) Essai sens Y

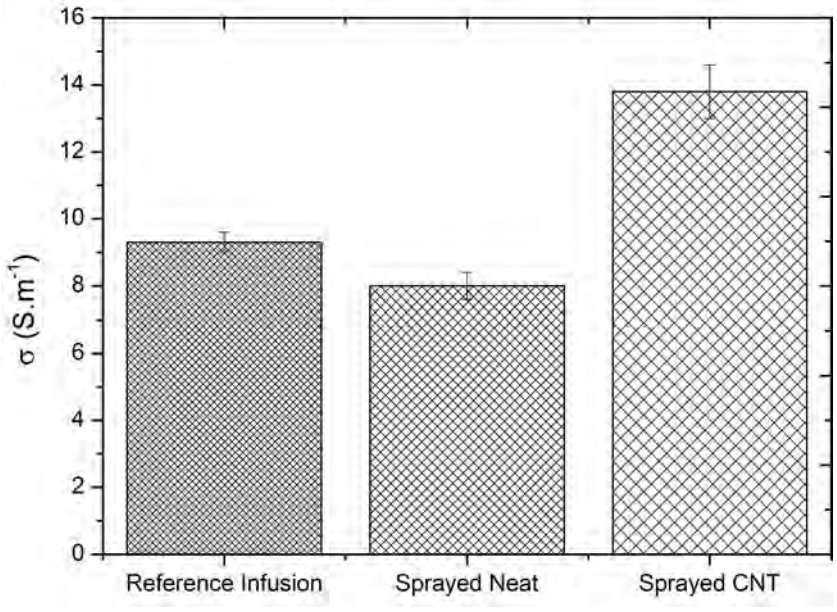

(d) Conductivité électrique sens Y

Figure 10 – Conductivité électrique en courant continu

À la lumière de ces investigations, nous notons que la mesure de la conductivité

électrique en courant continu produit des résultats reproductibles. Ces résultats montrent une légère influence défavorable du procédé de dépôt par pulvérisation et une influence positive, bien que modérée, des NTC dans les directions où la conductivité est régie par les propriétés de la matrice (sens Z et Y). En sens X, où la conductivité est dominée par la conductivité élevée des fibres de carbone, une mesure reproductible est rendue impossible par la faible valeur de la résistance de l'échantillon, qui dans ce cas est du même ordre de grandeur que la résistance de contact échantillon / électrode.

Spectroscopie diélectrique dynamique

Des mesures en spectroscopie diélectrique dynamique ont été réalisées en sens transverse (sens Z) sur les mêmes échantillons que ceux testés en courant continu. Les spectres des conductivités ont été obtenus pour des fréquences de 10^{-1} à 10^{6} Hz et des températures de -150 à +150°C.

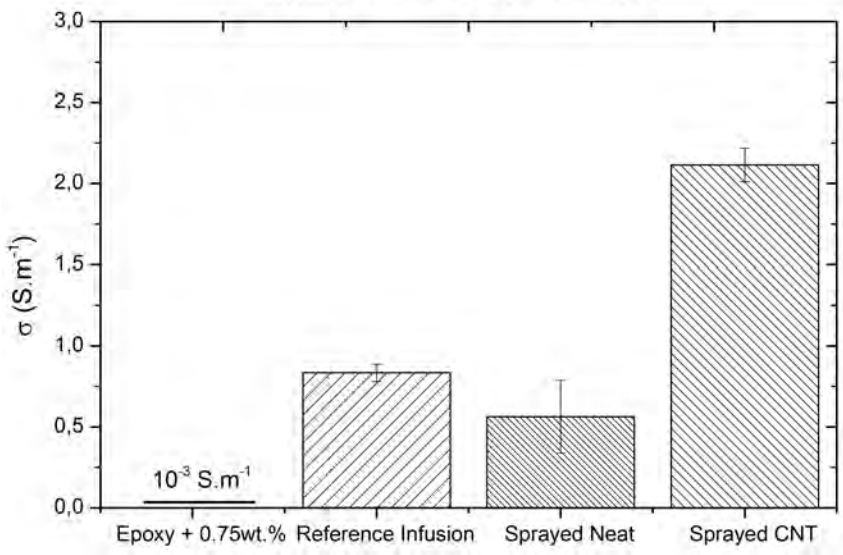

Figure 11 – Conductivité électrique en courant continu mesurée via SDD

La figure 11 présente les valeurs de conductivité électrique en courant continu, mesurée via SDD. On note premièrement que ces valeurs sont en parfait accord avec les mesures présentées au paragraphe précédent (figure 10b), témoignant de la concordance de ces deux méthodes. Ces résultats confirment ceux obtenus précédemment et montrent une influence notable de la conductivité en sens transverse grâce aux nanotubes.

Propriétés mécaniques

Cette section présente les résultats des trois propriétés mécaniques étudiées : analyse mécanique dynamique, résistance au cisaillement interlaminaire et résistance à la propagation de fissure.

La figure 12 présente trois essais de spectrométrie mécanique, et en particulier la tangente de l'angle de perte *tan* δ pour un échantillon représentatif par matériaux. L'étude détaillée de spectres montrent que ni le procédé de pulvérisation, ni l'ajout des nanotubes n'ont d'influence sur les processus de relaxation du polymère. De même, l'étude du pic de relaxation principal (relaxation α) et en particulier de la hauteur et largeur à mi-hauteur de ce pic ne montre pas d'influence de ces deux paramètres sur l'homogénéité du réseau.

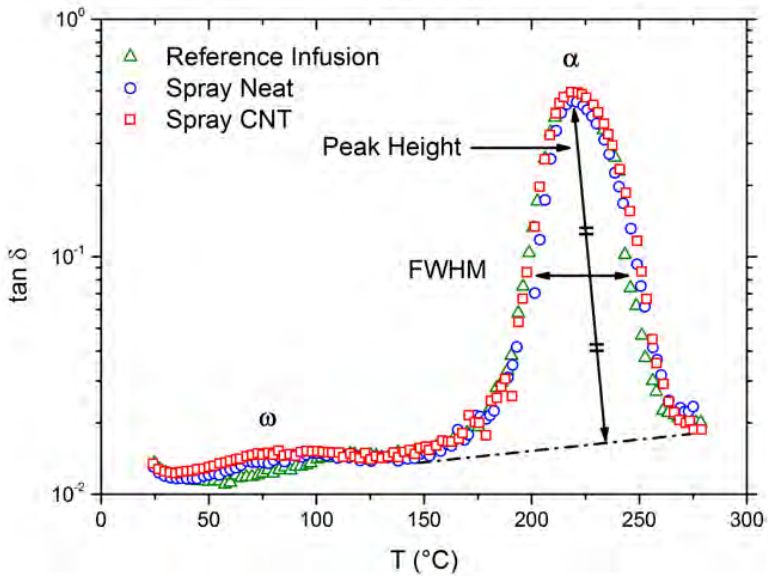

Figure 12 – Évolution de tan δ pour les trois types de matériaux produits

La figure 13 présente les valeurs moyennes (ainsi que l'écart-type) de résistance au cisaillement interlaminaire pour les trois types de matériaux produits. En complément, une étude du profil de fracture des éprouvettes a permis de s'assurer de la nature interlaminaire de la rupture. À la lumière de ces résultats on constate une influence défavorable du procédé de pulvérisation et des nanotubes de carbone. On note toutefois que cette dégradation de la résistance au cisaillement interlaminaire est très modérée et reste de l'ordre de l'erreur de mesure. Cette diminution pourrait être due à une dégradation de la qualité de l'interface fibre / matrice ou à une fragilisation de la matrice par les nanotubes.

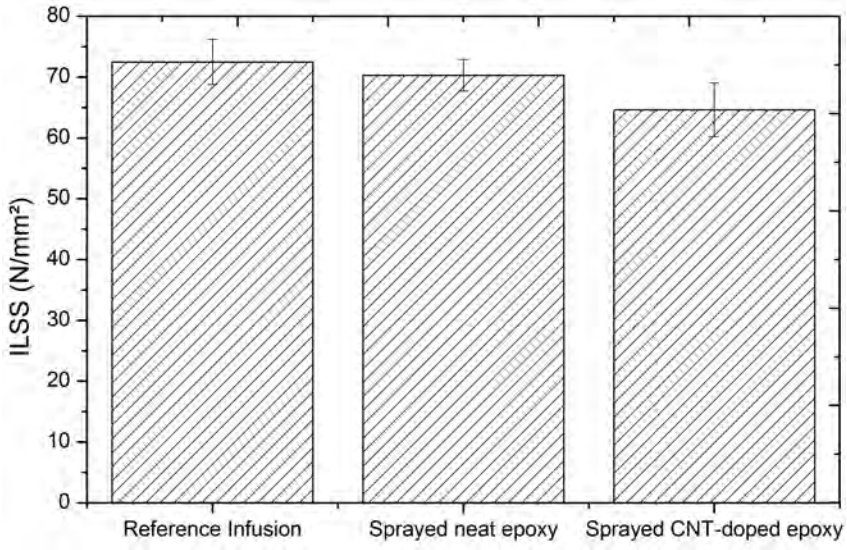

Figure 13 – Valeurs de résistance au cisaillement interlaminaire pour les trois types de matériaux produits

Le tableau 3 regroupe les résultats des essais de délaminage en mode I et reporte les taux de restitution d'énergie pour les trois matériaux (valeurs moyennes). L'analyse de ces tests est rendue difficile par l'importante dispersion des résultats. Néanmoins il peut être noté qu'une augmentation de la valeur de G_I est observée pour les éprouvettes mise en œuvre par pulvérisation. Celle-ci pourrait être due à une augmentation de l'épaisseur de la couche de matrice située à l'interface entre deux plis de fibres de carbone. En second lieu, on note que les échantillons contenant des NTC présentent un taux de restitution d'énergie situé au même niveau que les échantillons références. Cette diminution pourrait être due, à l'instar de la résistance au cisaillement, à une dégradation de la qualité de l'interface fibre / matrice ou à une fragilisation de la matrice par les nanotubes.

	$G_I(J.m^{-2})$
Référence (VAP)	423 ± 47
Spray MVR 444 seule	557 ± 61
Spray 0,75 %. NTC	400 ± 32

Tableau 3 – Valeurs moyennes de GI_c pour les trois types de matériaux produits

Conclusion et perspectives

L'étude bibliographique réalisée en préambule à ce travail de thèse a mis en évidence que l'inhomogénéité de la conductivité électrique des composites stratifiés était un frein à l'utilisation de ces derniers dans l'industrie aéronautique. C'est pourquoi l'objectif premier de ce travail a été l'augmentation et l'homogénéisation de la conductivité électrique en sens transverse des composites à renforts fibres de carbone. En réponse à cette problématique, il a été proposé d'insérer des nanotubes de carbone en tant que charge conductrice, créant ainsi un matériau multifonctionnel. Cependant, la revue de l'état de l'art a également permis de relever les différents verrous s'opposant à la mise en œuvre de composites chargés en nanotubes à l'aides des techniques usuelles (filtration des nanotubes, réagglomération, augmentation de la viscosité de la résine chargée). C'est pourquoi, un procédé innovant de pulvérisation des dispersion NTC / époxy sur plis de fibres de carbone secs a été développé, permettant la mise en œuvre de composites à renforts fibres de carbone chargés en NTC.

En parallèle, il était important de se pencher sur l'analyse des propriétés thermocinétiques, rhéologiques et électriques de nanocomposites NTC / époxy. L'état de dispersion des NTC au sein de la matrice a pu être déterminée grâce à l'analyse des propriétés diélectriques des nanocomposites, permettant également de déterminer le ratio optimal entre taux de charge et conductivité électrique. L'étude de la viscosité à basse fréquence a montré que le comportement des dispersions en fonction de la température semble suivre deux tendances différentes en fonction du taux de charge en NTC. Ce comportement pourrait être associé à une manifestation mécanique du phénomène de formation de l'amas percolant. L'analyse des propriétés thermocinétiques des dispersions a permis de recueillir d'importants paramètres permettant de mener à bien la mise en œuvre des stratifiés.

En dernier lieu, les propriétés électriques et mécaniques des composites à renforts fibres de carbone dopés en nanotubes de carbone ont été étudiés. Une influence des NTC sur la conductivité électrique des composites est mise en lumière, contribuant à l'homogénéisation de la conductivité électrique dans le stratifié. Répondant à notre problématique initiale, cette augmentation légère mais sensible permet l'intégration et l'homogénéisation

de la fonction conductivité électrique au sein d'un matériau composite multifonctionnel. À l'opposé, peu d'influence des NTC sur les propriétés mécaniques de composites n'a pu être observé dans ce travail de thèse.

Perspectives

Cependant, ceci est à mettre en perspective avec les attentes industrielles dans le domaine de la conductivité électrique des composites. Par exemple, afin d'être apte à supporter les effets indirects d'un impact foudre, une conductivité électrique supérieure à 10^2 S.m^{-1} est requise.

La résistance aux impacts des matériaux composites est un point crucial, l'évaluation de la résilience des matériaux composites chargés en nanotubes reste à explorer. De même, les attentes industrielles actuelles en matière de dissipation thermique dans les matériaux composites structuraux encouragent l'évaluation de la conductivité thermique de nos matériaux.

En dernier lieux, il est bon de noter que la méthode de pulvérisation développée dans ce travail de thèse pourrait être appliqué à d'autres nanoparticules conductrices. Le travail de Lonjon [139] a permis de mettre en œuvre des nanocomposites conducteurs polymère / nanofils métalliques, atteignant une conductivité électrique de 10^2 S.m^{-1}. Une application de ces deux techniques aux plis extérieurs des stratifiés apparait potentiellement intéressante en tant que matériaux structural ou revêtement anti-foudre.

TITRE : Mise en œuvre de composites structuraux conducteurs par pulvérisation de dispersions NTC / résine époxy sur nappes fibres de carbone

RÉSUMÉ :

Ce travail présente un procédé innovant de mise en œuvre des composites basé sur le dépôt par pulvérisation des dispersions NTC / époxy a été développé. Une mise en œuvre avec succès de composites à renforts fibres de carbone chargés en nanotubes a montré l'adéquation de ce procédé afin de créer un matériau multi-échelles, où l'insertion de nanotubes de carbone en tant que charge conductrice confère au composite à renforts macroscopiques (fibre de carbone) une nouvelle dimension nanoscopique (nanotubes de carbone).

En second lieu, les propriétés électriques et mécaniques des composites à renforts fibres de carbone dopés en nanotubes de carbones ont été étudiés. Une influence des NTC sur la conductivité électrique des composites est mise en lumière, contribuant à l'homogénéisation de la conductivité électrique dans le stratifié. Répondant à notre problématique initiale, cette augmentation légère mais sensible permet l'intégration et l'homogénéisation de la fonction conductivité électrique au sein d'un matériau composite multifonctionnel. À l'opposé, peu d'influence des NTC sur les propriétés mécaniques de composites n'a pu être observé dans ce travail de thèse.

TITLE : Manufacturing of conductive structural composites through spraying of CNTs / epoxy dispersions on dry carbon fiber plies

ABSTRACT :

The main goal of this work was to create multiscale Carbon Fiber-Reinforced Polymers by inserting carbon nanotubes in the matrix of the composite material to improve and homogenize the through-thickness electrical conductivity. Multiscale composites manufacturing was proposed through addition of carbon nanotubes to a standard composite conferring a nano-dimension to the material.

A spray deposition technique of CNT / epoxy mixtures was developed. CNT-doped CFRP material in which the matrix came exclusively from the spraying process were successfully produced.

An influence of carbon nanotubes on the transverse (Z direction) and orthogonal (Y direction) electrical conductivity could be obtained. A slight but noticeable increase of the conductivity was achieved. More than the inherent values reached, the electrical conductivity was homogenized throughout the whole laminate. This achievement could be one step in order to solve the issue of "edge-glow" on aeronautical structures.